

The isospin-3 three-particle K -matrix at NLO in ChPT

Jorge Baeza-Ballesteros,^a Johan Bijnens,^b Tomáš Husek,^{b,c} Fernando Romero-López,^d Stephen R. Sharpe,^e and Mattias Sjö^b

^a*IFIC, CSIC-Universitat de València, 46980 Paterna, Spain*

^b*Department of Physics, Lund University, Box 118, SE 22100 Lund, Sweden*

^c*Institute of Particle and Nuclear Physics, Charles University, V Holešovičkách 2, 180 00 Prague, Czech Republic*

^d*CTP, Massachusetts Institute of Technology, Cambridge, MA 02139, USA*

^e*Physics Department, University of Washington, Seattle, WA 98195-1560, USA*

E-mail: jorge.baeza@ific.uv.es, johan.bijnens@hep.lu.se,
husek@ipnp.mff.cuni.cz, fernando@mit.edu, srsharpe@uw.edu,
mattias.sjo@hep.lu.se

ABSTRACT: The three-particle K -matrix, $\mathcal{K}_{df,3}$, is a scheme-dependent quantity that parametrizes short-range three-particle interactions in the relativistic-field-theory three-particle finite-volume formalism. In this work, we compute its value for systems of three pions at maximal isospin through next-to-leading order (NLO) in Chiral Perturbation Theory (ChPT). We compare the values to existing lattice QCD results and find that the agreement between lattice QCD data and ChPT in the first two coefficients of the threshold expansion of $\mathcal{K}_{df,3}$ is significantly improved with respect to leading order once NLO effects are incorporated.

KEYWORDS: Chiral Lagrangian, Hadronic Spectroscopy, Structure and Interactions, Lattice QCD

Contents

1	Introduction	1
2	The three-particle K-matrix from ChPT	3
2.1	The role of $\mathcal{K}_{\text{df},3}$ in the three-particle formalism	3
2.2	Relation between \mathcal{M}_3 and $\mathcal{K}_{\text{df},3}$ in ChPT	7
2.3	A note on off-shell conventions	9
2.4	Explicit calculation of $\mathcal{K}_{\text{df},3}^{\text{LO}}$ for $3\pi^+$ scattering	10
2.5	Procedure to calculate $\mathcal{K}_{\text{df},3}$ at NLO	12
3	Summary of results	13
3.1	Complete results	14
3.2	Comparison to lattice results	15
3.3	Range of validity of the threshold expansion	17
4	Details of the calculation of $\mathcal{K}_{\text{df},3}^{\text{NLO}}$	19
4.1	General form of the threshold expansion	19
4.2	Threshold expansion of the non-OPE part of \mathcal{M}_3	21
4.2.1	Threshold expansion of A_J	22
4.2.2	Threshold expansion of A_C	23
4.2.3	The full non-OPE threshold expansion	24
4.3	Bull's head subtraction contribution	25
4.3.1	Threshold expansion	26
4.3.2	Hadamard finite-part integration	27
4.3.3	Analytic approximation	28
4.3.4	Direct numerical evaluation	29
4.3.5	The full bull's head subtraction	31
4.4	OPE diagrams	32
4.4.1	Expression for $\text{Re } \mathcal{M}_{2,\text{off}}^{\text{NLO}}$	33
4.4.2	Decomposition of $t_2 u_2$	34
4.4.3	s -wave contributions	35
4.4.4	d -wave contributions	36
4.4.5	The full OPE contribution	37
5	Conclusions and outlook	38
A	Dependence on the cutoff	39
B	Loop integrals	40

C	Cancellation of imaginary parts	42
C.1	Bull’s head diagram	42
C.2	OPE diagrams	44
C.3	Remaining diagrams	45
D	Threshold expansion using single-parameter kinematic configurations	45
E	An integration method for less well-behaved \mathcal{M}_3	47
	References	51

1 Introduction

Lattice QCD provides a systematically improvable approach to calculate strongly-interacting processes, including several that are inaccessible in experiment. One example is the scattering of three particles, e.g., $3\pi^+ \rightarrow 3\pi^+$. Experimentally, such processes can be very difficult due to the challenge of creating and scattering three beams and because all hadrons (except the nucleons) are short-lived. By contrast, lattice QCD provides a method for obtaining multihadron scattering amplitudes and allows one to treat the strong force in isolation, thus rendering the lightest mesons (and some other hadrons) stable due to the absence of weak and electromagnetic interactions.

The extraction of scattering amplitudes from lattice QCD is a very active topic of research (see refs. [1–8] for recent reviews), and, in particular, three-particle processes have recently received a lot of attention. The formalism to extract these amplitudes from the three-particle finite-volume spectrum computed on the lattice has been developed over the last decade [9–39], using three main approaches, and has been applied to results from lattice simulations for a number of scattering amplitudes [40–53]. So far, the system that has been most extensively explored is that of three pions at maximal isospin, i.e., $3\pi^+ \rightarrow 3\pi^+$ scattering. Several of these works (refs. [44, 47, 48, 52]) use the relativistic-field-theory (RFT) three-particle finite-volume formalism, which parametrizes short-range three-body interactions via an intermediate cutoff-dependent quantity, the three-particle K -matrix, $\mathcal{K}_{\text{df},3}$. As explained in ref. [14], $\mathcal{K}_{\text{df},3}$ is related to the physical three-particle amplitude, \mathcal{M}_3 , via integral equations.

An alternative approach to QCD is the use of effective field theories, with Chiral Perturbation Theory (ChPT) [54, 55] being the paradigm for meson dynamics at low energies. Besides its many phenomenological applications, the synergy between ChPT and lattice QCD is indeed frequently exploited in the literature. ChPT expressions allow one to address the quark-mass dependence, discretization effects, and finite-volume effects for certain quantities. To highlight one example, the $\pi\pi$ scattering lengths can be very well constrained by combining lattice QCD results at heavier-than-physical pion masses with ChPT extrapolations to the real-world value of the mass; see the dedicated chapter in the

FLAG report [56] and refs. [57–59]. Given the recent progress in three-particle scattering amplitudes [60, 61], one hopes that a similar path can be followed for three-pion quantities. So far, however, comparisons between ChPT and lattice QCD results for three-pion systems have only been qualitative.

The leading-order (LO) ChPT prediction for $\mathcal{K}_{\text{df},3}$ for the $3\pi^+$ system was determined in ref. [44]. When compared to lattice QCD results from refs. [44, 47, 52], however, a significant disagreement was observed. This finding was surprising, given how well the two-particle counterpart, the maximal-isospin $\pi\pi$ K -matrix, is described by LO ChPT. It is thus important to understand the cause of this discrepancy. One source could be systematic errors in the lattice QCD calculation, since extracting $\mathcal{K}_{\text{df},3}$ from the finite-volume spectrum is numerically challenging as the shifts in the finite-volume energy levels from their free values are primarily determined by two-particle interactions. Another source could be the importance of higher-order ChPT corrections. In this work, we address the latter possibility by determining the next-to-leading-order (NLO) predictions for $\mathcal{K}_{\text{df},3}$.

The first step in this direction was carried out in refs. [60, 61], where the three-meson scattering amplitude, \mathcal{M}_3 , was determined to NLO for a number of mesonic effective theories, including the one relevant for pions, i.e., ChPT with two quark flavors. It is, however, not obvious how to connect \mathcal{M}_3 to $\mathcal{K}_{\text{df},3}$, since their relation, based on integral equations, needs to be inverted. The aim of this work is to combine the results of ref. [60] with the RFT approach to provide the NLO ChPT prediction for $\mathcal{K}_{\text{df},3}$. We focus here on the case of three pions at maximal isospin, where most of the lattice QCD data is available.

The derivation of the RFT formalism in ref. [13] leads to $\mathcal{K}_{\text{df},3}$ having the key properties of being real, smooth, and invariant under the same symmetries as \mathcal{M}_3 (i.e. Lorentz, parity, and time-reversal symmetries). In particular, all the branch cuts present in \mathcal{M}_3 due to unitarity (two- and three-particle cuts), as well as the single-particle pole due to one-particle exchange (OPE), are absent in $\mathcal{K}_{\text{df},3}$ by construction.¹ An important aspect of an NLO ChPT calculation is that it can provide a check of these properties (and the RFT derivation) much more extensively than the LO result.

Since $\mathcal{K}_{\text{df},3}$ is smooth, it can be expanded about threshold, constrained only by the above-mentioned symmetries. Such a “threshold expansion” is the three-particle analog of the effective-range expansion for the two-particle phase shift (or K -matrix). It has been worked out for the $3\pi^+$ scattering amplitude up to quadratic order as an expansion in relativistic invariants. As described in ref. [22], at this order there are only five unknown constants² in $\mathcal{K}_{\text{df},3}$, i.e., \mathcal{K}_0 , \mathcal{K}_1 , \mathcal{K}_2 , \mathcal{K}_A , and \mathcal{K}_B ; see eq. (2.2). The leading two orders, \mathcal{K}_0 and \mathcal{K}_1 , give rise only to isotropic terms, i.e., those that are independent of the angles between particles. Angular dependence enters through the \mathcal{K}_A and \mathcal{K}_B terms. At LO in ChPT, ref. [44] finds that all terms but \mathcal{K}_0 and \mathcal{K}_1 vanish. At NLO, all five terms are expected to be nonzero, and our aim here is to determine their values.

Several technical complications need to be addressed to obtain the NLO result for $\mathcal{K}_{\text{df},3}$. First, a relation between $\mathcal{K}_{\text{df},3}$ and \mathcal{M}_3 that is valid at NLO in ChPT has to be

¹The absence of the OPE pole is the reason why this is denoted a df = “divergence-free” quantity.

²In ref. [22], the constants are called $\mathcal{K}_{\text{df},3}^{\text{iso}}$, $\mathcal{K}_{\text{df},3}^{\text{iso},1}$, $\mathcal{K}_{\text{df},3}^{\text{iso},2}$, $\mathcal{K}_{\text{df},3}^{(2,A)}$ and $\mathcal{K}_{\text{df},3}^{(2,B)}$, respectively, where “iso” marks the coefficients of the isotropic terms. We have chosen to use an abbreviated notation here.

established. As we will show, both at LO and NLO, the relation between $\mathcal{K}_{\text{df},3}$ and \mathcal{M}_3 is algebraic and linear, which simplifies the subsequent calculation. Second, $\mathcal{K}_{\text{df},3}$ depends, in general, on a cutoff function, and is thus unphysical. This cutoff function appears in the subtraction to cancel the aforementioned divergences in \mathcal{M}_3 , and evaluating its contribution requires a tailored numerical approach. Third, a strategy to isolate the different terms in the threshold expansion of $\mathcal{K}_{\text{df},3}$ is needed, both in the contributions that are analytical as well as in those that can only be evaluated numerically. Here, we succeeded in having an essentially fully analytical result checked by numerical calculations.

Once the NLO results for the different terms in the threshold expansion of $\mathcal{K}_{\text{df},3}$ have been worked out, we can compare to lattice QCD data. In particular, we use the results of ref. [52], which provides values for different coefficients of the threshold expansion at three values of the pion mass. As we will see, the agreement in \mathcal{K}_0 and \mathcal{K}_1 between lattice QCD results and ChPT is significantly improved once NLO effects are incorporated. It is, however, interesting to note that NLO effects seem to be rather large, in particular in \mathcal{K}_1 .

The remainder of this paper is structured as follows. In sec. 2, we provide the necessary background to compute $\mathcal{K}_{\text{df},3}$ in ChPT at NLO. Sec. 3 then presents the central results of this paper, while we leave the technical part of the calculation to sec. 4. Finally, some conclusions are presented in sec. 5. This paper contains 5 appendices, detailing the cutoff dependence of $\mathcal{K}_{\text{df},3}$ (appendix A) and the loop integrals in \mathcal{M}_3 (appendix B), verifying the cancellation of imaginary parts in $\mathcal{K}_{\text{df},3}$ (appendix C), and supplementing sec. 4.2 (appendix D) and sec. 4.3 (appendix E).

2 The three-particle K -matrix from ChPT

In this section, we provide the necessary background to compute $\mathcal{K}_{\text{df},3}$ at NLO in ChPT. Sec. 2.1 introduces $\mathcal{K}_{\text{df},3}$ and describes its role in the three-particle formalism, and sec. 2.2 establishes its connection to \mathcal{M}_3 at NLO in ChPT. Then, an explicit calculation of $\mathcal{K}_{\text{df},3}$ at LO is provided in sec. 2.4, and the strategy to follow at NLO is outlined in sec. 2.5. We defer all technical details of the computation to sec. 4.

2.1 The role of $\mathcal{K}_{\text{df},3}$ in the three-particle formalism

The three-particle finite-volume formalism for identical scalar particles without two-to-three transitions was derived in ref. [13]. In (isospin-symmetric) QCD, it applies for three pions or three kaons at maximal isospin, $I = 3$. We will focus here on the former case. The central equation of the formalism is the quantization condition, whose solutions correspond to the energy levels E_n of a three-pion system with total three-momentum \mathbf{P} in a box of side L ,

$$\det \left[F_3^{-1}(E, \mathbf{P}, L) + \mathcal{K}_{\text{df},3}(E^*) \right] = 0 \quad \text{at} \quad E = E_n. \quad (2.1)$$

This is valid in the energy range where only three-pion intermediate states can go on shell, i.e., $M_\pi < E^* < 5M_\pi$,³ with E^* the total energy in the center-of-mass frame (CMF). F_3 is

³In the following, M_π will denote the renormalized mass of the pions, i.e., $p_i^2 = M_\pi^2$ for on-shell pions of momenta p_i . In amplitude calculations, this is called the “physical” mass to distinguish it from the non-

a quantity that depends on the volume, kinematic functions and two-particle interactions, and $\mathcal{K}_{\text{df},3}$ is a real, Lorentz-invariant and smooth function of E^* that parametrizes short-range three-particle interactions. Both quantities are matrices in a space that describes the kinematics of three on-shell particles, and the determinant is taken over those indices. In particular, the choice in the RFT formalism is to describe the three-particle system as composed by a pair of particles with angular momentum indices ℓ and m , usually called the *interacting pair* or *dimer*, plus a third particle with three-momentum \mathbf{k} , called the *spectator*. Note that $\mathcal{K}_{\text{df},3}$ is a scheme-dependent quantity, with the scheme being determined by the choice of a cutoff function applied to the momentum of the spectator particle. This function ensures that the matrices appearing in the quantization conditions have finite size. For more details on the implementation of the formalism, we refer the reader to refs. [20, 22, 26, 36].

The key feature of eq. (2.1) needed for this work is that, given a set of $3\pi^+$ finite-volume energy levels, $\mathcal{K}_{\text{df},3}$ can be extracted by fitting the predicted spectrum to the measured one. For this, one needs a parametrization of $\mathcal{K}_{\text{df},3}$ in terms of few independent quantities. A systematic approach is to expand $\mathcal{K}_{\text{df},3}$ in terms of relativistic invariants organized by the distance to the three-particle threshold. To reduce the number of independent parameters, one can use the fact that $\mathcal{K}_{\text{df},3}$ has the same symmetries as the scattering amplitude, i.e., parity, time-reversal and particle-exchange symmetries. This leads to the threshold expansion worked out in ref. [22]. As explained in that work, only five independent terms contribute to the expansion up to quadratic order:

$$M_\pi^2 \mathcal{K}_{\text{df},3} = \mathcal{K}_0 + \mathcal{K}_1 \Delta + \mathcal{K}_2 \Delta^2 + \mathcal{K}_A \Delta_A + \mathcal{K}_B \Delta_B + \mathcal{O}(\Delta^3), \quad (2.2)$$

where the following kinematic quantities have been defined:

$$\begin{aligned} \Delta &\equiv -\frac{1}{2} \sum_{i,j} \tilde{t}_{ij} = \frac{P^2 - 9M_\pi^2}{9M_\pi^2}, \\ \Delta_A &\equiv \sum_i (\Delta_i^2 + \Delta_i'^2) - \Delta^2, \quad \Delta_B \equiv \sum_{i,j} \tilde{t}_{ij}^2 - \Delta^2. \end{aligned} \quad (2.3)$$

Here, $P = (E, \mathbf{P})$ is the total four-momentum of the system, and we define

$$\begin{aligned} \tilde{t}_{ij} &\equiv \frac{(p_i - k_j)^2}{9M_\pi^2}, \\ \Delta_j &\equiv \sum_i \tilde{t}_{ij} + \Delta = \frac{(P - k_j)^2 - 4M_\pi^2}{9M_\pi^2}, \\ \Delta_i' &\equiv \sum_j \tilde{t}_{ij} + \Delta = \frac{(P - p_i)^2 - 4M_\pi^2}{9M_\pi^2}. \end{aligned} \quad (2.4)$$

We choose k_1, k_2, k_3 to be the incoming momenta, and p_1, p_2, p_3 the outgoing ones, so that $P = k_1 + k_2 + k_3 = p_1 + p_2 + p_3$. We reiterate that \mathcal{K}_X with $X = 0, 1, 2, A, B$ are renormalized mass appearing in the Lagrangian. In the lattice community, the “physical” mass typically refers to the real-world value $M_{\pi,\text{phys}} \approx 139.570$ MeV. In this work we will use the latter convention, and so M_π will in general be different from $M_{\pi,\text{phys}}$.

unknown, dimensionless constants to be determined. As noted in the introduction, the only terms that lead to nontrivial dependence on the relative angles in the initial or final three-particle state are Δ_A and Δ_B . Moreover, only Δ_B leads to contributions with overall angular momentum differing from zero.

Once the coefficients of eq. (2.2) are determined from lattice QCD simulation, one has to connect the scheme-dependent $\mathcal{K}_{\text{df},3}$ to the physical scattering amplitude, \mathcal{M}_3 . The relation between both quantities was derived in ref. [14] and involves integral equations. In this paper, we use that relation extensively, so as to obtain $\mathcal{K}_{\text{df},3}$ at a consistent order in ChPT provided the corresponding prediction for \mathcal{M}_3 . Therefore, we reproduce here the key results from ref. [14]. For numerical solutions of the integral equations, see refs. [62, 63].

We begin by recalling the kinematic variables used in the RFT approach. As already anticipated, the configuration of three on-shell particles is described by singling out one as a spectator with three-momentum \mathbf{k} , and boosting the interacting pair to their CMF, in which the two particles of the pair have three-momentum \mathbf{a}_k^* and $-\mathbf{a}_k^*$, respectively.⁴ The magnitude of these momenta is denoted $q_{2,k}^* \equiv |\mathbf{a}_k^*|$ and is given by

$$q_{2,k}^{*2} = \frac{1}{4}(E_{2,k}^{*2} - 4M_\pi^2), \quad \text{with} \quad E_{2,k}^{*2} = (P - k)^2, \quad (2.5)$$

where $E_{2,k}^*$ is the energy of the pair in their rest frame. Expressing the initial-state kinematics this way, and expressing the final state analogously as a spectator and an interacting pair with three-momenta \mathbf{p} and $\pm\mathbf{a}_p^*$, respectively, the three-particle amplitude can be written as a function of the spectator momenta and the *directions* of the pair momenta,

$$\mathcal{M}_3(\mathbf{p}, \hat{\mathbf{a}}_p^*; \mathbf{k}, \hat{\mathbf{a}}_k^*), \quad (2.6)$$

since magnitudes are fixed by eq. (2.5); the hats denote unit vectors. Here and in what follows, the dependence on P is left implicit. This description is somehow redundant, as it involves 10 (11 if we include P^2) variables, while there are only 8 independent kinematic quantities describing a general three-to-three process. In particular, the rotational invariance of the amplitude in, say, the overall CMF is not taken into account.⁵ Nevertheless, these variables are the natural choice in the RFT approach.

A further step is to decompose the angular dependence in the pair CMFs into spherical harmonics:⁶

$$\mathcal{M}_3(\mathbf{p}, \hat{\mathbf{a}}_p^*; \mathbf{k}, \hat{\mathbf{a}}_k^*) = \sum_{\ell' m' \ell m} 4\pi Y_{\ell' m'}^*(\hat{\mathbf{a}}_p^*) \mathcal{M}_3(\mathbf{p}, \mathbf{k})_{\ell' m'; \ell m} Y_{\ell m}(\hat{\mathbf{a}}_k^*). \quad (2.7)$$

⁴Here * indicates that quantities are expressed in the CMF of the interacting pair, and the subscript is used to emphasize that the quantity is expressed in the CMF of the pair for which the spectator has that particular momentum.

⁵A convenient set of 8 parameters, from which the 11-parameter set $\{P^2, \mathbf{p}, \hat{\mathbf{a}}_p^*, \mathbf{k}, \hat{\mathbf{a}}_k^*\}$ is easy to obtain, is $\{E^*, |\mathbf{p}|, |\mathbf{k}|, \psi, \hat{\mathbf{a}}_p^*, \hat{\mathbf{a}}_k^*\}$, where E is the total CMF energy and ψ is the angle between \mathbf{p} and \mathbf{k} in the overall CMF. The remaining three degrees of freedom correspond to rotations of the full system.

⁶Later in this paper, we discuss the real and imaginary parts of quantities like \mathcal{M}_3 . When doing so, the fact that, in the standard basis, the spherical harmonics are complex should be ignored. One can show that the spherical harmonics arise as overall factors in the unitarity-like relations, and it is the imaginary part of the remainder of the expression that matters. To avoid this issue in numerical calculations, one can use the real spherical harmonics, as is done in present implementations of the three-particle quantization condition (see, e.g., ref. [22]).

This is needed because, as will be seen shortly, some of the subtractions that appear in the definition of the divergence-free version of \mathcal{M}_3 depend on the pair angular momenta. Subsequent relations will be written for $\mathcal{M}_3(\mathbf{p}, \mathbf{k})_{\ell' m'; \ell m}$, with the angular momentum indices treated as matrix indices and often left implicit. Other three-particle quantities entering the following equations, such as $\mathcal{K}_{\text{df},3}$ itself, are also written in this hybrid notation. For two-particle quantities, in which the spectator is unchanged, we follow ref. [14] and label them with a single spectator momentum,⁷ e.g.,

$$\mathcal{M}_2(\mathbf{p})_{\ell' m'; \ell m} = \delta_{\ell' \ell} \delta_{m' m} \mathcal{M}_{2,\ell}(q_{2,p}^*), \quad (2.8)$$

and similarly for the two-particle phase-space factor,

$$\rho(\mathbf{p})_{\ell' m'; \ell m} = \delta_{\ell' \ell} \delta_{m' m} \bar{\rho}(q_{2,p}^*), \quad \bar{\rho}(q_{2,p}^*) \equiv -i \frac{q_{2,p}^*}{16\pi E_{2,p}^*}, \quad (2.9)$$

which we only define above threshold, i.e., for $E_{2,p}^* \geq 2M_\pi$, as this is all we need in this work. A full definition of $\rho(\mathbf{p})$ is given in ref. [14], including its subthreshold behavior, where it is real and cutoff-dependent.

We are now ready to define the divergence-free three-particle amplitude, $\mathcal{M}_{\text{df},3}$:

$$\mathcal{M}_{\text{df},3}(\mathbf{p}, \mathbf{k}) = \mathcal{M}_3(\mathbf{p}, \mathbf{k}) - \mathcal{S} \left\{ \mathcal{D}^{(u,u)}(\mathbf{p}, \mathbf{k}) \right\}. \quad (2.10)$$

Here, \mathcal{S} indicates symmetrization over choices of initial and final spectators (9 terms in total), while $\mathcal{D}^{(u,u)}$ is the unsymmetrized subtraction term, with (u, u) indicating unsymmetrized for both final and initial states. This symmetrization procedure is explained in detail in ref. [14], and we give only specific examples below. It is important to keep in mind that \mathcal{M}_3 and $\mathcal{K}_{\text{df},3}$ are, by definition, fully symmetrized quantities.

The subtraction term solves an integral equation that can be expanded in powers of \mathcal{M}_2 to the order we need as

$$\mathcal{D}^{(u,u)}(\mathbf{p}, \mathbf{k}) = -\mathcal{M}_2(\mathbf{p}) G^\infty(\mathbf{p}, \mathbf{k}) \mathcal{M}_2(\mathbf{k}) + \int_r \mathcal{M}_2(\mathbf{p}) G^\infty(\mathbf{p}, \mathbf{r}) \mathcal{M}_2(\mathbf{r}) G^\infty(\mathbf{r}, \mathbf{k}) \mathcal{M}_2(\mathbf{k}) + \dots, \quad (2.11)$$

where $\int_r \equiv \int d^3r / [2\omega_r (2\pi)^3]$, with $\omega_r = \sqrt{\mathbf{r}^2 + M_\pi^2}$, and⁸

$$G^\infty(\mathbf{p}, \mathbf{k})_{\ell' m'; \ell m} = \left(\frac{k_p^*}{q_{2,p}^*} \right)^{\ell'} \frac{4\pi Y_{\ell' m'}(\hat{\mathbf{k}}_p^*) H(x_p) H(x_k) Y_{\ell m}^*(\hat{\mathbf{p}}_k^*)}{b_{pk}^2 - M_\pi^2 + i\epsilon} \left(\frac{p_k^*}{q_{2,k}^*} \right)^\ell. \quad (2.12)$$

Here, $b_{pk} \equiv P - p - k$, and $H(x)$ is a smooth cutoff function that is 0 when $x \leq 0$ and 1 when $x \geq 1$, with $x_k \equiv (P - k)^2 / (4M_\pi^2)$ and similarly for x_p .⁹ Note that k_p^* refers to the

⁷An alternative notation involving two variables and an adjustment of factors of the energy, 2ω , has been used in some subsequent works, e.g., ref. [32].

⁸Comparing to eq. (81) of ref. [14], we note that here we use the relativistic form of the denominator, which is needed to obtain a relativistically invariant $\mathcal{K}_{\text{df},3}$.

⁹In the range $0 < x < 1$, we let

$$H(x) = \exp \left[-\frac{1}{x} \exp \left(-\frac{1}{1-x} \right) \right]$$

in accordance with, for example, eqs. (28) and (29) of ref. [13], but any smooth function that interpolates between the constant values may be used. Some other choices of $H(x)$ are studied in appendix A.

magnitude of \mathbf{k} taken in the CMF of the pair associated with p , and analogously for p_k^* . We stress that the cutoff functions do not violate Lorentz symmetry, because x_k and x_p are both Lorentz invariant.

The factors of $k_p^*/q_{2,p}^*$ and $p_k^*/q_{2,k}^*$ in G^∞ result from the analysis of the power-law volume-dependent contributions to the *finite-volume* correlator. In particular, it is important in that analysis that the dependence on \mathbf{k}_p^* and \mathbf{p}_k^* is smooth near threshold, and this requires the presence of the harmonic polynomials, e.g., $(k_p^*)^\ell Y_{\ell m}(\hat{\mathbf{k}}_p^*)$, rather than the spherical harmonics alone. We stress that the factors of $k_p^*/q_{2,p}^*$ and $p_k^*/q_{2,k}^*$ imply that the sum over angular momentum indices cannot be performed analytically.

Some features of $\mathcal{D}^{(u,u)}$ will be important below and we comment on them here. First, it depends only on the *on-shell* two-particle amplitudes. Second, while in general one needs to keep the entire infinite series in $\mathcal{D}^{(u,u)}$ to determine $\mathcal{M}_{\text{df},3}$, when working at some fixed order in a perturbative expansion such as ChPT, only a finite subset of the terms in eq. (2.11) appear. Finally, we stress that $\mathcal{D}^{(u,u)}$ depends on the choice of cutoff function, and is thus not a physical quantity.

With $\mathcal{M}_{\text{df},3}$ in hand, the full relation to $\mathcal{K}_{\text{df},3}$ is given by¹⁰

$$\mathcal{M}_{\text{df},3}(\mathbf{p}, \mathbf{k}) = \mathcal{S} \left\{ \int_s \int_r \mathcal{L}^{(u,u)}(\mathbf{p}, \mathbf{s}) \mathcal{T}(\mathbf{s}, \mathbf{r}) \mathcal{R}^{(u,u)}(\mathbf{r}, \mathbf{k}) \right\}, \quad (2.13)$$

where

$$\mathcal{L}^{(u,u)}(\mathbf{p}, \mathbf{k}) \equiv \left[\frac{1}{3} - \mathcal{M}_2(\mathbf{p}) \rho(\mathbf{p}) \right] \bar{\delta}(\mathbf{p} - \mathbf{k}) - \mathcal{D}^{(u,u)}(\mathbf{p}, \mathbf{k}) \rho(\mathbf{k}), \quad (2.14)$$

$$\mathcal{R}^{(u,u)}(\mathbf{p}, \mathbf{k}) \equiv \bar{\delta}(\mathbf{p} - \mathbf{k}) \left[\frac{1}{3} - \rho(\mathbf{p}) \mathcal{M}_2(\mathbf{p}) \right] - \rho(\mathbf{p}) \mathcal{D}^{(u,u)}(\mathbf{p}, \mathbf{k}), \quad (2.15)$$

with $\bar{\delta}(\mathbf{p} - \mathbf{k}) \equiv 2\omega_k (2\pi)^3 \delta^{(3)}(\mathbf{p} - \mathbf{k})$, and, finally,

$$\mathcal{T}(\mathbf{p}, \mathbf{k}) \equiv \mathcal{K}_{\text{df},3}(\mathbf{p}, \mathbf{k}) - \int_s \int_r \mathcal{K}_{\text{df},3}(\mathbf{p}, \mathbf{s}) \rho(\mathbf{s}) \mathcal{L}^{(u,u)}(\mathbf{s}, \mathbf{r}) \mathcal{K}_{\text{df},3}(\mathbf{r}, \mathbf{k}) + \dots \quad (2.16)$$

The last equation shows the first two terms in the expansion of the integral equation for \mathcal{T} in powers of $\mathcal{K}_{\text{df},3}$.

2.2 Relation between \mathcal{M}_3 and $\mathcal{K}_{\text{df},3}$ in ChPT

ChPT describes the low-energy regime of QCD in terms of mesonic degrees of freedom. It allows a perturbative determination of mesonic observables in terms of momenta and masses and as a function of some a priori unknown parameters—the so-called low-energy constants (LECs). These can be determined from experiment or first principles (the latter usually via matching to lattice QCD). We refer the unfamiliar reader to refs. [64, 65] for an introduction to ChPT and to refs. [60, 61] for brief summaries of what is needed for NLO three-meson scattering. In this work, we restrict ourselves to the case of two-flavor ChPT.

Regarding the integral equations that are part of the RFT formalism, we can implement the usual ChPT power counting by expanding in powers of $1/F_\pi^2$, where F_π is the pion decay

¹⁰Here and below, we have rearranged some factors of $2\omega_r$ relative to ref. [14] in order to simplify the notation.

constant.¹¹ From here on, we will focus on the $3\pi^+$ system, and so \mathcal{M}_2 and \mathcal{M}_3 will refer to the two-particle $I = 2$ and three-particle $I = 3$ scattering amplitudes, respectively. We note that $\mathcal{M}_2 = \mathcal{O}(1/F_\pi^2)$ and $\mathcal{M}_3 = \mathcal{O}(1/F_\pi^4)$. Since \mathcal{L} and \mathcal{R} begin at $\mathcal{O}(1)$,

$$\mathcal{L}^{(u,u)\text{LO}}(\mathbf{p}, \mathbf{k}) = \frac{1}{3}\bar{\delta}(\mathbf{p} - \mathbf{k}) = \mathcal{R}^{(u,u)\text{LO}}(\mathbf{p}, \mathbf{k}), \quad (2.17)$$

we have that $\mathcal{K}_{\text{df},3} = \mathcal{O}(1/F_\pi^4)$, and thus that $\mathcal{T}^{\text{LO}} = \mathcal{K}_{\text{df},3}^{\text{LO}}$. Putting this together and noting that the symmetrization of $\mathcal{K}_{\text{df},3}/9$ simply yields $\mathcal{K}_{\text{df},3}$, the LO version of eq. (2.13) reduces to

$$\mathcal{K}_{\text{df},3}^{\text{LO}}(\mathbf{p}, \mathbf{k}) = \mathcal{M}_{\text{df},3}^{\text{LO}}(\mathbf{p}, \mathbf{k}) = \mathcal{M}_3^{\text{LO}}(\mathbf{p}, \mathbf{k}) - \mathcal{S}\left\{\mathcal{D}^{(u,u)\text{LO}}(\mathbf{p}, \mathbf{k})\right\}, \quad (2.18)$$

$$\mathcal{D}^{(u,u)\text{LO}}(\mathbf{p}, \mathbf{k}) = -\mathcal{M}_2^{\text{LO}}(\mathbf{p})G^\infty(\mathbf{p}, \mathbf{k})\mathcal{M}_2^{\text{LO}}(\mathbf{k}). \quad (2.19)$$

The second equation can be further simplified by noting that $\mathcal{M}_2^{\text{LO}}$ is purely s -wave, so we can make the replacement

$$G^\infty(\mathbf{p}, \mathbf{k}) \longrightarrow G_{ss}^\infty(\mathbf{p}, \mathbf{k}), \quad G_{ss}^\infty(\mathbf{p}, \mathbf{k})_{\ell'm';\ell m} \equiv \delta_{\ell'0}\delta_{m'0}\delta_{\ell 0}\delta_{m 0} \frac{H(x_p)H(x_k)}{b_{pk}^2 - M_\pi^2 + i\epsilon}. \quad (2.20)$$

We can also rewrite the expression for $\mathcal{K}_{\text{df},3}$ as

$$\mathcal{K}_{\text{df},3}^{\text{LO}}(\mathbf{p}, \mathbf{k}) = \mathcal{S}\left\{\mathcal{K}_{\text{df},3}^{(u,u)\text{LO}}(\mathbf{p}, \mathbf{k})\right\} = \mathcal{S}\left\{\mathcal{M}_3^{(u,u)\text{LO}}(\mathbf{p}, \mathbf{k}) - \mathcal{D}^{(u,u)\text{LO}}(\mathbf{p}, \mathbf{k})\right\}, \quad (2.21)$$

where $\mathcal{M}_3^{(u,u)}$ is the unsymmetrized amplitude. This form was used to perform the LO calculation of $\mathcal{K}_{\text{df},3}$ in ref. [44], which we reproduce below in sec. 2.4. We note that the subtraction produces a divergence-free quantity that is automatically real.

Moving to NLO, we need to keep terms up to $\mathcal{O}(1/F_\pi^6)$. We note that the second term in the right-hand side of eq. (2.16) is $\mathcal{O}(1/F_\pi^8)$, so we still have $\mathcal{T} = \mathcal{K}_{\text{df},3}$ at NLO. Since $\mathcal{D}^{(u,u)} = \mathcal{O}(1/F_\pi^4)$, the NLO expressions for $\mathcal{L}^{(u,u)}$ and $\mathcal{R}^{(u,u)}$ are equal and given by

$$\mathcal{L}^{(u,u)\text{NLO}}(\mathbf{p}, \mathbf{k}) = -\mathcal{M}_2^{\text{LO}}(\mathbf{p})\rho(\mathbf{p})\bar{\delta}(\mathbf{p} - \mathbf{k}) = \mathcal{R}^{(u,u)\text{NLO}}(\mathbf{p}, \mathbf{k}). \quad (2.22)$$

Here, we are adopting the notation, also used below, that NLO indicates the next-to-leading-order contribution alone rather than the sum of LO and NLO contributions. Applying these results to eq. (2.13), we find

$$\mathcal{M}_{\text{df},3}^{\text{NLO}}(\mathbf{p}, \mathbf{k}) = \mathcal{K}_{\text{df},3}^{\text{NLO}}(\mathbf{p}, \mathbf{k}) - \frac{1}{3}\mathcal{S}\left\{\mathcal{K}_{\text{df},3}^{\text{LO}}(\mathbf{p}, \mathbf{k})\rho(\mathbf{k})\mathcal{M}_2^{\text{LO}}(\mathbf{k}) + \mathcal{M}_2^{\text{LO}}(\mathbf{p})\rho(\mathbf{p})\mathcal{K}_{\text{df},3}^{\text{LO}}(\mathbf{p}, \mathbf{k})\right\}. \quad (2.23)$$

Using the equality of $\mathcal{K}_{\text{df},3}$ and $\mathcal{M}_{\text{df},3}$ at LO, this can be reorganized into

$$\mathcal{K}_{\text{df},3}^{\text{NLO}}(\mathbf{p}, \mathbf{k}) = \mathcal{M}_{\text{df},3}^{\text{NLO}}(\mathbf{p}, \mathbf{k}) + \frac{1}{3}\mathcal{S}\left\{\mathcal{M}_{\text{df},3}^{\text{LO}}(\mathbf{p}, \mathbf{k})\rho(\mathbf{k})\mathcal{M}_2^{\text{LO}}(\mathbf{k}) + \mathcal{M}_2^{\text{LO}}(\mathbf{p})\rho(\mathbf{p})\mathcal{M}_{\text{df},3}^{\text{LO}}(\mathbf{p}, \mathbf{k})\right\}. \quad (2.24)$$

¹¹Regarding what is considered “physical”, F_π is treated the same way as M_π . Its real-world value is $F_{\pi,\text{phys}} \approx 92.2$ MeV.

The final quantity that we need is the NLO part of the subtraction term $\mathcal{D}^{(u,u)}$, which is given by

$$\begin{aligned} \mathcal{D}^{(u,u)\text{NLO}}(\mathbf{p}, \mathbf{k}) = & -\mathcal{M}_2^{\text{LO}}(\mathbf{p})G^\infty(\mathbf{p}, \mathbf{k})\mathcal{M}_2^{\text{NLO}}(\mathbf{k}) - \mathcal{M}_2^{\text{NLO}}(\mathbf{p})G^\infty(\mathbf{p}, \mathbf{k})\mathcal{M}_2^{\text{LO}}(\mathbf{k}) \\ & + \int_r \mathcal{M}_2^{\text{LO}}(\mathbf{p})G_{ss}^\infty(\mathbf{p}, \mathbf{r})\mathcal{M}_2^{\text{LO}}(\mathbf{r})G_{ss}^\infty(\mathbf{r}, \mathbf{k})\mathcal{M}_2^{\text{LO}}(\mathbf{k}). \end{aligned} \quad (2.25)$$

Note that we have made the replacement $G^\infty \rightarrow G_{ss}^\infty$ in the final term since there all two-particle interactions are LO and thus purely s -wave. Accordingly, this replacement cannot be made in the other two terms, since $\mathcal{M}_2^{\text{NLO}}$ contains all (even) partial waves.

The final equation we need to completely specify the NLO contribution to $\mathcal{K}_{\text{df},3}$ is

$$\mathcal{M}_{\text{df},3}^{\text{NLO}}(\mathbf{p}, \mathbf{k}) = \mathcal{M}_3^{\text{NLO}}(\mathbf{p}, \mathbf{k}) - \mathcal{S}\left\{\mathcal{D}^{(u,u)\text{NLO}}(\mathbf{p}, \mathbf{k})\right\}. \quad (2.26)$$

The procedure is thus, given $\mathcal{M}_3^{\text{NLO}}$, to subtract $\mathcal{D}^{(u,u)\text{NLO}}$, eq. (2.25), after symmetrization, and then add in the “ ρ terms” on the right-hand side of eq. (2.24). In fact, the latter are purely imaginary since both LO amplitudes are real, and thus, given the fact that $\mathcal{K}_{\text{df},3}$ is real, we obtain a simplified result

$$\mathcal{K}_{\text{df},3}^{\text{NLO}}(\mathbf{p}, \mathbf{k}) = \text{Re } \mathcal{M}_{\text{df},3}^{\text{NLO}}(\mathbf{p}, \mathbf{k}). \quad (2.27)$$

In principle, we do not need to calculate the ρ terms. However, an important cross-check on the formalism and the calculations can be obtained by showing explicitly that the imaginary part of $\mathcal{K}_{\text{df},3}$ vanishes based on the unitarity of off-shell amplitudes. This is presented in appendix C.

2.3 A note on off-shell conventions

The subtraction term \mathcal{D} naturally separates into a part that cancels the OPE poles, namely the symmetrization of the first line of eq. (2.25), and a remainder. Below, we will find it useful to similarly separate \mathcal{M}_3 into an OPE and a non-OPE part. The same separation of $\mathcal{M}_{\text{df},3}$ and $\mathcal{K}_{\text{df},3}$ follows from this. However, this separation (unlike that of \mathcal{D}) is not unique.

Feynman diagrams can be categorized as either OPE (e.g., figs. 1a and 10) or non-OPE (e.g., figs. 1b, 8, and 9), but the contribution of each diagram in ChPT depends on the parametrization of the Nambu–Goldstone manifold.¹² This dependence must cancel when all contributions are summed into a physical amplitude, but separating based on diagrams does introduce parametrization dependence into the OPE and non-OPE parts.

Alternatively, one may view the OPE part as two four-point amplitudes with one leg off-shell, with the OPE propagator joining the off-shell legs. The off-shell four-point amplitude can be modified by the addition of a smooth function of the kinematic variables that vanishes on shell, and the remainder of the complete amplitude is deferred to the non-OPE part. Thus, we say that the separation is determined by an *off-shell convention*.

¹²See appendix B of ref. [61] for an in-depth discussion on parametrizations.

Note that each parametrization will naturally give rise to a specific off-shell convention, as can be seen in appendix E.

Here, we follow the off-shell convention of ref. [60], where the off-shell amplitude is defined by directly replacing the on-shell Mandelstam variables by their off-shell counterparts in a particular form of the on-shell four-pion amplitude.¹³ In this approach, the off-shell amplitude is unique up to the freedom to rewrite the on-shell amplitude using $s + t + u = 4M_\pi^2$, which does not hold off-shell. This prescription leads to the same OPE and non-OPE parts independently of the underlying initial parametrization, and both parts are separately scale-independent. Nevertheless, we stress that the separation into parts depends on a choice, and that only their sum is physical; also, contributions from individual diagrams remain parametrization dependent. This is in contrast to the subtraction terms, which are unique up to the choice of cutoff function, since they are built from on-shell quantities.

2.4 Explicit calculation of $\mathcal{K}_{\text{df},3}^{\text{LO}}$ for $3\pi^+$ scattering

To illustrate the subtractions needed to obtain a divergence-free quantity, we work through the calculation of $\mathcal{M}_{\text{df},3}^{\text{LO}} = \mathcal{K}_{\text{df},3}^{\text{LO}}$ for the $3\pi^+$ system, the results of which were first presented in ref. [44]; see also the calculation of the corresponding quantities for $\pi^+\pi^+K^+$ and $\pi^+K^+K^+$ systems in ref. [36]. This calculation also illustrates how intermediate results may depend on the convention used for off-shell amplitudes, as described in the previous section, although the final result should be (and is) independent of such conventions.

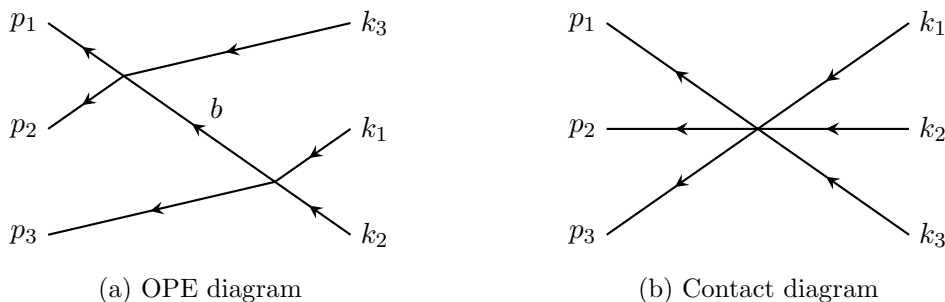


Figure 1: Feynman diagrams contributing to \mathcal{M}_3 at LO for maximal isospin. For diagram (a), there are an additional eight diagrams corresponding to the symmetrization of initial and final momenta.

To calculate $\mathcal{M}_{\text{df},3}^{\text{LO}}$, we use eq. (2.21). Only two diagrams contribute to $\mathcal{M}_3^{\text{LO}}$, which are shown in fig. 1, and only the first of them, the OPE diagram, requires a subtraction, that is given by eq. (2.19). We consider the OPE contributions first.

The results are simplified by the fact that $\mathcal{M}_2^{\text{LO}}$ is purely s -wave, so we need only keep the $\ell' = \ell = 0$ contribution to $\mathcal{K}_{\text{df},3}$. We obtain (with the s -wave limitation indicated by

¹³This form is presented in eqs. (18) and (23) of ref. [60] and repeated (for maximum isospin) in eqs. (2.31) and (4.58) here. Ultimately, it comes from the form used in ref. [66], which is not entirely arbitrary but rather based on crossing symmetry considerations.

the subscripts s and using the momentum labeling of fig. 1)

$$\begin{aligned} \mathcal{K}_{\text{df},3,s}^{(u,u)\text{LO,OPE}}(\mathbf{p}_3, \mathbf{k}_1) \\ = -\mathcal{M}_{2,\text{off}}^{\text{LO}}(\mathbf{p}_3) \frac{1}{b^2 - M_\pi^2 + i\epsilon} \mathcal{M}_{2,\text{off}}^{\text{LO}}(\mathbf{k}_3) + \mathcal{M}_{2s}^{\text{LO}}(\mathbf{p}_3) G_{ss}^\infty(\mathbf{p}_3, \mathbf{k}_3) \mathcal{M}_{2s}^{\text{LO}}(\mathbf{k}_3). \end{aligned} \quad (2.28)$$

Here, $\mathcal{M}_{2,\text{off}}^{\text{LO}}$ is the two-particle amplitude with a single leg off shell. Since both p_3 and k_3 are on shell, the H functions in G_{ss}^∞ both equal unity, and we can combine the terms to find the following result:

$$\begin{aligned} \mathcal{K}_{\text{df},3,s}^{(u,u)\text{LO,OPE}}(\mathbf{p}_3, \mathbf{k}_3) = -\delta\mathcal{M}_{2,\text{off}}^{\text{LO}}(\mathbf{p}_3) \frac{1}{b^2 - M_\pi^2 + i\epsilon} \delta\mathcal{M}_{2,\text{off}}^{\text{LO}}(\mathbf{k}_3) \\ - \delta\mathcal{M}_{2,\text{off}}^{\text{LO}}(\mathbf{p}_3) \frac{1}{b^2 - M_\pi^2 + i\epsilon} \mathcal{M}_{2s}^{\text{LO}}(\mathbf{k}_3) - \mathcal{M}_{2s}^{\text{LO}}(\mathbf{p}_3) \frac{1}{b^2 - M_\pi^2 + i\epsilon} \delta\mathcal{M}_{2,\text{off}}^{\text{LO}}(\mathbf{k}_3), \end{aligned} \quad (2.29)$$

where we define the difference between the off- and on-shell amplitudes,

$$\delta\mathcal{M}_{2,\text{off}}^{\text{LO}}(\mathbf{p}) = \mathcal{M}_{2,\text{off}}^{\text{LO}}(\mathbf{p}) - \mathcal{M}_{2s}^{\text{LO}}(\mathbf{p}). \quad (2.30)$$

As we will see explicitly below, this quantity is proportional to $b^2 - M_\pi^2$ and thus cancels the poles appearing in eq. (2.29).

Using the results and notation of ref. [60], the $I = 2$ $\pi\pi$ off-shell amplitude is

$$\begin{aligned} \mathcal{M}_{2,\text{off}}^{\text{LO}}(\mathbf{p}_3) &= A^{(2)}(t_2, u_2, s_2) + A^{(2)}(u_2, s_2, t_2) \\ &= \frac{1}{F_\pi^2} (t_2 + u_2 - 2M_\pi^2) \\ &= \frac{1}{F_\pi^2} [-s_2 + 2M_\pi^2 + (b^2 - M_\pi^2)] = \frac{1}{F_\pi^2} [-2p_1 \cdot p_2 + (b^2 - M_\pi^2)], \end{aligned} \quad (2.31)$$

where we use the subscript 2 on the Mandelstam variables to indicate that these are two-particle quantities, while $(b^2 - M_\pi^2)$ is the off-shellness of one of the legs. For example, using the labeling of momenta given in fig. 1a and focusing on the left vertex, we have $s_2 = (p_1 + p_2)^2$, $t_2 = (k_3 - p_1)^2$, and $u_2 = (k_3 - p_2)^2$, with $s_2 + t_2 + u_2 = 3M_\pi^2 + b^2$. The on-shell amplitude $\mathcal{M}_{2s}^{\text{LO}}$ is then obtained by setting $b^2 = M_\pi^2$. Given these results, eq. (2.29) yields

$$F_\pi^4 \mathcal{K}_{\text{df},3,s}^{(u,u)\text{LO,OPE}}(\mathbf{p}_3, \mathbf{k}_3) = 2p_1 \cdot p_2 + 2k_1 \cdot k_2 - (b^2 - M_\pi^2). \quad (2.32)$$

To symmetrize, we use the following relations:

$$\mathcal{S}\{2p_1 \cdot p_2\} = \mathcal{S}\{2k_1 \cdot k_2\} = 3P^2 - 9M_\pi^2, \quad \mathcal{S}\{b^2 - M_\pi^2\} = 9M_\pi^2 - P^2, \quad (2.33)$$

and we arrive at the final OPE contribution to $\mathcal{M}_{\text{df},3}^{\text{LO}}$,

$$F_\pi^4 \mathcal{M}_{\text{df},3}^{\text{LO,OPE}} = 6(P^2 - 3M_\pi^2) - (9M_\pi^2 - P^2) = 7P^2 - 27M_\pi^2. \quad (2.34)$$

The contribution from the contact term (six-point vertex) of fig. 1b can be read off from eqs. (30), (33), and (34) of ref. [60] which, however, describes the interaction of six pion

fields $\pi^{f_1}(p_1)\pi^{f_2}(p_2)\pi^{f_3}(p_3)\pi^{f_4}(p_4)\pi^{f_5}(p_5)\pi^{f_6}(p_6)$, with flavor indices $f_i = 1, 2, 3$, in the “all-incoming” convention. In this language, our amplitude corresponds to the interaction of $\pi^+(k_1)\pi^+(k_2)\pi^+(k_3)\pi^-(-p_1)\pi^-(-p_2)\pi^-(-p_3)$. The connection between our conventions and those of ref. [60] is given by using $\pi^\pm = (\pi^1 \pm i\pi^2)/\sqrt{2}$ and replacing $\{p_1, \dots, p_6\}$ by $\{k_1, k_2, k_3, -p_1, -p_2, -p_3\}$. Thus,

$$\begin{aligned} \mathcal{M}_{\text{df},3}^{\text{LO},6\text{pt}} &= A^{(2)}(k_1, -p_1, k_2, -p_2, k_3, -p_3) + A^{(2)}(k_1, -p_2, k_2, -p_1, k_3, -p_3) \\ &\quad + A^{(2)}(k_1, -p_1, k_2, -p_3, k_3, -p_2) + A^{(2)}(k_1, -p_2, k_2, -p_3, k_3, -p_1) \\ &\quad + A^{(2)}(k_1, -p_3, k_2, -p_1, k_3, -p_2) + A^{(2)}(k_1, -p_3, k_2, -p_2, k_3, -p_1), \end{aligned} \quad (2.35)$$

with

$$F_\pi^4 A^{(2)}(k_1, -p_1, k_2, -p_2, k_3, -p_3) = -2k_1 \cdot p_1 - 2k_2 \cdot p_2 - 2k_3 \cdot p_3 + 3M_\pi^2. \quad (2.36)$$

Here, no subtraction or symmetrization is needed. Summing all six terms, we find

$$F_\pi^4 \mathcal{M}_{\text{df},3}^{\text{LO},6\text{pt}} = -4P^2 + 18M_\pi^2. \quad (2.37)$$

Combining the OPE and contact terms, we finally obtain

$$F_\pi^4 \mathcal{M}_{\text{df},3}^{\text{LO}} = 3P^2 - 9M_\pi^2 = M_\pi^2(18 + 27\Delta), \quad (2.38)$$

which agrees with the result of ref. [44]. However, we note that the values for the separate OPE and contact contributions are not the same as in that reference, due to our different off-shell conventions.

2.5 Procedure to calculate $\mathcal{K}_{\text{df},3}$ at NLO

Thanks to eq. (2.27), the determination of our main result, $\mathcal{K}_{\text{df},3}^{\text{NLO}}$, is equivalent to calculating $\text{Re } \mathcal{M}_{\text{df},3}^{\text{NLO}}$. We subdivide the calculation into multiple pieces according to the following schematic equation, which is also represented graphically in fig. 2:¹⁴

$$\text{Re } \mathcal{M}_{\text{df},3}^{\text{NLO}} = \text{Re } \mathcal{M}_3^{\text{NLO},\text{non-OPE}} - \text{Re } \mathcal{D}^{\text{BH}} + \text{Re } \left\{ \mathcal{M}_3^{\text{NLO},\text{OPE}} - \mathcal{D}^{\text{NLO},\text{OPE}} \right\}. \quad (2.39)$$

Employing this separation, the one-particle-reducible diagrams contribute to the term $\mathcal{M}_3^{\text{NLO},\text{OPE}}$, while the remainder of the full $I = 3$ amplitude is denoted $\mathcal{M}_3^{\text{NLO},\text{non-OPE}}$. Recall from sec. 2.3 that $\mathcal{M}_3^{\text{NLO},\text{non-OPE}}$ and $\mathcal{M}_3^{\text{NLO},\text{OPE}}$, while parametrization- and scale-independent, depend on our choice of off-shell convention.

We find that the real part of $\mathcal{M}_3^{\text{NLO},\text{non-OPE}}$ is smooth at threshold, so it can be expanded directly without first subtracting any divergences, unlike for the imaginary part. Since the non-OPE contribution is smooth, the corresponding part of the subtraction must also be smooth, and can be calculated individually. This contribution, given by the third term in eq. (2.25), is the subtraction corresponding to the “bull’s head” (BH) triangle

¹⁴Colorblind- and monochrome-safe colors, courtesy of P. Tol (<https://personal.sron.nl/~pault/>), are used in figs. 2, 7, and 11.

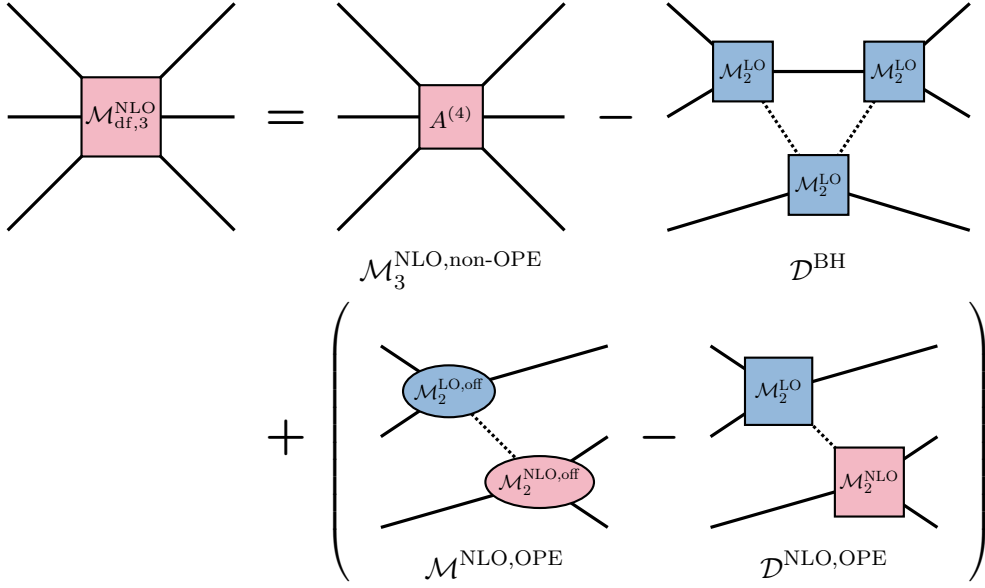


Figure 2: Sketch of eq. (2.39). Solid lines represent on-shell pions, while dotted lines are off-shell propagators. Square boxes indicate fully on-shell amplitudes, while oval boxes have one leg off shell (factors of G^∞ ensure only on-shell amplitudes are needed in \mathcal{D}). Finally, blue and pink filling indicate, respectively, LO and NLO quantities. We leave implicit that we take only the real parts of all quantities.

diagram shown below in fig. 9a. In eq. (2.39), \mathcal{D}^{BH} is the symmetrization of this term. It is the only piece that depends on the cutoff function $H(x)$.

Calculating each of these pieces leads to distinctive difficulties and methods of solution. Since the full calculation is rather long and technical, we first present the main results in sec. 3, and then describe the full calculation in sec. 4: In sec. 4.1, we provide a general form of the threshold expansion of $\mathcal{K}_{\text{df},3}$; sec. 4.2 then covers the full threshold expansion of $\text{Re } \mathcal{M}_3^{\text{NLO,non-OPE}}$, sec. 4.3 deals with $\text{Re } \mathcal{D}^{\text{BH}}$, and sec. 4.4 covers the $\text{Re}\{\mathcal{M}_3^{\text{NLO,OPE}} - \mathcal{D}^{\text{NLO,OPE}}\}$ term. All pieces can be computed analytically except $\text{Re } \mathcal{D}^{\text{BH}}$. Since the real part is applied term-by-term in eq. (2.39), each of secs. 4.2 to 4.4 gives a real, finite result. We explicitly verify the cancellation of imaginary parts in appendix C.

3 Summary of results

We now present, in sec. 3.1, the threshold expansion of $\mathcal{K}_{\text{df},3}$ at NLO in ChPT for the 3π system at maximal isospin, which constitutes the main result of this work. Some of the coefficients are then compared against lattice results from ref. [52] in sec. 3.2. Finally, we compare the threshold expansion to the full NLO result for a particular kinematic configuration in sec. 3.3.

3.1 Complete results

Including both LO and NLO contributions from ChPT, i.e., combining eqs. (2.38), (4.17), (4.47), and (4.86), the results are

$$\mathcal{K}_0 = \left(\frac{M_\pi}{F_\pi}\right)^4 18 + \left(\frac{M_\pi}{F_\pi}\right)^6 \left[-3\kappa(35 + 12 \log 3) - \mathcal{D}_0 + 111L + \ell_{(0)}^r \right], \quad (3.1a)$$

$$\mathcal{K}_1 = \left(\frac{M_\pi}{F_\pi}\right)^4 27 + \left(\frac{M_\pi}{F_\pi}\right)^6 \left[-\frac{\kappa}{20}(1999 + 1920 \log 3) - \mathcal{D}_1 + 384L + \ell_{(1)}^r \right], \quad (3.1b)$$

$$\mathcal{K}_2 = \left(\frac{M_\pi}{F_\pi}\right)^6 \left[\frac{207\kappa}{1400}(2923 - 420 \log 3) - \mathcal{D}_2 + 360L + \ell_{(2)}^r \right], \quad (3.1c)$$

$$\mathcal{K}_A = \left(\frac{M_\pi}{F_\pi}\right)^6 \left[\frac{9\kappa}{560}(21809 - 1050 \log 3) - \mathcal{D}_A - 9L + \ell_{(A)}^r \right], \quad (3.1d)$$

$$\mathcal{K}_B = \left(\frac{M_\pi}{F_\pi}\right)^6 \left[\frac{27\kappa}{1400}(6698 - 245 \log 3) - \mathcal{D}_B + 54L + \ell_{(B)}^r \right]. \quad (3.1e)$$

Here, $\kappa \equiv 1/(16\pi^2)$, $L \equiv \kappa \log(M_\pi^2/\mu^2)$, \mathcal{D}_X are cutoff-dependent numerical constants related to the bull's head subtraction (see sec. 4.3),¹⁵

$$\begin{aligned} \mathcal{D}_0 &\approx -0.0563476589, & \mathcal{D}_1 &\approx 0.129589681, & \mathcal{D}_2 &\approx 0.432202370, \\ \mathcal{D}_A &\approx 9.07273890 \cdot 10^{-4}, & \mathcal{D}_B &\approx 1.62394747 \cdot 10^{-4}, \end{aligned} \quad (3.2)$$

and we have defined the following linear combinations of LECs:

$$\begin{aligned} \ell_{(0)}^r &= -288\ell_1^r - 432\ell_2^r - 36\ell_3^r + 72\ell_4^r, & \ell_{(1)}^r &= -612\ell_1^r - 1170\ell_2^r + 108\ell_4^r, \\ \ell_{(2)}^r &= -432\ell_1^r - 864\ell_2^r, & \ell_{(A)}^r &= 27\ell_1^r + \frac{27}{2}\ell_2^r, & \ell_{(B)}^r &= -162\ell_1^r - 81\ell_2^r. \end{aligned} \quad (3.3)$$

A numerical comparison of the different contributions to each coefficient at the physical point is given in table 1. Above, $\ell_i^r \equiv \ell_i^r(\mu)$ are scale-dependent LECs, with μ being the renormalization scale. Different scales are related via

$$\ell_i^r(\mu_2) = \ell_i^r(\mu_1) + \frac{\gamma_i \kappa}{2} \log \frac{\mu_1^2}{\mu_2^2}, \quad (3.4)$$

with

$$\gamma_1 = 1/3, \quad \gamma_2 = 2/3, \quad \gamma_3 = -1/2, \quad \gamma_4 = 2. \quad (3.5)$$

In combination with the L terms, this ensures the scale independence of the results in eq. (3.1) and thus of $\mathcal{K}_{\text{df},3}$. Often, scale-independent variants of the LECs, $\bar{\ell}_i$, are used. They are related to ℓ_i^r via

$$\ell_i^r(\mu) = \kappa \frac{\gamma_i}{2} \left(\bar{\ell}_i + \log \frac{M_{\pi,\text{phys}}^2}{\mu^2} \right), \quad (3.6)$$

where $M_{\pi,\text{phys}} \approx 139.57$ MeV is the real-world pion mass. The $\bar{\ell}_i$ are fairly well known, either from phenomenology or from lattice QCD.

¹⁵All digits shown are exact, and we have computed the values numerically to much higher precision, with the first twenty digits being verified by at least two independent methods. Higher-precision values and codes for calculating them are available upon request.

	$(\frac{F_\pi}{M_\pi})^6 \mathcal{K}_0$	$(\frac{F_\pi}{M_\pi})^6 \mathcal{K}_1$	$(\frac{F_\pi}{M_\pi})^6 \mathcal{K}_2$	$(\frac{F_\pi}{M_\pi})^6 \mathcal{K}_A$	$(\frac{F_\pi}{M_\pi})^6 \mathcal{K}_B$
non-OPE	-2.04(28)	-3.75(61)	1.43(37)	3.00(14)	0.25(28)
OPE	0.50(53)	-1.8(1.0)	-5.11(58)	-2.76(15)	-0.22(37)
BH, excl. \mathcal{D}_X	-1.16234	-3.35289	-1.67334	1.97425	0.08225
BH, only \mathcal{D}_X	0.05635	-0.12959	-0.43220	-0.00091	-0.00016
Total NLO	-2.65(26)	-9.04(46)	-5.79(24)	2.212(16)	0.118(93)
	\mathcal{K}_0	\mathcal{K}_1	\mathcal{K}_2	\mathcal{K}_A	\mathcal{K}_B
LO	94.5186	141.778	0	0	0
NLO	-31.9(3.1)	-108.8(5.5)	-69.6(2.9)	26.62(19)	1.4(1.1)
Total	62.6(3.1)	34.0(5.5)	-69.6(2.9)	26.62(19)	1.4(1.1)

Table 1: Numerical comparison of the different contributions to $\mathcal{K}_{\text{df},3}$ presented in eq. (3.1), evaluated at the physical point, $M_{\pi,\text{phys}} = 139.57$ MeV, $F_{\pi,\text{phys}} = 92.2$ MeV. Errors inherited from the LECs, as listed in eq. (3.7), are given where applicable; the BH (bull’s head subtraction) numbers are exact up to rounding. The top part of the table covers the NLO contributions, with factors of M_π/F_π removed. In the bottom part, these factors are included so that LO and NLO can be compared; the uncertainty of M_π/F_π is not taken into account. The LO piece comes from eq. (2.38). Of the NLO pieces, non-OPE comes from eq. (4.17), OPE from eq. (4.86), and BH from eq. (4.47), with the numerical residues \mathcal{D}_X , also given in eq. (3.2), separated out.

3.2 Comparison to lattice results

We are now in position to compare our results to lattice determinations of $\mathcal{K}_{\text{df},3}$. Several works [44, 47, 48, 52] have applied the RFT formalism to the study of three pions at maximal isospin, and in all cases similar qualitative disagreement with LO ChPT predictions was found. We will see that this can be explained by NLO ChPT contributions. In particular, we compare to ref. [52], which studied the scattering process for pion masses of 200, 280 and 340 MeV. Note this is the only work in which $\mathcal{K}_{\text{df},3}$ has been (partially) determined to quadratic order. The disagreement with LO ChPT in \mathcal{K}_0 and \mathcal{K}_1 is seen also in ref. [47] and is resolved similarly at NLO, but we do not include this in the plots due to its large uncertainties.

We take the following reference values for the scale-independent LECs,

$$\bar{\ell}_1 = -0.4(6), \quad \bar{\ell}_2 = 4.3(1), \quad \bar{\ell}_3 = 3.07(64), \quad \bar{\ell}_4 = 4.02(45), \quad (3.7)$$

where $\bar{\ell}_1$ and $\bar{\ell}_2$ are determined by combining experiment, ChPT and dispersion relations [67], while $\bar{\ell}_3$ and $\bar{\ell}_4$ come from the averaged $N_f = 2 + 1$ lattice QCD results [56], based on refs. [68–72]. We also take into account correlations between $\bar{\ell}_1$ and $\bar{\ell}_2$ using the covariance matrix from ref. [67]:

$$\text{Cov}(\bar{\ell}_1, \bar{\ell}_2) = \begin{pmatrix} 0.35 & -0.033 \\ -0.033 & 0.012 \end{pmatrix}. \quad (3.8)$$

Although the results in eq. (3.1) are independent of the choice of μ , it is customary in lattice computations to choose μ such that the results depend only on M_π/F_π . In our case this can be achieved by taking $\mu = 4\pi F_\pi$ in the L terms of eq. (3.1), and approximating it as $\mu \approx 4\pi F_{\pi,\text{phys}}$ in eq. (3.6). This approximation only impacts the results for $\mathcal{K}_{\text{df},3}$ at NNLO since F_π is independent of M_π at LO. With this choice, for example, eq. (3.1a) can be rewritten as

$$\mathcal{K}_0 = \left(\frac{M_\pi}{F_\pi}\right)^4 18 + \left(\frac{M_\pi}{F_\pi}\right)^6 \left[-3\kappa(35 + 12 \log 3) - \mathcal{D}_0 + 111\kappa \log \frac{\xi}{\xi_{\text{phys}}} + \kappa \bar{\ell}_{(0)} \right], \quad (3.9)$$

with $\bar{\ell}_{(0)} = -48\bar{\ell}_1 - 144\bar{\ell}_2 + 9\bar{\ell}_3 + 72\bar{\ell}_4$, $\xi \equiv M_\pi^2/(4\pi F_\pi)^2$ and $\xi_{\text{phys}} \equiv M_{\pi,\text{phys}}^2/(4\pi F_{\pi,\text{phys}})^2$.

In fig. 3, we compare the ChPT predictions for \mathcal{K}_0 and \mathcal{K}_1 including NLO contributions to lattice results. We also show the LO predictions for comparison. We observe how the agreement with the lattice results is vastly improved by the inclusion of NLO terms. For \mathcal{K}_0 the addition of the NLO term leads to smaller values that are closer to the lattice results, while for \mathcal{K}_1 the correction produces a change of sign (for all except very small pion masses) that brings the sign and rough magnitude into agreement with that of the lattice results. A conservative interpretation of these results could be that, since the NLO corrections are so large, particularly for \mathcal{K}_1 , the convergence of the chiral expansion is poor in the regime where lattice results have been obtained and the ChPT results cannot be trusted. A more optimistic interpretation is that the NLO results are, for some reason, larger than the LO contributions, but are nevertheless reliable. This could be because new classes of diagrams, such as the bull's-head diagram, appear at NLO. In either view, however, the discrepancy between lattice results and LO ChPT is resolved.

Due to the similarity between the ChPT prediction and the lattice results, as an exercise we perform a fit to the lattice data for \mathcal{K}_0 and \mathcal{K}_1 to estimate how well the values of the LECs in eq. (3.3) can be constrained. We obtain the following results:

$$\begin{aligned} \ell_{(0)}^r &= 1.55(11), & \chi^2/\text{dof} &= 2.93/2, \\ \ell_{(1)}^r &= 4.09(25), & \chi^2/\text{dof} &= 0.36/2, \end{aligned} \quad (3.10)$$

which are not that dissimilar to those computed using eq. (3.7),

$$\ell_{(0)}^r = 1.19(25), \quad \ell_{(1)}^r = 2.71(46). \quad (3.11)$$

These fits are also shown in fig. 3.

We show the predictions for \mathcal{K}_2 , \mathcal{K}_A and \mathcal{K}_B in fig. 4. Here there are only NLO contributions, since these quantities vanish at LO in ChPT. In the case of \mathcal{K}_B , we also compare the expectations to results from ref. [52]. This time, however, we observe a much larger discrepancy, with the ChPT prediction taking the opposite sign to the lattice results, although the magnitude is roughly correct. This discrepancy is superficially similar to that between \mathcal{K}_1 and its leading nonzero prediction in ChPT, so it is possible that it is resolved by NNLO terms.

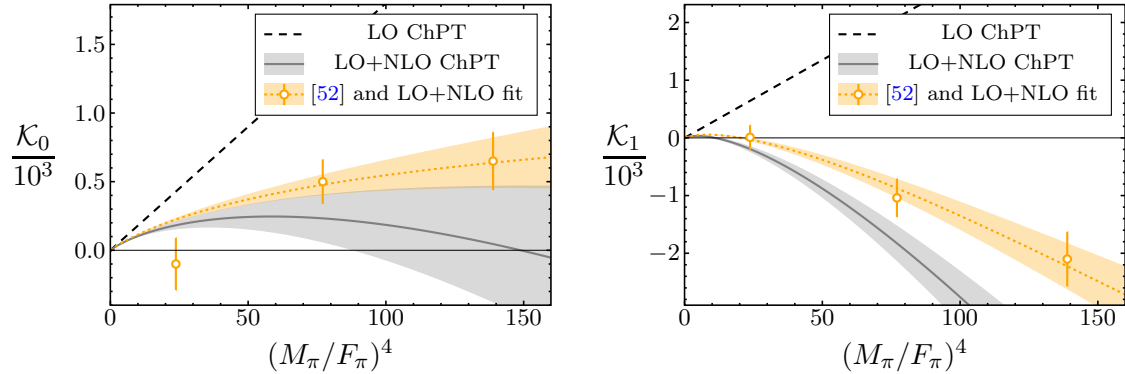


Figure 3: LO (dashed black line) and NLO (grey line and band) ChPT predictions for \mathcal{K}_0 (left) and \mathcal{K}_1 (right) as functions of $(M_\pi/F_\pi)^4$, using LECs from refs. [56, 67] [see eq. (3.7)]. These are compared to lattice results from ref. [52] (orange points); for reference, the physical point is at $(M_{\pi,\text{phys}}/F_{\pi,\text{phys}})^4 \approx 5.25$. We also present the best fit to the lattice data (dotted orange line and orange band).

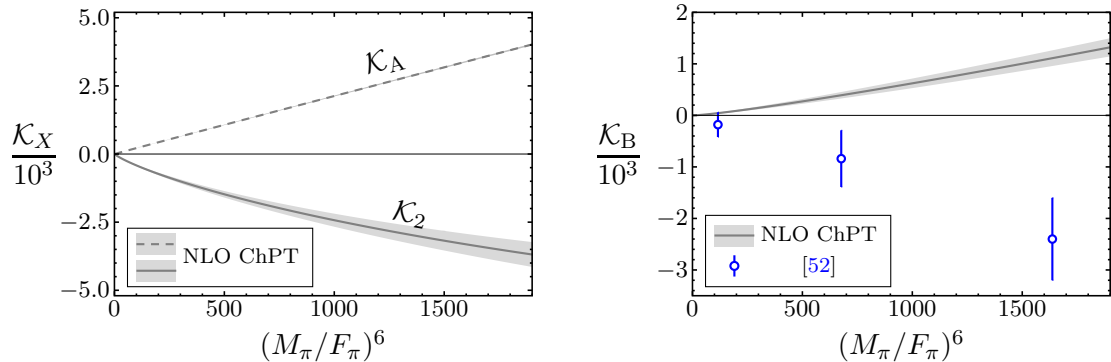


Figure 4: NLO ChPT predictions for \mathcal{K}_2 (left panel, solid line), \mathcal{K}_A (left panel, dashed line) and \mathcal{K}_B (right panel, solid line) as a function of $(M_\pi/F_\pi)^6$, using LECs from refs. [56, 67] [see eq. (3.7)]. In the case of \mathcal{K}_B , we compare to lattice results from ref. [52] (blue points); for reference, the physical point is at $(M_{\pi,\text{phys}}/F_{\pi,\text{phys}})^6 \approx 12.0$. Note that all three coefficients vanish at LO in ChPT.

3.3 Range of validity of the threshold expansion

The determination of $\mathcal{K}_{\text{df},3}$ in ref. [52] assumes that the threshold expansion truncated at quadratic order provides an accurate representation of the full amplitude up to the inelastic threshold at $E^* = 5M_\pi$. Our results allow a test of this assumption, as we can compare the threshold expansion against the full result evaluated numerically for a particular kinematical configuration. Throughout this section, we make use of momentum family 1 (see table 2 in appendix D). We have checked that the results for other kinematic families are comparable.

In fig. 5 we perform this test for the total $\mathcal{K}_{\text{df},3}^{\text{NLO}}$, both for the physical pion mass and for $M_\pi = 340$ MeV, the latter being the heaviest pion mass used in ref. [52]. In both

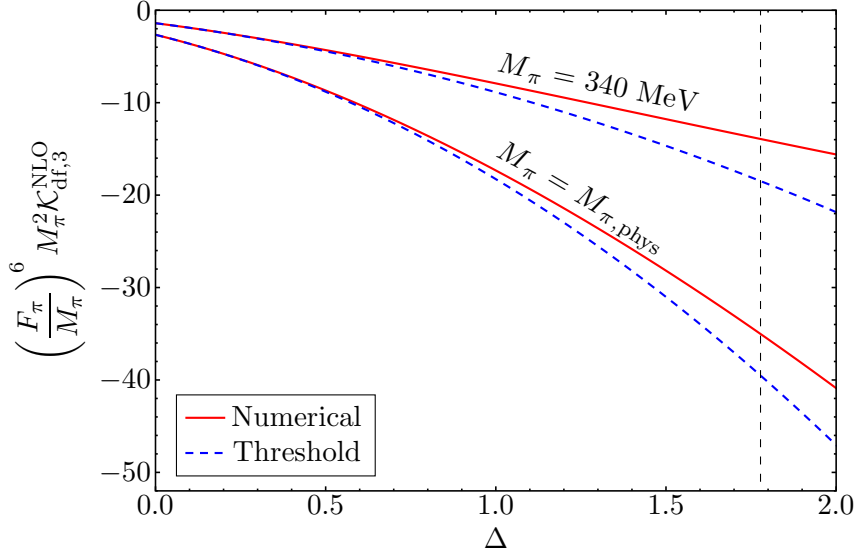


Figure 5: Comparison between numerical results and the threshold expansion for $\mathcal{K}_{df,3}$, evaluated for momentum family 1 (see table 2). The comparison is presented for $M_\pi = M_{\pi,\text{phys}}$ and $M_\pi = 340$ MeV, the latter corresponding to the heaviest pion mass used in ref. [52]. The dashed vertical line indicates the inelastic threshold, which occurs at $E^* = 5M_\pi$.

cases, we observe that the threshold expansion works reasonably well up to the inelastic threshold, where the discrepancy is $\sim 10\%$ for physical pions, and $\sim 20\%$ in the heavier case. As expected, the convergence is better for smaller pion masses.

We can perform the same comparison separately for each of the three components appearing in eq. (2.39) and fig. 2. This is presented in fig. 6 for $M_\pi = 340$ MeV. We recall from sec. 2.3 that each of the three components is independent of the renormalization scale in ChPT, although they do depend on the off-shell convention. Of the three, only the BH subtraction depends on the cutoff function H . We observe that the difference is $\lesssim 5\%$ at the inelastic threshold in the case of the non-OPE and the BH subtraction contribution, while for the OPE part it is $\sim 30\%$.

For the OPE contribution we can also study the convergence as higher partial waves of the interacting pair are included. The threshold expansion contains only s - and d -waves, while the full result contains all even pair partial waves.¹⁶ In fig. 7 we show the contributions of the first three nonzero partial waves to the numerical result for the OPE contribution for $M_\pi = 340$ MeV. We find a rapid convergence with ℓ . In particular, the contribution is negligible below the inelastic threshold for $\ell \geq 4$. A similar result holds for smaller pion masses.

¹⁶The decomposition into partial waves is obtained by evaluating $\text{Re} \mathcal{M}_{df,3}^{(u,u)\text{NLO,OPE}}$ using eq. (4.49), and decomposing $\mathcal{M}_{2,\ell,\text{off}}^{\text{NLO}}$ into partial waves by numerical integration.

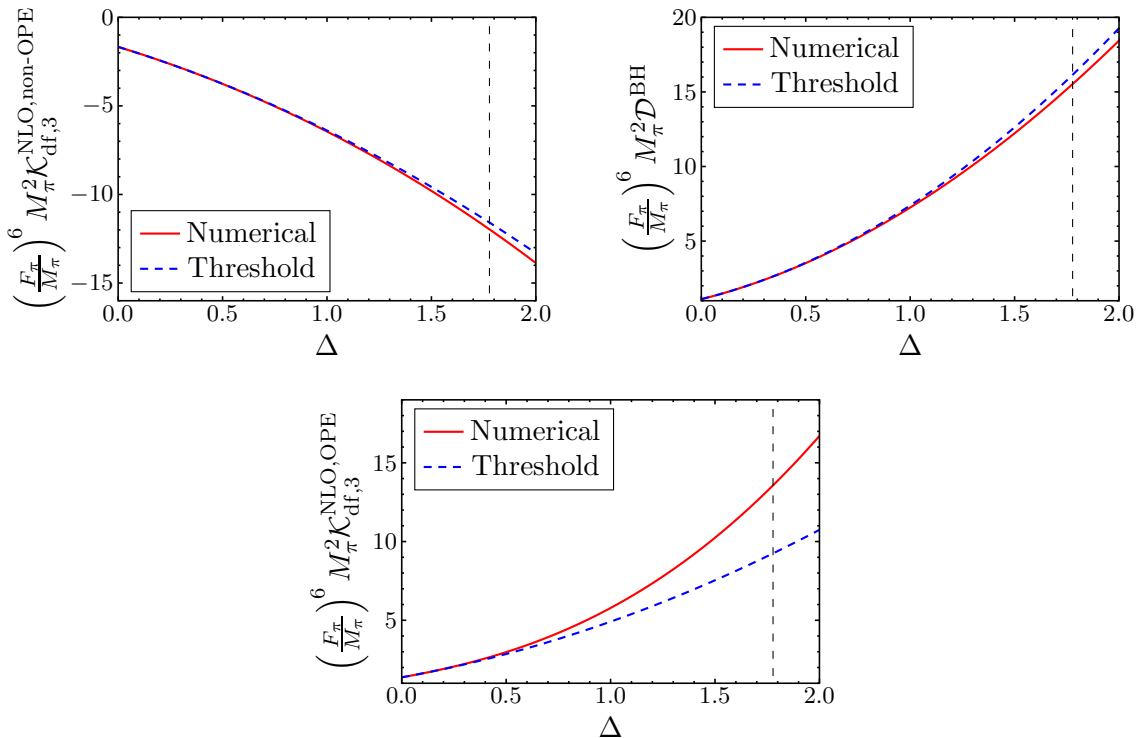


Figure 6: Comparison between numerical results and the threshold expansion for the different terms in the right-hand side of eq. (2.39), evaluated for momentum family 1 (see table 2). The panels correspond to the terms in the right-hand side of eq. (2.39): the non-OPE (top left), the BH subtraction (top right) and the OPE (bottom) contributions to $\mathcal{K}_{\text{df},3}$. The black vertical line indicates the inelastic threshold, which occurs at $E^* = 5M_\pi$. The comparison is made for $M_\pi = 340$ MeV, corresponding to the heaviest pion mass used in ref. [52].

4 Details of the calculation of $\mathcal{K}_{\text{df},3}^{\text{NLO}}$

In this section, we go in detail through the calculation outlined in sec. 2.5 to obtain the results of sec. 3. Given the length of the expressions, the algebra is done with either Wolfram Mathematica [73] or FORM [74], and is cross-checked independently by several of the authors. Likewise, all numerical calculations are performed using Mathematica or C++, using *CHIRON* [75], *LoopTools* [76] and *GSL* [77], with independent cross-checks and preferably using several different methods.

4.1 General form of the threshold expansion

Throughout the calculation of $\mathcal{K}_{\text{df},3}^{\text{NLO}}$, it will often be useful to work with $\mathcal{K}_{\text{df},3}^{(u,u)}$, the unsymmetrized version of $\mathcal{K}_{\text{df},3}$. These quantities are related by $\mathcal{K}_{\text{df},3} = \mathcal{S}\{\mathcal{K}_{\text{df},3}^{(u,u)}\}$, where \mathcal{S} indicates symmetrization of both initial and final states, as in eq. (2.10). It is thus necessary to identify the form of the terms that can contribute to $\mathcal{K}_{\text{df},3}^{(u,u)}$ up to quadratic

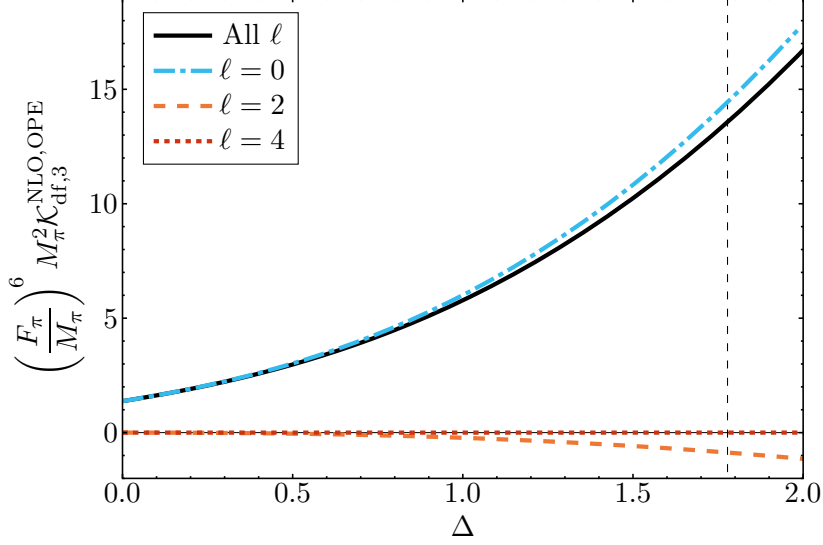


Figure 7: Comparison of contributions to $\mathcal{K}_{\text{df},3}^{\text{NLO,OPE}}$ from different interacting pair partial waves, numerically evaluated for momentum family 1 (see table 2). Results are shown for $M_\pi = 340$ MeV, corresponding to the heaviest pion mass in ref. [52]. The black solid line is the full result including all partial waves, and the dashed vertical line indicates the inelastic threshold. Contributions for $\ell \gtrsim 4$ are negligible.

order.¹⁷

The symmetries that constrain $\mathcal{K}_{\text{df},3}^{(u,u)}$ are the same as those for a 2+1 theory (i.e., with two identical particles and one that is different). Thus, we can use the threshold expansion for the latter theories derived in ref. [34]:¹⁸

$$\begin{aligned} \mathcal{K}_{\text{df},3}^{(u,u)} = & c_0 + c_1 \Delta + c_2 \Delta_3^S + c_3 \tilde{t}_{33} \\ & + c_4 \Delta^2 + c_5 \Delta \Delta_3^S + c_6 \Delta \tilde{t}_{33} + c_7 \Delta_3 \Delta_3' + c_8 (\Delta_3^S)^2 + c_9 \Delta_3^S \tilde{t}_{33} + c_{10} \tilde{t}_{33}^2 \\ & + c_{11} \mathcal{Q}_{--} + c_{12} \mathcal{Q}_{+-} + c_{13} \mathcal{Q}_{3-} + c_{14} \mathcal{Q}_{tu} + \mathcal{O}(\Delta^3). \end{aligned} \quad (4.1)$$

Some quantities used above have already been defined in eq. (2.4). Moreover, $\Delta_3^S \equiv \Delta_3 + \Delta_3'$ and

$$\begin{aligned} \mathcal{Q}_{--} & \equiv 4 \left[\frac{p_- \cdot k_-}{9M_\pi^2} \right]^2, & \mathcal{Q}_{+-} & \equiv 2 \left(\frac{p_+ \cdot k_-}{9M_\pi^2} \right)^2 + 2 \left(\frac{p_- \cdot k_+}{9M_\pi^2} \right)^2, \\ \mathcal{Q}_{3-} & \equiv 4 \frac{p_- \cdot k_+}{9M_\pi^2} \frac{p_- \cdot k_3}{9M_\pi^2} + 4 \frac{p_+ \cdot k_-}{9M_\pi^2} \frac{p_3 \cdot k_-}{9M_\pi^2}, & \mathcal{Q}_{tu} & \equiv \tilde{t}_{13} \tilde{t}_{23} + \tilde{t}_{31} \tilde{t}_{32}, \end{aligned} \quad (4.2)$$

with $p_\pm = p_1 \pm p_2$ and $k_\pm = k_1 \pm k_2$. Here, the initial and final spectators are taken to have momenta k_3 and p_3 , respectively. We note that, in eq. (4.1), only terms on the final line contain values of ℓ other than zero.

¹⁷Note that in this subsection, all statements concerning $\mathcal{K}_{\text{df},3}/\mathcal{K}_{\text{df},3}^{(u,u)}$ apply equally well to $\mathcal{M}_{\text{df},3}/\mathcal{M}_{\text{df},3}^{(u,u)}$ or $\mathcal{D}/\mathcal{D}^{(u,u)}$, for those cases in which divergences are absent such that the threshold expansion is well-defined.

¹⁸Two operators are missed by the analysis of ref. [34], \mathcal{Q}_{3-} and \mathcal{Q}_{tu} . Note that we have used a somewhat different basis than in ref. [34].

Symmetrizing $\mathcal{K}_{\text{df},3}^{(u,u)}$ then leads to the following contributions to $\mathcal{K}_{\text{df},3}$:

$$\mathcal{K}_0 = 9c_0, \quad (4.3a)$$

$$\mathcal{K}_1 = 9c_1 + 6c_2 - 2c_3, \quad (4.3b)$$

$$\mathcal{K}_2 = 9c_4 + 6c_5 - 2c_6 + c_7 + 5c_8 - c_9 + c_{10} + 4c_{11} + 2c_{12} - 2c_{13} + \frac{1}{2}c_{14}, \quad (4.3c)$$

$$\mathcal{K}_A = 3c_8 + c_9 - 3c_{11} + c_{12} + 4c_{13} + \frac{1}{2}c_{14}, \quad (4.3d)$$

$$\mathcal{K}_B = c_{10} + 9c_{11} + 3c_{12} - 6c_{13} - c_{14}. \quad (4.3e)$$

As expected, several terms from $\mathcal{K}_{\text{df},3}^{(u,u)}$ are often combined in each term in $\mathcal{K}_{\text{df},3}$ because of the larger symmetry of the latter. Note that some of the terms that are purely s -wave in eq. (4.1) can lead to nontrivial angular dependence after symmetrization, and thus contribute to \mathcal{K}_A and \mathcal{K}_B , because there can be nonzero angular momentum between the spectator and the pair.

We also make use of another basis of operators, in which all quantities are expressed in terms of \tilde{t}_{ij} [defined in eq. (2.4)], for expanding the symmetrized K -matrix directly. We can write

$$\mathcal{K}_{\text{df},3} = c'_0 + c'_1 \mathcal{Q}'_0 + c'_2 \mathcal{Q}'_1 + c'_3 \mathcal{Q}'_2 + c'_4 \mathcal{Q}'_3 + \mathcal{O}(\Delta^3), \quad (4.4)$$

where

$$\begin{aligned} \mathcal{Q}'_0 &\equiv S[\tilde{t}_{11}] &&= -2\Delta, \\ \mathcal{Q}'_1 &\equiv S[\tilde{t}_{11}\tilde{t}_{11}] &&= \Delta^2 + \Delta_B, \\ \mathcal{Q}'_2 &\equiv S[\tilde{t}_{11}\tilde{t}_{12} + \tilde{t}_{11}\tilde{t}_{21}] &&= \frac{1}{2}(2\Delta^2 + \Delta_A - 2\Delta_B), \\ \mathcal{Q}'_3 &\equiv S[\tilde{t}_{11}\tilde{t}_{22} + \tilde{t}_{21}\tilde{t}_{12}] &&= \frac{1}{2}(2\Delta^2 - \Delta_A + \Delta_B). \end{aligned} \quad (4.5)$$

Here, we have indicated the relation to the basis used in eq. (2.2). Employing these relations, we find that the coefficients in eq. (2.2) are given by

$$\begin{aligned} \mathcal{K}_0 &= c'_0, & \mathcal{K}_1 &= -2c'_1, & \mathcal{K}_2 &= c'_2 + c'_3 + 2c'_4, \\ \mathcal{K}_A &= c'_3 - c'_4, & \mathcal{K}_B &= c'_2 - 2c'_3 + c'_4. \end{aligned} \quad (4.6)$$

The requirement for the two methods of expansion to agree serves as a cross-check. Specifically, eqs. (4.3) and (4.6) [or, equivalently, eqs. (2.2) and (4.4)] must match.

4.2 Threshold expansion of the non-OPE part of \mathcal{M}_3

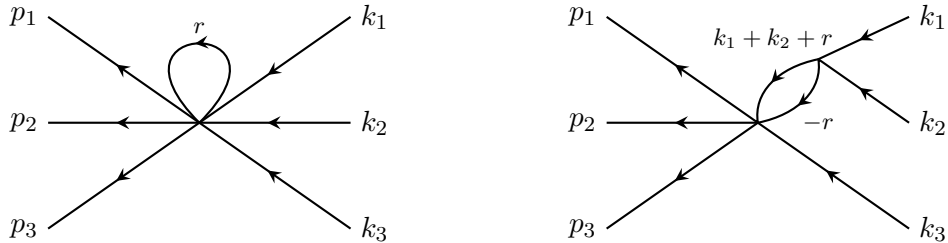


Figure 8: Examples of non-OPE NLO diagrams for which no subtraction is needed.

In this section, we focus on threshold-expanding the non-OPE piece of the amplitude in eq. (2.39). This is the piece related to one-particle-irreducible diagrams, like those in figs. 8 and 9, for which the contribution to $\mathcal{K}_{\text{df},3}$ can be computed independently of any subtraction. For the $I = 3$ system, this contribution is given by

$$\begin{aligned} \mathcal{M}_{\text{df},3}^{\text{NLO,non-OPE}} &= A^{(4)}(k_1, -p_1, k_2, -p_2, k_3, -p_3) + A^{(4)}(k_1, -p_2, k_2, -p_1, k_3, -p_3) \\ &+ A^{(4)}(k_1, -p_1, k_2, -p_3, k_3, -p_2) + A^{(4)}(k_1, -p_2, k_2, -p_3, k_3, -p_1) \\ &+ A^{(4)}(k_1, -p_3, k_2, -p_1, k_3, -p_2) + A^{(4)}(k_1, -p_3, k_2, -p_2, k_3, -p_1), \end{aligned} \quad (4.7)$$

where $A^{(4)}$ is defined in eq. (35) of ref. [60], and we have converted to our conventions as described above eq. (2.35).

This part of the amplitude can be divided as

$$A^{(4)} = A_C + A_J + A_\pi + A_L + A_l, \quad (4.8)$$

where the division is similar to that in eq. (35) of ref. [60], although here we group some terms together. In particular, A_C is the part that contains the \bar{C} functions, i.e., \bar{C} , \bar{C}_{11} and \bar{C}_{21} (\bar{C}_3 does not contribute to $I = 3$), A_J contains all terms with \bar{J} functions, and A_π , A_L , and A_l are terms containing only factors of κ , L or LECs, respectively (see sec. 3.1 and appendix B for definitions). Some of these amplitudes have imaginary parts, but we only need to calculate the real parts since the imaginary parts do not contribute to $\mathcal{K}_{\text{df},3}$ [see eq. (2.27)].

The computation of c'_i [following eq. (4.4)] is straightforward for A_l , A_L , and A_π . The results for the latter two are given in eq. (4.19). The remaining parts, which contain loop integrals, require more care. As is shown in the following subsections, they can be expanded in terms of squared momenta that are either small or close to threshold. These can then be straightforwardly related to \tilde{t}_{ij} and $\Delta_i^{(j)}$ through eq. (2.4). Alternatively, one can use (at least) three different particular kinematic configurations to numerically determine the corresponding coefficients in the Δ variables. This cross-check is described in appendix D.

4.2.1 Threshold expansion of A_J

Terms containing $\bar{J}(q^2)$ functions must be expanded about either $q^2 = 0$ or $q^2 = 4M_\pi^2$ (the two-particle threshold). In the notation of ref. [60], $A_J = A_J^{(1)} + A_J^{(2)}$, where all \bar{J} functions in $A_J^{(1)}$ are expanded about $q^2 = 4M_\pi^2$, while in $A_J^{(2)}$ both cases appear. It is, however, easy to separate $A_J^{(2)}$ in two parts, each of which contains one single case. Using again the notation of ref. [60] [in particular eq. (B9) thereof],

$$\begin{aligned} A_J^{(2)} &= (R_{132456} + R_{241356} + R_{152634} + R_{152634} + R_{261543} + R_{536412} + R_{645321} \\ &+ R_{142356} + R_{231456} + R_{251634} + R_{162543} + R_{635421} + R_{546312}) A_{J,0}^{(2)}, \end{aligned} \quad (4.9)$$

where R_{ijklmn} indicates an operator, acting on $A_{J,0}^{(2)}$, that permutes $p_1 \rightarrow p_i$, $p_2 \rightarrow p_j$, etc., with $\{p_1, \dots, p_6\} = \{k_1, k_2, k_3, -p_1, -p_2, -p_3\}$ as described above eq. (2.35). It is easy to check that, after projecting to $I = 3$, the first line above leads to terms that contain \bar{J}

functions that have to be expanded about the two-particle threshold, while the second has those that need to be expanded around $q^2 = 0$.

Using the definition (B.3), the expansions in the two cases are

$$\frac{1}{\kappa} \text{Re } \bar{J}(4M_\pi^2 + \bar{s}) = 2 - \frac{1}{2} \frac{\bar{s}}{M_\pi^2} + \frac{1}{12} \frac{\bar{s}^2}{M_\pi^4} - \frac{1}{60} \frac{\bar{s}^3}{M_\pi^6} + \mathcal{O}(\bar{s}^4), \quad (4.10)$$

$$\frac{1}{\kappa} \bar{J}(t) = \frac{1}{6} \frac{t}{M_\pi^2} + \frac{1}{60} \frac{t^2}{M_\pi^4} + \frac{1}{420} \frac{t^3}{M_\pi^6} + \mathcal{O}(t^4). \quad (4.11)$$

Note that only $\text{Re } \bar{J}$, not $\text{Im } \bar{J}$, is smooth at threshold. After conversion to threshold-expansion parameters, the results are given in eq. (4.20).

4.2.2 Threshold expansion of A_C

All \bar{C} , which are functions of three pairs of momenta as defined in appendix B, can be expanded either for all three pairs being small or one small and the other two near threshold. Given that the expansions are analytic, for $\text{Re } \mathcal{M}_{\text{df},3}^{\text{NLO,non-OPE}}$ the Feynman integrals can be performed naïvely with a principal-value prescription. For C , defined in eq. (B.4), the starting point is the Feynman-parameter representation

$$C \equiv C(p_1, p_2, \dots, p_6) = -\kappa \int_0^1 dx dy dz \frac{\delta(1-x-y-z)}{M_\pi^2 - xyq_1^2 - yzq_2^2 - zxq_3^2}, \quad (4.12)$$

with $q_1 = p_1 + p_2$, $q_2 = p_3 + p_4$ and $q_3 = p_5 + p_6$. For the three q_i^2 small, we straightforwardly expand the denominator and then perform the Feynman integrals, arriving at

$$\frac{C}{\kappa} = -\frac{1}{2M_\pi^2} - \frac{1}{24M_\pi^4} (q_1^2 + q_2^2 + q_3^2) - \frac{1}{180M_\pi^6} (q_1^4 + q_2^4 + q_3^4 + q_1^2 q_2^2 + q_2^2 q_3^2 + q_3^2 q_1^2) + \dots \quad (4.13)$$

For the expansion about threshold, take for example q_1^2 , \bar{s}_2 , and \bar{s}_3 small, where $\bar{s}_2 = q_2^2 - 4M_\pi^2$ and $\bar{s}_3 = q_3^2 - 4M_\pi^2$. We can write the Feynman parametrization of C as

$$\begin{aligned} C &= -\kappa \int_0^1 dx dy dz \frac{\delta(1-x-y-z)}{M_\pi^2 - 4M_\pi^2(yz + zx) - xyq_1^2 - yz\bar{s}_2 - zx\bar{s}_3} \\ &= -\kappa \int_0^1 dx dy dz \frac{\delta(1-x-y-z)}{M_\pi^2(1-2z)^2 - xyq_1^2 - yz\bar{s}_2 - zx\bar{s}_3}. \end{aligned} \quad (4.14)$$

Since we know the integral is analytic above threshold, we expand naïvely in q_1^2 , \bar{s}_2 , and \bar{s}_3 and perform the Feynman integrals, first doing the x, y integrals and then the z integral using the principal-value prescription, discarding the imaginary part. In particular, after expanding and performing the x, y integrals, one obtains integrals of the type

$$\mathcal{P} \int_0^1 dz \frac{1}{(1-2z)^n} = \frac{1}{2} \mathcal{P} \int_{-1}^1 dv \frac{1}{v^n} = \frac{1}{4} \int_\pi^0 e^{-in\theta} de^{i\theta} + \frac{1}{4} \int_\pi^0 e^{in\theta} de^{-i\theta}, \quad (4.15)$$

where we changed variables to $v \equiv 1 - 2z$ and implemented the principal-value (\mathcal{P}) prescription as the average of the contours above and below the singularity at $v = 0$ in the

complex plane, letting $v = e^{\pm i\theta}$.¹⁹ The integrals vanish for odd values of n and are equal to $-1/(n-1)$ for even values. This way, the result for eq. (4.14) becomes

$$\begin{aligned} \frac{C}{\kappa} &= \frac{1}{2M_\pi^2} + \frac{1}{M_\pi^4} \left(\frac{5}{72} q_1^2 - \frac{1}{24} \bar{s}_2 - \frac{1}{24} \bar{s}_3 \right) \\ &\quad + \frac{1}{M_\pi^6} \left[\frac{2}{225} q_1^4 - \frac{1}{90} q_1^2 (\bar{s}_2 + \bar{s}_3) + \frac{1}{180} (\bar{s}_2^2 + \bar{s}_3^2 + \bar{s}_2 \bar{s}_3) \right] + \dots \end{aligned} \quad (4.16)$$

The other triangle integrals are expanded using the same methods. We have checked the expansions numerically against *LoopTools* [76]. The contributions to $\mathcal{K}_{\text{df},3}$ from A_C are given in eq. (4.21).

4.2.3 The full non-OPE threshold expansion

Performing the expansion described above to second order, we find that the total contributions from $\text{Re } \mathcal{M}_{\text{df},3}^{\text{NLO,non-OPE}}$ are

$$\frac{F_\pi^6}{M_\pi^6} \mathcal{K}_0 \supset 14\kappa + 33L + 36(8\ell_1^r + \ell_3^r - 2\ell_4^r), \quad (4.17a)$$

$$\frac{F_\pi^6}{M_\pi^6} \mathcal{K}_1 \supset -\frac{35}{2}\kappa + 12L + 36(20\ell_1^r + \ell_2^r - 4\ell_4^r), \quad (4.17b)$$

$$\frac{F_\pi^6}{M_\pi^6} \mathcal{K}_2 \supset -\frac{9747}{50}\kappa - 216L + 324(2\ell_1^r + \ell_2^r), \quad (4.17c)$$

$$\frac{F_\pi^6}{M_\pi^6} \mathcal{K}_A \supset \frac{576}{5}\kappa - 54L - 81(2\ell_1^r - 3\ell_2^r), \quad (4.17d)$$

$$\frac{F_\pi^6}{M_\pi^6} \mathcal{K}_B \supset -\frac{13797}{50}\kappa - 162L + 243(2\ell_1^r + \ell_2^r). \quad (4.17e)$$

For comparison, the LO results from the non-OPE diagram in fig. 1b are

$$\frac{F_\pi^4}{M_\pi^4} \mathcal{K}_0 \supset -18, \quad \frac{F_\pi^4}{M_\pi^4} \mathcal{K}_1 \supset -26. \quad (4.18)$$

This is specific to our off-shell convention (see sec. 2.3).

The results for the separate parts of $A^{(4)}$ in eq. (4.8) are as follows. The part stemming from A_l can be directly read from eq. (4.17) as the terms containing ℓ_i^r . The remaining parts not containing \bar{J} or \bar{C} loop functions, i.e., A_π and A_L , give

$$\begin{aligned} \frac{F_\pi^6}{M_\pi^4} \mathcal{K}_{\text{df},3}^{\text{NLO,non-OPE}} &\supset 17\kappa + 33L + \Delta(10\kappa + 48L) + \Delta^2 \left(-\frac{387}{2}\kappa - \frac{351}{2}L \right) \\ &\quad + \Delta_A \left(-\frac{495}{8}\kappa - \frac{675}{8}L \right) + \Delta_B \left(-\frac{1323}{8}\kappa - \frac{1215}{8}L \right). \end{aligned} \quad (4.19)$$

The part A_J containing solely \bar{J} functions, using the results from sec. 4.2.1, reads

$$\begin{aligned} \frac{F_\pi^6}{M_\pi^4} \mathcal{K}_{\text{df},3}^{\text{NLO,non-OPE}} &\supset -72\kappa + \Delta(-223\kappa) + \Delta^2 \left(-\frac{243}{4}\kappa \right) \\ &\quad + \Delta_A \left(\frac{1233}{4}\kappa \right) + \Delta_B \left(-\frac{117}{2}\kappa \right), \end{aligned} \quad (4.20)$$

¹⁹We refer readers unfamiliar with principal values for multiple poles to ref. [78].

and the \overline{C} functions of A_C , calculated employing the methods presented in sec. 4.2.2, all together give

$$\begin{aligned} \frac{F_\pi^6}{M_\pi^4} \mathcal{K}_{\text{df},3}^{\text{NLO,non-OPE}} \supset & 69\kappa + \Delta \left(-36L + \frac{391}{2}\kappa \right) + \Delta^2 \left(-\frac{81}{2}L + \frac{5931}{100}\kappa \right) \\ & + \Delta_A \left(\frac{243}{8}L - \frac{5247}{40}\kappa \right) + \Delta_B \left(-\frac{81}{8}L - \frac{10413}{200}\kappa \right). \end{aligned} \quad (4.21)$$

The sum of eqs. (4.19) to (4.21), plus the ℓ_i^r terms, gives eq. (4.17).

4.3 Bull's head subtraction contribution

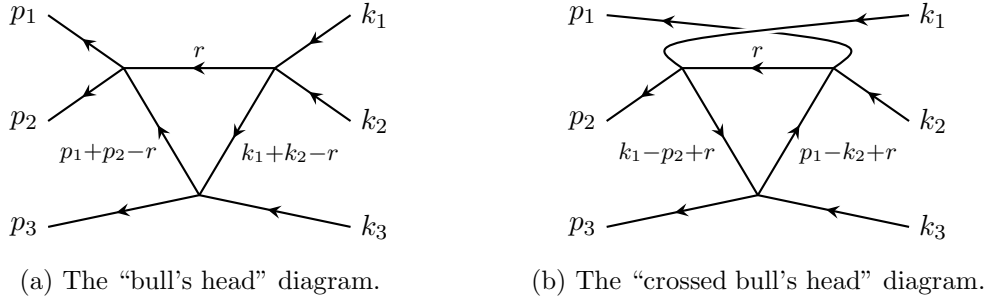


Figure 9: Two configurations of the triangle-loop diagram, of which only (a) requires subtraction [in the form of $\mathcal{D}^{(u,u)\text{BH}}$, eq. (4.23)]. There are a total of 15 diagrams with the triangle topology, of which 9 correspond to the configuration (a) [so their sum corresponds to the symmetrization of (a)] and 6 to the configuration (b).

The BH piece of the subtraction, \mathcal{D}^{BH} in eq. (2.39), concerns the symmetrization of the final term in eq. (2.11), which subtracts the “bull’s head” diagram in fig. 9a. This is the only cutoff-dependent contribution to $\mathcal{K}_{\text{df},3}^{\text{NLO}}$, and due to the integral over $H(x)$, it requires numerical evaluation.

Since there are only s -wave contributions, the subtraction term reduces to

$$\mathcal{D}^{(u,u)\text{BH}}(\mathbf{p}_3, \mathbf{k}_3) = -\frac{1}{F_\pi^6} (2p_1 \cdot p_2) I(\mathbf{p}_3, \mathbf{k}_3) (2k_1 \cdot k_2), \quad (4.22)$$

$$I(\mathbf{p}_3, \mathbf{k}_3) \equiv \int_r \frac{H(x_r) [(P-r)^2 - 2M_\pi^2] H(x_r)}{[(p_+ - r)^2 - M_\pi^2 + i\epsilon] [(k_+ - r)^2 - M_\pi^2 + i\epsilon]}, \quad (4.23)$$

where $p_+ \equiv p_1 + p_2$, $k_+ \equiv k_1 + k_2$, and $x_r \equiv (P-r)^2/(4M_\pi^2)$. For brevity, we define $G(r; p_+, k_+)$ (not to be confused with G^∞ above) such that

$$\mathcal{D}^{(u,u)\text{BH}} = -\frac{1}{F_\pi^6} (2p_1 \cdot p_2) (2k_1 \cdot k_2) \int_r H^2(x_r) G(r; p_+, k_+). \quad (4.24)$$

We stress that r is on-shell and that the integral is Lorentz-invariant.

4.3.1 Threshold expansion

The integrand of eq. (4.23) can be expressed to any order in the threshold expansion using $\Delta, \Delta_3, \Delta'_3$, and \tilde{t}_{33} only. Since the amplitude is free of singularities in the real part, it follows that the real part of the subtraction is also singularity-free. However, due to possible singularities in the integrand, some manipulations need to be done before the coefficients can be evaluated.

Starting with eq. (4.23), we stay in the CMF of the whole system, where $\mathbf{P} = \mathbf{0}$ and $(P-r)^2 = E^2 - 2E\omega_r + M_\pi^2$, and set $d^3r = r^2 dr \cos\theta d\phi$. We rewrite the first denominator as

$$(p_+ - r)^2 - M_\pi^2 = p_+^2 - 2\mathbf{p}_+ \cdot \mathbf{r} = p_+^2 - 2E_{p_+}\omega_r + 2\mathbf{p}_+ \cdot \mathbf{r} \equiv 4M_\pi^2 - 4M_\pi\omega_r + \Delta_{p_+}, \quad (4.25)$$

which defines Δ_{p_+} ; Δ_{k_+} is defined similarly from the second denominator. Note that $p_+ = (E_{p_+}, \mathbf{p}_+)$ is the momentum of the two-pion system. We then expand naively in Δ_{p_+} and Δ_{k_+} , which are both $\mathcal{O}(\sqrt{\Delta})$, so

$$I(\mathbf{p}_3, \mathbf{k}_3) = \int_r H^2(x_r) [E^2 - 2E\omega_r - M_\pi^2] \sum_{a,b=0}^{\infty} \frac{\Delta_{p_+}^a \Delta_{k_+}^b}{(4M_\pi^2 - 4M_\pi\omega_r)^{a+b+2}}, \quad (4.26)$$

and cut off the sums at a suitable order. After that, we can perform all angular integrals using

$$\int d\cos\theta d\phi (\mathbf{p}_+ \cdot \mathbf{r})(\mathbf{k}_+ \cdot \mathbf{r}) = 4\pi \frac{r^2}{3} \mathbf{p}_+ \cdot \mathbf{k}_+ \quad (4.27)$$

and its generalizations.²⁰ Finally, we expand the explicit and implicit [via $E = 3M_\pi\sqrt{1 + \Delta}$ and $x_r = (E^2 - 2E\omega_r + M_\pi^2)/4M_\pi^2$] dependence on Δ to the order needed. We will show in sec. 4.3.2 that naively expanding $H(x_r)$ this way is valid, despite the non-analyticity of H .

The remaining integral over r can be rewritten as an integral over ω_r . Introducing the variable z , defined via $\omega_r = M_\pi(1 + 2z^2)$ so that $r^2 dr / [2\omega_r(2\pi)^3] = M_\pi^2 z^2 \sqrt{1 + z^2} dz / (2\pi^3)$, leads to integrals of the type

$$H_{m,n} \equiv \frac{1}{\pi^2} \int_0^{1/\sqrt{3}} dz \frac{\sqrt{1+z^2}}{z^m} \frac{d^n}{dx^n} [H^2(x)]. \quad (4.28)$$

Since $x = 1 - 3z^2$, the integration limits are $x = 1$ at $z = 0$ and $x = 0$ at $z = 1/\sqrt{3}$. Due to H and all its derivatives vanishing at $x = 0$, the E -dependence in the upper limit of the integral is not captured by the expansion, meaning this is an expansion of asymptotic nature. However, as can be seen in the upper-right panel of fig. 6, the expansion to

²⁰The general case can be compactly written as

$$\int d\cos\theta d\phi \prod_{a=1}^{2n} (\mathbf{p}_a \cdot \mathbf{r}) = 4\pi \frac{r^{2n}}{(2n+1)!!} \delta^{i_1 i_2 \dots i_{2n}} p_1^{i_1} p_2^{i_2} \dots p_n^{i_{2n}}$$

(the case with an odd number of \mathbf{p}_a vanishes by symmetry). Repeated indices are summed, and $\delta^{i_1 \dots i_n}$ generalizes the Kronecker δ to the totally symmetric tensor obtained by summing all distinct ways of distributing the indices i_1, \dots, i_{2n} among n Kronecker δ 's, i.e., $\delta^{ijkl} = \delta^{ij}\delta^{kl} + \delta^{ik}\delta^{jl} + \delta^{il}\delta^{jk}$, etc.

quadratic order approximates the full numerical result very well for the range of energies of interest.

We will return to the evaluation of $H_{m,n}$ in sec. 4.3.2. For now, we use it to state the result, which to second order in the threshold expansion is

$$\begin{aligned}
\frac{F_\pi^6}{M_\pi^4} \text{Re } \mathcal{D}^{(u,u)\text{BH}} &= \left(\frac{3}{2}H_{0,0} - \frac{1}{4}H_{2,0}\right) + \left(\frac{21}{4}H_{0,1} + \frac{1}{8}H_{4,0}\right)\Delta + \left(\frac{81}{16}H_{0,0} - \frac{9}{32}H_{2,0} - \frac{3}{32}H_{4,0}\right)\Delta_3^S \\
&+ \left(\frac{9}{16}H_{0,0} + \frac{15}{32}H_{2,0} - \frac{3}{32}H_{4,0}\right)\tilde{t}_{33} + \left(\frac{63}{8}H_{0,2} - \frac{33}{64}H_{0,1} - \frac{13}{256}H_{6,0} - \frac{19}{64}H_{4,0}\right)\Delta^2 \\
&+ \left(\frac{63}{4}H_{0,1} + \frac{3}{64}H_{6,0} + \frac{3}{32}H_{4,0}\right)\Delta\Delta_3^S + \left(\frac{9}{128}H_{6,0} - \frac{63}{128}H_{4,0} + \frac{27}{64}H_{2,0}\right)\Delta\tilde{t}_{33} \\
&+ \left(-\frac{9}{32}H_{4,0} + \frac{81}{32}H_{2,0} - \frac{81}{16}H_{2,0}\right)(\Delta_3^S)^2 + \left(\frac{891}{32}H_{0,0} - \frac{243}{64}H_{2,0} - \frac{9}{64}H_{4,0}\right)\Delta_3\Delta_3' \\
&+ \left(-\frac{9}{128}H_{6,0} + \frac{9}{64}H_{4,0} + \frac{189}{128}H_{2,0} + \frac{81}{64}H_{0,0}\right)\Delta_3^S\tilde{t}_{33} \\
&+ \left(-\frac{27}{640}H_{6,0} + \frac{27}{160}H_{4,0} + \frac{297}{640}H_{2,0} + \frac{81}{320}H_{0,0}\right)\tilde{t}_{33}^2. \tag{4.29}
\end{aligned}$$

This is the same expansion as in eq. (4.1), but only a subset of the terms is needed. The integration-by-parts relation

$$\begin{aligned}
H_{m,n+1} + H_{m-2,n+1} &= \frac{1}{6}[(2-m)H_{m,n} - (m+1)H_{m+2,n}] \\
&- \frac{1}{6}\left[(f'_{m-1}(z) + f'_{m+1}(z))\frac{d^n}{dx^n}H^2(x)\right]_0^{1/\sqrt{3}}, \tag{4.30}
\end{aligned}$$

where f_n is defined in eq. (4.32), has been used extensively in simplifying eq. (4.29); the ‘‘surface terms’’ [the second line of eq. (4.30)] vanish identically, but are revisited in sec. 4.3.3. After symmetrization over all 9 possibilities, analogous to eq. (4.3), we get

$$\begin{aligned}
\frac{F_\pi^6}{M_\pi^4} \text{Re } \mathcal{D}^{\text{BH}} &= \left[\frac{27}{2}H_{0,0} - \frac{9}{4}H_{2,0}\right] + \Delta\left[\frac{117}{4}H_{0,0} - \frac{21}{8}H_{2,0} + \frac{3}{4}H_{4,0} + \frac{189}{4}H_{0,1}\right] \\
&+ \Delta^2\left[\frac{243}{160}H_{0,0} + \frac{2241}{320}H_{2,0} - \frac{423}{160}H_{4,0} - \frac{369}{1280}H_{6,0} + \frac{5751}{64}H_{0,1} + \frac{567}{8}H_{0,2}\right] \\
&+ \Delta_A\left[-\frac{891}{64}H_{0,0} + \frac{1161}{128}H_{2,0} - \frac{45}{64}H_{4,0} - \frac{9}{128}H_{6,0}\right] \\
&+ \Delta_B\left[\frac{81}{320}H_{0,0} + \frac{297}{640}H_{2,0} + \frac{27}{160}H_{4,0} - \frac{27}{640}H_{6,0}\right], \tag{4.31}
\end{aligned}$$

where $\mathcal{D}^{\text{BH}} = \mathcal{S}\{\mathcal{D}^{(u,u)\text{BH}}\}$ is the bull’s head term in eq. (2.39).

4.3.2 Hadamard finite-part integration

Eq. (4.28) for $n = 0$ and $m > 0$ has a troublesome singularity in the endpoint $z = 0$, so it is not possible to naively apply the Cauchy principal value to evaluate $H_{m,n}$. However, it is possible to use the *Hadamard finite-part* prescription. Let us present its (rather simple) application before turning to the question of its validity. We define the functions $f_m(z)$ via

$$\frac{d}{dz}f_m(z) = \frac{1}{\pi^2}\frac{\sqrt{1+z^2}}{z^m}. \tag{4.32}$$

Using partial integration on eq. (4.28), we arrive at

$$H_{m,0} = f_m(z)H^2(x)\Big|_{z=0}^{1/\sqrt{3}} - \int_0^{1/\sqrt{3}} dz f_m(z)(-6z)\frac{d}{dx}H^2(x), \tag{4.33}$$

an expression that is independent of the integration constant in $f_m(z)$. The $z = 0$ limit of the first term is singular, whereas the second term (the integral) is non-singular since derivatives of $H(x)$ vanish exponentially as $z \rightarrow 0$ or $x \rightarrow 1$. The $z = 1/\sqrt{3}$ or $x = 0$ limit vanishes by construction since H and its derivatives all vanish at $x = 0$. The Hadamard finite part of $H_{m,0}$ is obtained by dropping the singular $z = 0$ limit, and if the prescription is valid, $\mathcal{D}^{(u,u)\text{BH}}$ is obtained by replacing all divergent $H_{m,n}$ with their finite parts.

It is at first not obvious that the Hadamard finite-part prescription is valid in our case, since the standard proofs involve complex integrals that break down due to the non-analyticity of $H(x)$. However, ref. [79] presents a proof using only smoothness criteria, which our integrands do satisfy. It also requires $m > 1$, but $H_{0,0}$ is non-singular, and we do not need $H_{1,0}$ (which only has an integrable singularity). Lastly, the prescription of course requires $\mathcal{D}^{(u,u)\text{BH}}$ to be finite, but we know from sec. 4.2 that such is the case, at least for the real part: $\text{Re}\mathcal{M}_3$ lacks the divergences that $\mathcal{D}^{(u,u)\text{BH}}$ would subtract.

As a last remark, we note that the Hadamard finite-part integration validates the naïve threshold expansion used to obtain eq. (4.28), which involved Taylor expanding $H(x)$. This Taylor series converges for $0 < x < 1$, but the convergence is extremely poor in the vicinity of the essential singularities at the endpoints. However, after applying eq. (4.33), all integrands contain a derivative of $H(x)$, which is exponentially suppressed near those endpoints. Therefore, nothing remains that is sensitive to the Taylor expansion in the region where it converges poorly. Thus, the non-analyticity of $H(x)$ causes no problems for our method.

4.3.3 Analytic approximation

The result eq. (4.33) is sufficient to obtain a numerical result for \mathcal{D}^{BH} : One simply evaluates the Hadamard finite part of $H_{m,n}$ numerically. However, it is possible, at least for a wide class of functions $H(x)$, to find an analytic approximation to eq. (4.28) that approximates \mathcal{D}^{BH} well, leaving a cutoff-dependent residue that must be evaluated numerically. Doing this, we are able to express $\mathcal{K}_{\text{df},3}$ almost entirely as an analytic, cutoff-independent expression, with small numerical cutoff-dependent corrections.

Letting $H^2(x) \equiv 1 + \tilde{H}^2(x)$, we get

$$H_{m,n} = \tilde{H}_{m,n} + \delta_{n,0} \frac{1}{\pi^2} \int_0^{1/\sqrt{3}} dz \frac{\sqrt{1+z^2}}{z^m}, \quad (4.34)$$

where $\tilde{H}_{m,n}$ is obtained by substituting $H(x) \rightarrow \tilde{H}(x)$ in eq. (4.28), and the remaining integral can be evaluated analytically, taking the Hadamard finite part when $m \neq 0$. Thus, making the choice $f_0(0) = 0$, we have

$$H_{m,n} = \tilde{H}_{m,n} + f_m(1/\sqrt{3}) \delta_{n,0}. \quad (4.35)$$

The analytic approximation is then obtained by setting $\tilde{H}_{m,n} = 0$, which allows everything

to be expressed in terms of $f_m \equiv f_m(1/\sqrt{3})$. We may thus rewrite eq. (4.31) as follows:

$$\begin{aligned} \frac{F_\pi^6}{M_\pi^4} \text{Re } \mathcal{D}^{\text{BH}} &= \left[\frac{27}{2} f_0 - \frac{9}{4} f_2 + \mathcal{D}_0 \right] + \Delta \left[36 f_0 - 6 f_2 - \frac{15}{16} f_4 + \mathcal{D}_1 \right] \\ &+ \Delta^2 \left[\frac{2313}{160} f_0 + \frac{171}{320} f_2 - \frac{1677}{640} f_4 - \frac{519}{1280} f_6 + \mathcal{D}_2 \right] \\ &+ \Delta_A \left[-\frac{891}{64} f_0 + \frac{1161}{128} f_2 - \frac{45}{64} f_4 - \frac{9}{128} f_6 + \mathcal{D}_A \right] \\ &+ \Delta_B \left[\frac{81}{320} f_0 + \frac{297}{640} f_2 + \frac{27}{160} f_4 - \frac{27}{640} f_6 + \mathcal{D}_B \right]. \end{aligned} \quad (4.36)$$

Here, \mathcal{D}_X are H -dependent numerical corrections stemming from $\tilde{H}_{m,n}$. They are defined by the requirement that eq. (4.36) equals eq. (4.31), and their values are given in eq. (3.2). In appendix A, we investigate the dependence of the \mathcal{D}_X upon the choice of cutoff function. Note that $\tilde{H}_{m,n} \rightarrow 0$ is not a good approximation for individual $H_{m,n}$, but as the smallness of \mathcal{D}_X shows, it clearly works at the level of \mathcal{D}^{BH} for our choice of H .

We stress that eq. (4.36) is *not* obtained by substituting $H_{m,n} \rightarrow f_m \delta_{n,0}$ in eq. (4.31), because the surface terms in eq. (4.30) do not vanish for $\tilde{H}_{m,n}$ and $f_m \delta_{n,0}$ separately. In other words, $H_{m,n} \rightarrow f_m \delta_{n,0}$ must be applied before eq. (4.30).

However, looking at eq. (4.30) for the $f_m \delta_{n,0}$ terms alone, we find that

$$(m+1)f_{m+2}(z) + (m-2)f_m(z) = -(1+z^2)f'_{m+1}(z). \quad (4.37)$$

This allows eq. (4.30) to be restated in a more symmetrical form as

$$\begin{aligned} H_{m,n+1} + H_{m-2,n+1} &= \frac{1}{6} \left[(2-m)H_{m,n} - (m+1)H_{m+2,n} \right] \\ &- \frac{1}{6} \left[\left[(2-m)f_m(z) - (m+1)f_{m+2}(z) \right] \frac{d^n}{dx^n} H^2(x) \right]_0^{1/\sqrt{3}}, \end{aligned} \quad (4.38)$$

but more importantly, since $f'_{m+1}(1/\sqrt{3})$ is just a rational number times κ , we can use eq. (4.37) to reduce eq. (4.36) entirely in terms of κ and $f_0 \equiv f_0(1/\sqrt{3}) = \frac{4}{3}\kappa(4+3\log 3)$:

$$\begin{aligned} \frac{F_\pi^6}{M_\pi^4} \text{Re } \mathcal{D}^{\text{BH}} &= \left[96\kappa + 9f_0 + \mathcal{D}_0 \right] + \Delta \left[296\kappa + 24f_0 + \mathcal{D}_1 \right] + \Delta^2 \left[\frac{5661}{50}\kappa + \frac{621}{40}f_0 + \mathcal{D}_2 \right] \\ &+ \Delta_A \left[-\frac{1764}{5}\kappa + \frac{135}{32}f_0 + \mathcal{D}_A \right] + \Delta_B \left[-\frac{612}{25}\kappa + \frac{189}{160}f_0 + \mathcal{D}_B \right]. \end{aligned} \quad (4.39)$$

4.3.4 Direct numerical evaluation

For a cross-check of the above results and for determining $\mathcal{D}^{(u,u)\text{BH}}$ further away from threshold, it is necessary to evaluate eq. (4.23) numerically without expansion. It is possible to evaluate it directly using numerical integration with a suitably chosen small $\epsilon > 0$, but the singularities in the integrand can lead to poor convergence or errors. Nevertheless, we have successfully performed this direct integration with 20 digits of accuracy, more than sufficient to reproduce eq. (3.2). In this subsection, however, we present a less numerically demanding approach, which complements and validates the direct evaluation. Another approach, making no assumptions about the smoothness of \mathcal{M}_3 , is presented in appendix E.

We note that the singularities in the integrand of eq. (4.23) occur only where $H(x_r) = 1$,²¹ so we separate

$$\int_r H^2(x_r) G(r; p_+, k_+) = \int_r \tilde{H}^2(x_r) G(r; p_+, k_+) \theta(R - |\mathbf{r}|) + \int_r G(r; p_+, k_+) \theta(R - |\mathbf{r}|), \quad (4.40)$$

for some suitable cutoff R such that $H(x_r) = 0$ when $|\mathbf{r}| > R$. Here, θ is the Heaviside step function and $\tilde{H}^2(x_r) \equiv H^2(x_r) - 1$ is the same as in sec. 4.3.1. The first term on the right-hand side is free from singularities and safe to evaluate numerically, while the second term, now free from $H(x_r)$, admits further simplification. This is easier in the CMF of $p_+ + k_+$, similar to the Breit frame in scattering, which we mark by \diamond . Setting up the \mathbf{r}^\diamond -integration in spherical coordinates with suitably aligned axes, i.e.,

$$\begin{aligned} \mathbf{r}^\diamond &= (r \sin \theta \cos \phi, r \sin \theta \sin \phi, r \cos \theta), \\ -\mathbf{p}_+^\diamond &= \mathbf{k}_+^\diamond = (0, 0, q), \quad \mathbf{P}^\diamond = (0, Q \sin \gamma, Q \cos \gamma), \end{aligned} \quad (4.41)$$

where we reuse the symbol r as $|\mathbf{r}^\diamond|$, we find

$$G^\diamond(r; p_+, k_+) = \frac{a_1 + a_2 \cos \theta + a_3 \sin \theta \sin \phi}{(b_1 - c \cos \theta)(b_2 + c \cos \theta)}, \quad (4.42)$$

where

$$\begin{aligned} a_1 &= E^2 - M_\pi^2 - 2E^\diamond \omega_r, & a_2 &= 2rQ \cos \gamma, & a_3 &= 2rQ \sin \gamma, \\ b_1 &= p_+^2 - 2p_{+0}^\diamond \omega_r + i\epsilon, & b_2 &= k_+^2 - 2k_{+0}^\diamond \omega_r + i\epsilon, & c &= 2rq. \end{aligned} \quad (4.43)$$

Eq. (4.42) is a convenient parametrization for evaluating the first term in eq. (4.40), which must be performed in the same frame as the second in order for the integration limits to match. More importantly it allows the angular integrals in the second term to be performed analytically, leaving

$$\int_r G^\diamond(r; p_+, k_+) \theta(R - r) = \int_0^R \frac{2\pi r^2 dr}{2\omega_r^\diamond (2\pi)^3} g(a_1, a_2; b_1, b_2; c), \quad (4.44)$$

where

$$g(a_1, a_2; b_1, b_2; c) = \begin{cases} \frac{2a_1}{b_1 b_2}, & \text{if } c = 0, \\ \sum_{i=1,2} \frac{A_i}{c(b_1 + b_2)} [\log(b_i + c) - \log(b_i - c)] & \text{otherwise,} \end{cases} \quad (4.45)$$

²¹This follows from the construction of $\mathcal{K}_{\text{df},3}$, but can also be proven directly as follows. At the pole where $(p_+ - r)^2 = M_\pi^2$,

$$4M_\pi^2 x_r = (P - r)^2 = (p_3 + p_+ - r)^2 = p_3^2 + (p_+ - r)^2 + 2p_3 \cdot (p_+ - r) = 2M_\pi^2 + 2\omega_{p_3} \omega_{p_+ - r},$$

where in the last equality we dropped the spatial part by going to the rest frame of either momentum. We have $\omega_{p_3} \geq m$ and $|\omega_{p_+ - r}| \geq m$, so as long as $(p_+ - r)$ has positive energy, this proves that $x_r \geq 1$. At threshold, $\omega_{p_+ - r} = 2m - m$ is positive, and since it is an analytic function of the kinematics, there is a path from threshold to any other configuration, and such a path clearly does not involve a switch to the negative-energy branch. The same holds for $(k_+ - r)^2 = M_\pi^2$.

with

$$A_1 = a_1 + \frac{a_2 b_1}{c}, \quad A_2 = a_1 - \frac{a_2 b_2}{c}. \quad (4.46)$$

There are singularities at $b_1 + b_2 = 0$ and $b_i = \pm c$, both of which are regulated by the $+i\epsilon$ from the propagators. Even without regulation, the singularities are integrable, except at threshold where actual divergences develop at $b_1 + b_2 \rightarrow 0$ and $r \rightarrow 0$. These cancel to keep $\mathcal{D}^{(u,u)\text{BH}}$ finite, but nevertheless present a numerical problem.

We have used three successful approaches to numerically evaluating eq. (4.44), providing cross-checks against each other, against the brute-force evaluation of eq. (4.23), and against the semi-analytic threshold expansion in the previous sections.

One method is to keep ϵ small but finite, giving an integrand with narrow spikes rather than singularities, which is numerically manageable with the right precautions. For sufficiently small ϵ , the ϵ -dependence of the result is very weak, and the $\epsilon \rightarrow 0$ limit is well approximated. It suffers stability issues near threshold, and we find that $\sqrt{\epsilon} \lesssim \Delta$ is required.

Another method is to deform the integration path into the complex plane, using, e.g., $r = z - i\alpha z(1 - z)$ for $z \in [0, R]$, where $\alpha > 0$ is arbitrary. With reasonably large α (but smaller than $4M_\pi$ to avoid the $\omega_r = 0$ pole at $r = iM_\pi$), the path avoids the singularities by a wide margin, allowing $\epsilon = 0$ and giving a smooth integrand that is easy to integrate. The deformation crosses some branch cuts if near thresholds, so it is only usable for the real part, and it cannot reach the threshold limit due to the divergence at $r \rightarrow 0$.

The third method is to express the $\epsilon \rightarrow 0$ limit in terms of Cauchy principal values, i.e., we replace the arguments of the logarithms in eq. (4.45) with their absolute values. This approach is full of subtleties, requiring careful consideration of the details in ref. [78]. Basically, in addition to the principal-value part, we need to add the naïve double-pole contribution multiplied by a factor of 2.

4.3.5 The full bull's head subtraction

Evaluating f_0 in eq. (4.39), the contributions of \mathcal{D}^{BH} to $\mathcal{K}_{\text{df},3}$ are

$$\frac{F_\pi^6}{M_\pi^6} \mathcal{K}_0 \supset -36\kappa(4 + \log 3) - \mathcal{D}_0, \quad (4.47a)$$

$$\frac{F_\pi^6}{M_\pi^6} \mathcal{K}_1 \supset -8\kappa(53 + 12 \log 3) - \mathcal{D}_1, \quad (4.47b)$$

$$\frac{F_\pi^6}{M_\pi^6} \mathcal{K}_2 \supset -\frac{27\kappa}{50}(363 + 115 \log 3) - \mathcal{D}_2, \quad (4.47c)$$

$$\frac{F_\pi^6}{M_\pi^6} \mathcal{K}_A \supset \frac{9\kappa}{40}(1468 - 75 \log 3) - \mathcal{D}_A, \quad (4.47d)$$

$$\frac{F_\pi^6}{M_\pi^6} \mathcal{K}_B \supset \frac{9\kappa}{200}(404 - 105 \log 3) - \mathcal{D}_B. \quad (4.47e)$$

The numerical values of these contributions are given in table 1. From there, we find that \mathcal{D}_X are indeed quite small compared to the full bull's head contributions: With the exception of \mathcal{D}_2 , they differ by more than an order of magnitude.

It is perhaps unexpected that the analytic approximation, which effectively amounts to the invalid cutoff choice $H(x) = \theta(x - 1)$, should be so accurate. However, as seen in sec. 4.3.4, the integral is dominated by the pole at small r , and $H(x_r)$ is very close to 1 in the vicinity of this pole. Conversely, the region where $H(x_r)$ differs meaningfully from 1 contributes very little. Appendix A looks more closely at this.

4.4 OPE diagrams

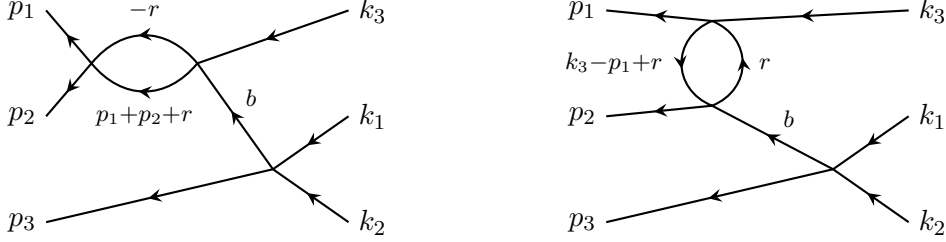


Figure 10: Examples of OPE NLO diagrams. There are also diagrams where the loop appears on the lower right.

The contributions of the OPE diagrams, such as those in fig. 10, can be computed analytically by directly performing the pertinent subtractions. Unlike in the LO case described in sec. 2.4, an additional challenge here is how to deal with the higher two-pion partial waves in the two-pion scattering subamplitude. While all partial waves appear in this subamplitude, it is possible to show that only two types of contributions are relevant at quadratic order: purely s -wave ones ($\ell = \ell' = 0$) and those with d -wave on one side ($\ell = 2, \ell' = 0$ or vice versa).

The starting point is the unsymmetrized version of the “master equation” (2.27), which we now restrict to OPE contributions:

$$\mathcal{K}_{\text{df},3}^{(u,u)\text{NLO,OPE}}(\mathbf{p}_3, \mathbf{k}_3)_{\ell'm',\ell m} = \text{Re} \mathcal{M}_{\text{df},3}^{(u,u)\text{NLO,OPE}}(\mathbf{p}_3, \mathbf{k}_3)_{\ell'm',\ell m}. \quad (4.48)$$

In turn, we need the definition of the divergence-free three-particle amplitude

$$\begin{aligned} \mathcal{M}_{\text{df},3}^{(u,u)\text{NLO,OPE}}(\mathbf{p}_3, \mathbf{k}_3)_{\ell'm',\ell m} \\ = \mathcal{M}_3^{(u,u)\text{NLO,OPE}}(\mathbf{p}_3, \mathbf{k}_3)_{\ell'm',\ell m} - \mathcal{D}^{(u,u)\text{NLO,OPE}}(\mathbf{p}_3, \mathbf{k}_3)_{\ell'm',\ell m}, \end{aligned} \quad (4.49)$$

where $\mathcal{M}_3^{(u,u)\text{NLO,OPE}}$ is given by one-particle-reducible diagrams like those shown in fig. 10. Before projection onto pair angular momenta, we have

$$\mathcal{M}_3^{(u,u)\text{NLO,OPE}} = -\mathcal{M}_{2,\text{off}}^{\text{NLO}}(\bar{s}'_2, t'_2, u'_2) \frac{1}{b^2 - M_\pi^2 + i\epsilon} \mathcal{M}_{2,\text{off}}^{\text{LO}}(\bar{s}_2, t_2, u_2) \quad (4.50)$$

$$- \mathcal{M}_{2,\text{off}}^{\text{LO}}(\bar{s}'_2, t'_2, u'_2) \frac{1}{b^2 - M_\pi^2 + i\epsilon} \mathcal{M}_{2,\text{off}}^{\text{NLO}}(\bar{s}_2, t_2, u_2), \quad (4.51)$$

where b is the momentum of the exchanged particle and

$$\begin{aligned} \bar{s}'_2 &\equiv (p_1 + p_2)^2 - 4M_\pi^2, & t'_2 &= (p_1 - k_3)^2, & u'_2 &= (p_2 - k_3)^2, \\ \bar{s}_2 &= (k_1 + k_2)^2 - 4M_\pi^2, & t_2 &= (k_1 - p_3)^2, & u_2 &= (k_2 - p_3)^2. \end{aligned} \quad (4.52)$$

The off-shell amplitudes have a single leg off shell (that of the exchanged particle), thus

$$\bar{s}_2 + t_2 + u_2 = b^2 - M_\pi^2 \equiv \bar{b}^2 = \bar{s}'_2 + t'_2 + u'_2. \quad (4.53)$$

The quantities \bar{s}_2 , \bar{s}'_2 , and \bar{b}^2 are defined so that they vanish at threshold (as do t_2 , u_2 , t'_2 and u'_2), and are thus convenient in a threshold expansion.

For the subtraction term, $\mathcal{D}^{(u,u)\text{NLO,OPE}}$, we must use the $\{\ell, m\}$ basis, where (keeping the indices implicit) we have

$$\begin{aligned} & \mathcal{D}^{(u,u)\text{NLO,OPE}}(\mathbf{p}_3, \mathbf{k}_3) \\ &= -\mathcal{M}_2^{\text{NLO}}(\mathbf{p}_3)G^\infty(\mathbf{p}_3, \mathbf{k}_1)\mathcal{M}_2^{\text{LO}}(\mathbf{k}_3) - \mathcal{M}_2^{\text{LO}}(\mathbf{p}_3)G^\infty(\mathbf{p}_3, \mathbf{k}_1)\mathcal{M}_2^{\text{NLO}}(\mathbf{k}_3), \end{aligned} \quad (4.54)$$

recalling eqs. (2.8) and (2.12) for relevant definitions. The absence of the subscript “off” on the factors of \mathcal{M}_2 in eq. (4.54) indicates that these amplitudes are all evaluated on shell.

Next, we note that $\mathcal{M}_2^{\text{LO}}$ contains only s -waves and is purely real,

$$F_\pi^2 \mathcal{M}_{2,\text{off}}^{\text{LO}}(s_2, t_2, u_2) = -2M_\pi^2 - \bar{s}_2 + \bar{b}^2. \quad (4.55)$$

Since the poles at $\bar{b}^2 = 0$ in $\mathcal{M}_3^{(u,u)}$ and $\mathcal{D}^{(u,u)}$ cancel, we are able to set $\epsilon \rightarrow 0$. Thus, to obtain the real part of $\mathcal{M}_{\text{df},3}^{(u,u)}$, we can use the expressions above with $\mathcal{M}_2^{\text{NLO}}$ replaced by its real part. Furthermore, since we are matching to the threshold expansion of $\mathcal{K}_{\text{df},3}^{(u,u)}$, keeping up to quadratic terms, we can expand $\text{Re } \mathcal{M}_2^{\text{NLO}}$ about threshold and drop terms of higher-than-cubic order in the quantities that vanish at threshold. Cubic order is required because of the \bar{b}^2 in the denominator coupled with the fact that $\mathcal{M}_2^{\text{LO}}$ does not vanish at threshold. It then turns out, as shown explicitly below, that the only term that contains other than s -waves is that proportional to $t_2 u_2$. Thus, we write

$$F_\pi^4 \text{Re } \mathcal{M}_{2,\text{off}}^{\text{NLO}}(\bar{s}_2, t_2, u_2) = F_\pi^4 \text{Re } \mathcal{M}_{2s,\text{off}}^{\text{NLO}}(\bar{s}_2, t_2, u_2) + e_{tu} t_2 u_2 + e'_{tu} \frac{(\bar{b}^2 - \bar{s}_2)}{M_\pi^2} t_2 u_2, \quad (4.56)$$

where the first term on the right-hand side contains the purely s -wave contributions. We treat the purely s -wave and the “ $t_2 u_2$ ” terms separately. The coefficients e_{tu} and e'_{tu} are real by construction.

4.4.1 Expression for $\text{Re } \mathcal{M}_{2,\text{off}}^{\text{NLO}}$

As explained in sec. 2.3, we use the choice of off-shell two-particle amplitude given in ref. [60]. For the $I = 2$ channel, the NLO amplitude is

$$F_\pi^4 \mathcal{M}_{2,\text{off}}^{\text{NLO}}(s, t, u) = A^{(4)}(t_2, u_2, s_2) + A^{(4)}(u_2, s_2, t_2), \quad (4.57)$$

where

$$\begin{aligned} A^{(4)}(s_2, t_2, u_2) &= d_1(t_2 - u_2)^2 + d_2 M_\pi^2 s_2 + d_3 s_2^2 + d_4 M_\pi^4 \\ &\quad + f_1(s_2)\bar{J}(s_2) + f_2(s_2, t_2)\bar{J}(t_2) + f_2(s_2, u_2)\bar{J}(u_2), \end{aligned} \quad (4.58)$$

$$f_1(s) = d_5 s^2 + d_6 M_\pi^2 s_2 + d_7 M_\pi^4, \quad (4.59)$$

$$f_2(s, t) = d_8 t^2 + d_9 t_2 M_\pi^2 + d_{10} s_2 M_\pi^2 + d_{11} s_2 t_2 + d_{12} M_\pi^4, \quad (4.60)$$

with the function \bar{J} defined in eq. (B.3). We revert to the standard Mandelstam variable s_2 rather than $\bar{s}_2 = s_2 - 4M_\pi^2$ in order to simplify the comparison with ref. [60]. The constants in the above expressions are [60]

$$\begin{aligned}
d_1 &= -\frac{5}{36}\kappa - \frac{1}{6}L + \frac{1}{2}\ell_2^r, \\
d_2 &= (N - \frac{29}{9})\kappa + (N - \frac{11}{3})L - 8\ell_1^r + 2\ell_4^r, \\
d_3 &= (\frac{11}{12} - \frac{1}{2}N)\kappa + (1 - \frac{1}{2}N)L + 2\ell_1^r + \frac{1}{2}\ell_2^r, \\
d_4 &= (\frac{20}{9} - \frac{1}{2}N)\kappa + (\frac{8}{3} - \frac{1}{2}N)L + 8\ell_1^r + 2\ell_3^r - 2\ell_4^r, \\
d_5 &= \frac{1}{2}N - 1, \quad d_6 = (3 - N), \quad d_7 = \frac{1}{2}N - 2, \\
d_8 &= \frac{1}{3}, \quad d_9 = -\frac{5}{3}, \quad d_{10} = -\frac{2}{3}, \quad d_{11} = \frac{1}{6}, \quad d_{12} = \frac{7}{3},
\end{aligned} \tag{4.61}$$

with $N = 3$, and remaining definitions are given below eq. (4.17). Imaginary parts arise only from the \bar{J} function. Its real part is analytic above threshold, and the expansions that we need are given in eq. (4.11). Combining these results, we obtain

$$\begin{aligned}
F_\pi^4 \text{Re } \mathcal{M}_{2,\text{off}}^{\text{NLO}}(\bar{s}_2, t_2, u_2) &= e_0 M_\pi^4 + e_1 M_\pi^2 \bar{s}_2 + e_2 \bar{s}_2^2 + e_3 M_\pi^2 \bar{b}^2 \\
&+ e_4 \bar{s}_2 \bar{b}^2 + e_5 (\bar{b}^2)^2 + e_{tu} t_2 u_2 \\
&+ e_6 \frac{\bar{s}_2^2 \bar{b}^2}{M_\pi^2} + e_7 \frac{\bar{s}_2 (\bar{b}^2)^2}{M_\pi^2} + e_8 \frac{(\bar{b}^2)^3}{M_\pi^6} + e'_{tu} \frac{(\bar{b}^2 - \bar{s}_2)}{M_\pi^2} t_2 u_2,
\end{aligned} \tag{4.62}$$

where the constants e_i and e_{tu} are known in terms of the d_i . Cubic terms \bar{s}_2^3 are not needed for the quadratic threshold expansion, since they give rise only to higher-order terms. The on-shell amplitude is obtained by setting $\bar{b} \rightarrow 0$.

4.4.2 Decomposition of $t_2 u_2$

As noted above, only the $t_2 u_2$ term in eq. (4.62) contains nonzero angular momenta in the pair CMF. To show this explicitly, we consider the final-state pair (with momenta p_1 and p_2) for which

$$t'_2 u'_2 = \frac{1}{4}(\bar{s}'_2 - \bar{b}^2)^2 - 4(\mathbf{a}_p^* \cdot \mathbf{k}_p^*)^2, \tag{4.63}$$

where \mathbf{a}_p^* and \mathbf{k}_p^* are the three-momenta \mathbf{p}_1 and \mathbf{k}_3 boosted to the CMF of the final-state pair. Their magnitudes are given by

$$|\mathbf{a}_p^*|^2 = q_{2,p}^{*2} = \frac{1}{4}\bar{s}'_2, \quad k_p^{*2} = \frac{(s'_2 - \bar{b}^2)^2}{4s'_2} - M_\pi^2. \tag{4.64}$$

To pull out the d -wave part, we use

$$(\mathbf{a}_p^* \cdot \mathbf{k}_p^*)^2 = q_{2,p}^{*2} k_p^{*2} \left[\frac{8\pi}{15} \sum_m Y_{2m}^*(\hat{\mathbf{a}}_p^*) Y_{2m}(\hat{\mathbf{k}}_p^*) + \frac{1}{3} \right]. \tag{4.65}$$

Thus, we can separate s - and d -wave parts as $t'_2 u'_2 = [t'_2 u'_2]_s + [t'_2 u'_2]_d$, where

$$[t'_2 u'_2]_s = \frac{1}{4}(\bar{s}'_2 - \bar{b}^2)^2 - \frac{4}{3}q_{2,p}^{*2} k_p^{*2}, \quad [t'_2 u'_2]_d = q_{2,p}^{*2} k_p^{*2} \frac{8\pi}{15} \sum_m Y_{2m}^*(\hat{\mathbf{a}}_p^*) Y_{2m}(\hat{\mathbf{k}}_p^*). \tag{4.66}$$

An analogous expression holds for $t_2 u_2$.

In the following, we will need the expansion of k_p^{*2} about threshold, which is given by

$$k_p^{*2} = \frac{1}{4}\bar{s}'_2 - \frac{1}{2}\bar{b}^2 + \frac{1}{16}(\bar{b}^2)^2 + \dots, \quad (4.67)$$

where the ellipsis contains terms of higher order that do not contribute at the order we work. Note that the partial-wave decomposition of the term $(\bar{b}^2 - \bar{s}_2)t_2 u_2$ is analogous since $(\bar{b}^2 - \bar{s}_2)$ is purely s -wave.

4.4.3 s -wave contributions

Including the $[t_2 u_2]_s$ and $(\bar{b}^2 - \bar{s}_2)[t_2 u_2]_s$ terms, the s -wave part of the real part of the NLO amplitude becomes

$$F_\pi^4 \text{Re } \mathcal{M}_{2s,\text{off}}^{\text{NLO}}(\bar{s}_2, \bar{b}^2) = e_0 M_\pi^4 + e_1 M_\pi^2 \bar{s}_2 + e'_2 \bar{s}_2^2 + e_3 M_\pi^2 \bar{b}^2 + e'_4 \bar{s}_2 \bar{b}^2 + e'_5 (\bar{b}^2)^2 \\ + e'_6 \frac{\bar{s}_2^2 \bar{b}^2}{M_\pi^2} + e'_7 \frac{\bar{s}_2 (\bar{b}^2)^2}{M_\pi^2} + e'_8 \frac{(\bar{b}^2)^3}{M_\pi^2} + \dots, \quad (4.68)$$

where

$$e'_2 = e_2 + \frac{1}{6}e_{tu}, \quad e'_4 = e_4 - \frac{1}{3}e_{tu}, \quad e'_5 = e_5 + \frac{1}{4}e_{tu}, \\ e'_6 = e_6 + \frac{1}{2}e'_{tu}, \quad e'_7 = e_7 - \frac{1}{48}e_{tu} - \frac{7}{12}e'_{tu}, \quad e'_8 = e_8 + \frac{1}{4}e'_{tu}. \quad (4.69)$$

We thus have

$$\mathcal{R}_s^{\text{NLO}}(\bar{s}_2) \equiv F_\pi^4 \text{Re } \mathcal{M}_{2s,\text{on}}^{\text{NLO}}(\bar{s}_2) = e_0 M_\pi^4 + e_1 M_\pi^2 \bar{s}_2 + e'_2 \bar{s}_2^2 + \dots, \quad (4.70)$$

$$\delta_s^{\text{NLO}}(\bar{s}_2, \bar{b}^2) \equiv F_\pi^4 \text{Re } \mathcal{M}_{2s,\text{off}}^{\text{NLO}}(\bar{s}_2) - F_\pi^4 \text{Re } \mathcal{M}_{2s,\text{on}}^{\text{NLO}}(\bar{s}_2) \\ = \bar{b}^2 \left(e_3 M_\pi^2 + e'_4 \bar{s}_2 + e'_5 \bar{b}^2 + e'_6 \frac{\bar{s}_2^2}{M_\pi^2} + e'_7 \frac{\bar{s}_2 \bar{b}^2}{M_\pi^2} + e'_8 \frac{(\bar{b}^2)^2}{M_\pi^2} + \dots \right). \quad (4.71)$$

The LO result from eq. (4.55) gives

$$\mathcal{R}_s^{\text{LO}}(\bar{s}_2) \equiv F_\pi^2 \mathcal{M}_{2s,\text{on}}^{\text{LO}}(\bar{s}_2) = -2M_\pi^2 - \bar{s}_2, \quad (4.72)$$

$$\delta_s^{\text{LO}}(\bar{b}^2) \equiv F_\pi^2 \mathcal{M}_{2s,\text{off}}^{\text{LO}}(\bar{s}_2, \bar{b}^2) - F_\pi^2 \mathcal{M}_{2s,\text{on}}^{\text{LO}}(\bar{s}_2) = \bar{b}^2. \quad (4.73)$$

We can now perform the required subtraction. Since we are considering purely s -wave terms, the projection onto pair angular momenta is trivial, and we can work with Mandelstam variables. Thus, the contribution of s -wave two-particle amplitudes is

$$-\bar{b}^2 F_\pi^6 \mathcal{K}_{\text{df},3}^{(u,u)\text{NLO,OPE},s} \\ = \mathcal{R}_s^{\text{NLO}}(\bar{s}'_2) \delta_s^{\text{LO}}(\bar{b}^2) + \delta_s^{\text{NLO}}(\bar{s}'_2, \bar{b}^2) \mathcal{R}_s^{\text{LO}}(\bar{s}_2) + \delta_s^{\text{NLO}}(\bar{s}'_2, \bar{b}^2) \delta_s^{\text{LO}}(\bar{b}^2) \\ + \mathcal{R}_s^{\text{LO}}(\bar{s}'_2) \delta_s^{\text{NLO}}(\bar{s}_2, \bar{b}^2) + \delta_s^{\text{LO}}(\bar{b}^2) \mathcal{R}_s^{\text{NLO}}(\bar{s}_2) + \delta_s^{\text{LO}}(\bar{b}^2) \delta_s^{\text{NLO}}(\bar{s}_2, \bar{b}^2). \quad (4.74)$$

Substituting the results above, we obtain

$$F_\pi^6 \mathcal{K}_{\text{df},3}^{(u,u)\text{NLO,OPE},s} = g_0^s M_\pi^4 + g_1^s M_\pi^2 (\bar{s}'_2 + \bar{s}_2) + g_2^s \bar{s}'_2 \bar{s}_2 + g_3^s (\bar{s}'_2 + \bar{s}_2)^2 \\ + g_4^s M_\pi^2 \bar{b}^2 + g_5^s \bar{b}^2 (\bar{s}'_2 + \bar{s}_2) + g_6^s (\bar{b}^2)^2 + \dots, \quad (4.75)$$

where the coefficients g_i^s are known in terms of the e_i , and the ellipsis indicates higher-order terms that are not needed.

The final step is to convert the variables to those used in the threshold expansion for $\mathcal{K}_{\text{df},3}^{(u,u)}$, eq. (4.1), using the results

$$\bar{s}'_2 + \bar{s}_2 = 9M_\pi^2 \Delta_3^S, \quad \bar{s}'_2 \bar{s}_2 = 81M_\pi^4 \Delta_3' \Delta_3, \quad \bar{b}^2 = 9M_\pi^2 (\Delta_3^S - \Delta - \tilde{t}_{33}). \quad (4.76)$$

In this way, we obtain the contributions to the coefficients c_1 – c_{10} in eq. (4.1) from the s -wave parts of \mathcal{M}_2 .

4.4.4 d -wave contributions

First, we consider the e_{tu} term, which gives a contribution of $[tu]_d$ to the NLO matrix element. Here, we must use the $\{k, \ell, m\}$ basis for $\mathcal{K}_{\text{df},3}$ since the subtraction is given in this basis. Specifically, the d -wave contribution to the subtraction of eq. (4.54) is, after recombining with spherical harmonics,

$$\begin{aligned} & \text{Re } \mathcal{D}^{(u,u)\text{NLO,OPE},d}(\{p_i\}, \{k_i\}) \\ &= - \sum_{m'} \sqrt{4\pi} Y_{2m'}(\hat{a}_p^*) \text{Re} \{ \mathcal{M}_{2,\ell'=2}^{\text{NLO}}(\mathbf{p}_3) \} \left(\frac{k_p^*}{q_{2,p}^*} \right)^2 \frac{\sqrt{4\pi} Y_{2m'}(\hat{k}_p^*)}{\bar{b}^2} \mathcal{M}_{2s}^{\text{LO}}(\mathbf{k}_3) + \leftrightarrow. \end{aligned} \quad (4.77)$$

Here, \leftrightarrow indicates the term in which the roles of the LO and NLO vertices are interchanged and the notation is as in sec. 4.4.2. The factor of $(k_p^*/q_{2,p}^*)^2$ arises from G^∞ , eq. (2.12). This contribution to $\mathcal{D}^{(u,u)}$ is to be subtracted from

$$\begin{aligned} & \text{Re } \mathcal{M}_3^{(u,u)\text{NLO,OPE},d}(\{p_i\}, \{k_i\}) \\ &= - \sum_{m'} \sqrt{4\pi} Y_{2m'}(\hat{a}_p^*) \text{Re} \{ \mathcal{M}_{2,\ell'=2,\text{off}}^{\text{NLO}}(\mathbf{p}_3) \} \frac{\sqrt{4\pi} Y_{2m'}(\hat{k}_p^*)}{\bar{b}^2} \mathcal{M}_{2s,\text{off}}^{\text{LO}}(\mathbf{k}_3) + \leftrightarrow. \end{aligned} \quad (4.78)$$

The key observation now is that, using the decomposition of the tu term given by eqs. (4.63) and (4.65),

$$\mathcal{M}_{2,\ell'=2,\text{off}}^{\text{NLO}}(\mathbf{p}_3) = -\frac{8}{15} q_{2,p}^{*2} k_p^{*2} \quad \text{and} \quad \mathcal{M}_{2,\ell'=2}^{\text{NLO}}(\mathbf{p}_3) = -\frac{8}{15} q_{2,p}^{*4}, \quad (4.79)$$

implying that

$$\mathcal{M}_{2,\ell'=2}^{\text{NLO}}(\mathbf{p}_3) \left(\frac{k_p^*}{q_{2,p}^*} \right)^2 = \mathcal{M}_{2,\ell'=2,\text{off}}^{\text{NLO}}(\mathbf{p}_3). \quad (4.80)$$

In other words, the barrier factor from G^∞ converts the on-shell amplitude appearing in the subtraction term into exactly the off-shell amplitude. Thus, the subtraction only picks out the difference between on- and off-shell values of $F_\pi^2 \mathcal{M}_2^{\text{LO}}$, given by $\delta_s^{\text{LO}}(\bar{b}^2) = \bar{b}^2$, and simply cancels the pole. One therefore obtains the contribution

$$F_\pi^6 \mathcal{K}_{\text{df},3}^{(u,u)\text{NLO,OPE},d} \supset -e_{tu} ([t'_2 u'_2]_d + [t_2 u_2]_d). \quad (4.81)$$

The two terms on the right-hand side contain $\{\ell', \ell\} = \{2, 0\}$ and $\{0, 2\}$, respectively. To convert to our standard basis, we use

$$[tu]_d = tu - [tu]_s, \quad (4.82)$$

with $[tu]_s$ given by eq. (4.66), and observe that $t'_2 u'_2 + t_2 u_2 = 81M_\pi^4 Q_{tu}$ [see eq. (4.2)], so that

$$F_\pi^6 \mathcal{K}_{\text{df},3}^{(u,u)\text{NLO,OPE},d} \supset e_{tu} (-81M_\pi^4 Q_{tu} + [t'_2 u'_2]_s + [t_2 u_2]_s). \quad (4.83)$$

The $[tu]_s$ terms can be expanded in powers of \bar{s}'_2 , \bar{s}_2 , and \bar{b}^2 , and lead to additional contributions of the form of eq. (4.75), with $g_i^s \rightarrow g_i^d$. These can then be converted to the standard variables of the threshold expansion as explained above and thus contribute to $c_1 - c_{10}$ in eq. (4.1).

Next, we consider the e'_{tu} term, which has the form $(\bar{b}^2 - \bar{s}_2)[tu]_d$. The analysis for the $\bar{s}_2[tu]_d$ part is the same as for $[tu]_d$ alone, leading to

$$F_\pi^6 \mathcal{K}_{\text{df},3}^{(u,u)\text{NLO,OPE},d} \supset -e'_{tu} \frac{\bar{s}_2}{M_\pi^2} (-81M_\pi^4 Q_{tu} + [t'_2 u'_2]_s + [t_2 u_2]_s). \quad (4.84)$$

Recalling that the subtraction has already been done, we note that all terms are of too high order to contribute.

Finally, we consider the $\bar{b}^2[tu]_d$ part of the NLO amplitude. Since this vanishes on shell, there is no subtraction term and we easily find

$$F_\pi^6 \mathcal{K}_{\text{df},3}^{(u,u)\text{NLO,OPE},d} \supset 2e'_{tu} ([t'_2 u'_2]_d + [t_2 u_2]_d) + \dots, \quad (4.85)$$

where the overall factor of 2 comes from the value of the LO amplitude at threshold. The remainder of the analysis is as for the $[tu]_d$ term above, except that $e_{tu} \rightarrow 2e'_{tu}$.

4.4.5 The full OPE contribution

Combining s - and d -wave contributions computed in secs. 4.4.3 and 4.4.4, we end up with expressions for c_1 through c_{10} and c_{14} in terms of the coefficients d_i ; there are no contributions to c_{11} , c_{12} , and c_{13} . We can now symmetrize using eqs. (4.3a) to (4.3e). We find that the contributions of the OPE diagrams at NLO are

$$\frac{F_\pi^6}{M_\pi^6} \mathcal{K}_0 \supset 25\kappa + 78L - 72(8\ell_1^r + 6\ell_2^r + \ell_3^r - 2\ell_4^r), \quad (4.86a)$$

$$\frac{F_\pi^6}{M_\pi^6} \mathcal{K}_1 \supset \frac{6831}{20}\kappa + 372L - 18(74\ell_1^r + 67\ell_2^r - 14\ell_4^r), \quad (4.86b)$$

$$\frac{F_\pi^6}{M_\pi^6} \mathcal{K}_2 \supset \frac{230481}{280}\kappa + 576L - 108(10\ell_1^r + 11\ell_2^r), \quad (4.86c)$$

$$\frac{F_\pi^6}{M_\pi^6} \mathcal{K}_A \supset -\frac{53199}{560}\kappa + 45L + \frac{27}{2}(14\ell_1^r - 17\ell_2^r), \quad (4.86d)$$

$$\frac{F_\pi^6}{M_\pi^6} \mathcal{K}_B \supset \frac{54171}{140}\kappa + 216L - 324(2\ell_1^r + \ell_2^r). \quad (4.86e)$$

For comparison, the LO results from the OPE diagram in fig. 1a are

$$\frac{F_\pi^4}{M_\pi^4} \mathcal{K}_0 \supset 36, \quad \frac{F_\pi^4}{M_\pi^4} \mathcal{K}_1 \supset 63. \quad (4.87)$$

Like eq. (4.18), this is specific to our off-shell convention (see sec. 2.3).

5 Conclusions and outlook

This work presents the NLO ChPT result for the isospin-3 three-particle K -matrix, $\mathcal{K}_{\text{df},3}$, which parametrizes three-particle interactions in the RFT three-particle finite-volume formalism [13, 14]. In particular, we have focused on the leading five terms in the threshold expansion. To determine $\mathcal{K}_{\text{df},3}$, we have used the three-pion amplitude calculated in ref. [60] combined with the relation between this amplitude and $\mathcal{K}_{\text{df},3}$ derived in ref. [14]. The main results of this work are summarized in sec. 3.1 and, in particular, in eq. (3.1).

Various simplifications play an important role in obtaining these results. The first is the result of eq. (2.27) that, at NLO in ChPT, $\mathcal{K}_{\text{df},3}$ is simply given by $\text{Re } \mathcal{M}_{\text{df},3}^{\text{NLO}}$, rather than requiring the solution of integral equations. The second simplification is that, although various contributions to $\mathcal{M}_{\text{df},3}^{\text{NLO}}$ can be singular at threshold, these singularities are absent in the real part of the total result. This allows us to obtain analytic results for the threshold expansion for almost all parts, the exception being the cutoff-dependent parts of the integrals appearing in the BH subtraction. The latter turn out to be numerically small.

One of the motivations for this work was to address the substantial discrepancy between lattice results for $\mathcal{K}_{\text{df},3}$ and the LO ChPT prediction [44, 47, 52]. Focusing on the results for the first two terms in the expansion of $\mathcal{K}_{\text{df},3}$, namely \mathcal{K}_0 and \mathcal{K}_1 , we find that the NLO corrections are able to resolve the large disagreement between lattice QCD and LO ChPT, thus increasing confidence on the extractions of $\mathcal{K}_{\text{df},3}$ from lattice calculations. We observe, however, that NLO effects are somewhat large in these two quantities. Regarding the term in the threshold expansion of $\mathcal{K}_{\text{df},3}$ that couples to d -waves, \mathcal{K}_B , we find a sign disagreement between the lattice QCD result and NLO ChPT result. While we do not have a definitive answer, we stress that the NLO ChPT contribution is the leading effect for \mathcal{K}_B . Potentially, NNLO effects could be large and account for the discrepancy.

Since we are using an expansion of $\mathcal{K}_{\text{df},3}$ about threshold, it is important to verify its convergence. This is necessary since at NLO in ChPT, $\mathcal{K}_{\text{df},3}$ has contributions to all orders in the threshold expansion due to the presence of loop integrals. To do so, in sec. 3.3, we address the validity of the truncation of $\mathcal{K}_{\text{df},3}$ at quadratic order. We find that for a pion mass of $M_\pi = 340$ MeV (the heaviest used in ref. [52]), the corrections beyond quadratic order account only for a 20% of the total at the 5π inelastic threshold. The corrections are even smaller for lighter masses. Similarly, two-pion partial waves with $\ell > 2$ in OPE diagrams, which do not enter the threshold expansion at quadratic order, only add a negligible contribution to the full $\mathcal{K}_{\text{df},3}$. We conclude that truncating the threshold expansion at quadratic order provides a good approximation to $\mathcal{K}_{\text{df},3}$.

Another timely question that we address is the cutoff dependence of $\mathcal{K}_{\text{df},3}$. All lattice QCD calculations using the RFT formalism have adopted the same choice of cutoff function.

However, this choice is not unique. In appendix A, we discuss how the NLO ChPT result varies for different cutoffs. Overall, we find that for a wide set of cutoff functions, the dependence is small, provided that the function does not drop to zero very rapidly below the two-pion threshold.

The results of this work can be extended to other systems, higher orders, or other EFTs. For instance, in preparation for future lattice QCD calculations, $\mathcal{K}_{\text{df},3}$ for other three-pion isospin channels could be derived since ref. [60] provides results for the six-pion amplitude for general isospin. A potential issue is that, due to the presence of resonances in two-particle subchannels and in the three-particle channel itself, the convergence of ChPT might be poor. Examples include σ and ρ in two-particle and ω and h_1 in three-particle channels. $\mathcal{K}_{\text{df},3}$ could also be computed for other systems of mixed mesons at maximal isospin, such as $\pi^+\pi^+K^+$ and $K^+K^+\pi^+$. In this case, the full amplitude is not available yet, and the results from ref. [60] would need to be extended to SU(3) ChPT. This is a very compelling follow-up in light of the recent lattice QCD results for such systems [80] and the observed tension with the LO ChPT prediction.

As shown by this work, the combination of EFTs and lattice QCD continues to be a potent tool for studying the hadron spectrum. This synergy has already yielded valuable insights into the three-hadron problem and will certainly keep contributing in the future.

Acknowledgments

The work of JBB was supported by the Spanish MU grant FPU19/04326. Additionally, JBB received support from the European project H2020-MSCA-ITN-2019//860881-HIDDeN and the staff exchange grant 101086085-ASYMMETRY, and from the Spanish AEI project PID2020-113644GB-I00/AEI/10.13039/501100011033. The work of FRL was supported in part by the U.S. Department of Energy (USDOE), Office of Science, Office of Nuclear Physics, under grant Contract Numbers DE-SC0011090 and DE-SC0021006. FRL also acknowledges financial support by the Mauricio and Carlota Botton Fellowship. The work of JB, TH and MS was supported by the Swedish Research Council grants contract numbers 2016-05996 and 2019-03779. TH also acknowledges support from Charles University Research Center (UNCE/SCI/013), Czech Republic. The work of SRS was supported in part by the USDOE grant No. DE-SC0011637.

JBB and FRL would like to thank the Physics Department at the University of Washington for its hospitality during a visit in which this work was initiated.

A Dependence on the cutoff

The cutoff function $H(x)$ is arbitrary so long as it is smooth and satisfies $H(x) = 0$ if $x \leq 0$ and $H(x) = 1$ if $x \geq 1$. Throughout this paper, we have been using the standard version

$$H(x) = \exp\left[-\frac{1}{x} \exp\left(-\frac{1}{1-x}\right)\right], \quad \text{when } 0 < x < 1, \quad (\text{A.1})$$

but ref. [15] and others consider a generalization thereof, corresponding to the replacement

$$x \rightarrow 1 + \frac{4}{3-\alpha}(x-1), \quad -1 \leq \alpha < 3, \quad (\text{A.2})$$

with $\alpha = -1$ corresponding to eq. (A.1). Larger α give sharper cutoffs, with the limit $\alpha \rightarrow 3$ being a step function, $H(x) \rightarrow \theta(x - 1)$. There is also the symmetric version

$$H(x) = \left[1 + \exp\left(\frac{1}{x} - \frac{1}{1-x}\right)\right]^{-1}, \quad \text{when } 0 < x < 1, \quad (\text{A.3})$$

which commonly appears in other areas, and which is more numerically well-behaved due to the lack of nested exponentials.

At NLO in ChPT, $\mathcal{K}_{\text{df},3}$ depends on $H(x)$ through the coefficients \mathcal{D}_X , defined in eq. (4.36). These are effectively the remainders of \mathcal{D}^{BH} after removing the analytic approximation obtained with $H(x) = \theta(x)$. With the standard cutoff choice, eq. (A.1), we obtain the values in eq. (3.2), which we restate here:

$$\begin{aligned} \mathcal{D}_0 &\approx -0.0563476589, & \mathcal{D}_1 &\approx 0.129589681, & \mathcal{D}_2 &\approx 0.432202370, \\ \mathcal{D}_A &\approx 9.07273890 \cdot 10^{-4}, & \mathcal{D}_B &\approx 1.62394747 \cdot 10^{-4}. \end{aligned} \quad (\text{A.4})$$

For comparison, with eq. (A.3) one instead obtains

$$\begin{aligned} \mathcal{D}_0 &\approx -0.0470650424, & \mathcal{D}_1 &\approx 0.107630347, & \mathcal{D}_2 &\approx 0.583361673, \\ \mathcal{D}_A &\approx -0.118643915, & \mathcal{D}_B &\approx -0.0400284275. \end{aligned} \quad (\text{A.5})$$

In fig. 11 we show the result for these quantities as a function of α in eq. (A.2).

A few features can be noted. Using the standard H , eq. (A.1), the analytic approximation is very good, in the sense that $|\mathcal{D}_X| \ll |\mathcal{K}_X|$. It is especially good for $X = \text{A, B}$. With larger α , the approximation of the quadratic order in the threshold expansion ($X = 2, \text{A, B}$) quickly grows worse, but in the leading orders ($X = 0, 1$) it grows better: Near $\alpha = 0.875$, \mathcal{K}_0 and \mathcal{K}_1 are almost exactly approximated. All \mathcal{D}_X diverge as $\alpha \rightarrow 3$, corresponding to extremely sharp cutoffs.

B Loop integrals

Let us bring up some basic definitions. Our notation, which follows ref. [60], differs from the standard Passarino–Veltman integrals by extra factors of $\kappa = 1/(16\pi^2)$. For the bubble integrals we use

$$\begin{aligned} B(q^2) &= \frac{1}{i} \int \frac{d^d \ell}{(2\pi)^d} \frac{1}{(\ell^2 - M_\pi^2) [(\ell - q)^2 - M_\pi^2]} \\ &= \kappa \frac{1}{\bar{\epsilon}} - \kappa - L + \bar{J}(q^2). \end{aligned} \quad (\text{B.1})$$

Following ChPT conventions, dimensional regularization in $4 - 2\epsilon$ dimensions uses

$$\frac{1}{\bar{\epsilon}} \equiv \frac{1}{\epsilon} - \gamma_E + \log 4\pi - \log \mu^2 + 1, \quad (\text{B.2})$$

where γ_E is the Euler–Mascheroni constant. We employ the standard definition for $\bar{J}(q^2)$:

$$\bar{J}(q^2) \equiv \kappa \left(2 + \beta \log \frac{\beta - 1}{\beta + 1} \right), \quad (\text{B.3})$$

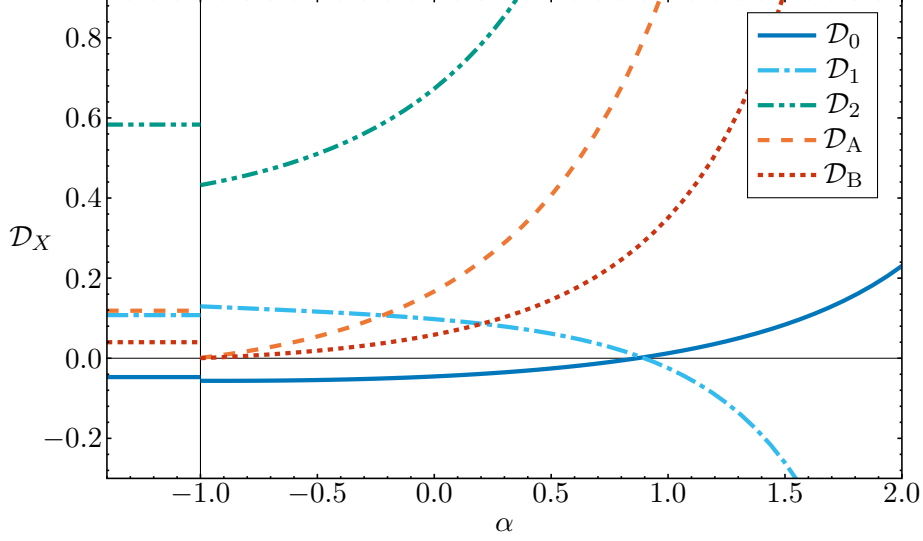


Figure 11: The numerical remainders \mathcal{D}_X as functions of the parameter α , employing eq. (A.1) together with eq. (A.2). All \mathcal{D}_X diverge as $\alpha \rightarrow 3$, while the standard $H(x)$ and the numerical values of eq. (3.2) are recovered at $\alpha = -1$. For comparison, the values obtained with the symmetric H , eq. (A.3), are shown to the left of $\alpha = -1$. The line $\mathcal{D}_X = 0$ corresponds to the analytic approximation in sec. 4.3.1 being exact.

with $\beta \equiv \beta(q^2) = \sqrt{1 - \frac{4M_\pi^2}{q^2}}$. Regarding the scalar triangle integrals, we have

$$C(p_1, p_2, \dots, p_6) = \frac{1}{i} \int \frac{d^d \ell}{(2\pi)^d} \frac{1}{(\ell^2 - M_\pi^2)[(\ell - q_1)^2 - M_\pi^2][(\ell + q_2)^2 - M_\pi^2]}, \quad (\text{B.4})$$

where $q_1 = p_1 + p_2$, $q_2 = p_3 + p_4$; for completeness, we also define $q_3 = p_5 + p_6$. The expressions for $\mathcal{M}_3^{\text{NLO}}$ also include the tensor integrals C_{11} and C_{21} (and C_3 , which does not contribute at $I = 3$); their definitions and properties are found in appendix A of ref. [60]. In all cases, \overline{C}_X denotes the UV-finite part of C_X , although among these integrals, only C_{21} is UV-divergent.

For the numerical evaluation of the triangle integrals we use *LoopTools* [76]. We also use the following analytic expression, which can be utilized once the tensor integrals are reduced to the scalar ones through the Passarino–Veltman reduction. The one-loop triangle function C (related to the standard C_0) can be written in terms of 12 dilogarithms as

$$\begin{aligned} \frac{1}{\kappa} C(p_1, p_2, \dots, p_6) &= C_0(q_1^2, q_2^2, q_3^2, M_\pi^2, M_\pi^2, M_\pi^2) \\ &= \sum_{\alpha_1, \alpha_2 \in \{-1, 1\}} \frac{\alpha_1}{\xi_1 \xi_2} \text{Li}_2 \left\{ \left(1 - \alpha_1 \xi_2 \right) \left[\frac{1}{1 - \alpha_2 \beta_1 \xi_2} + i \alpha_2 \text{sgn}\{q_1^2\} \epsilon \right] \right\} + \text{cycl.}, \quad (\text{B.5}) \end{aligned}$$

with $\lambda \equiv \lambda(q_1^2, q_2^2, q_3^2) > 0$ the Källén triangle function, $\beta_1 = \sqrt{1 - \frac{4M_\pi^2}{q_1^2}}$, $\xi_1 \equiv q_1^2 - q_2^2 - q_3^2$, $\xi_2 \equiv \sqrt{1 - 4q_2^2 q_3^2 / \xi_1^2}$, and “cycl.” standing for cyclic permutations in $\{q_1^2, q_2^2, q_3^2\}$.

C Cancellation of imaginary parts

To confirm that the formalism is working as it should, we would like to check that $\mathcal{K}_{\text{df},3}^{\text{NLO}}$, defined by eqs. (2.24) and (2.26), is indeed real, so that it is correct to use the master equation (2.27). This should be possible at a diagram-by-diagram level, with each small set of contributions to $\mathcal{M}_3^{\text{NLO}}$ matched with corresponding subtraction terms in $\mathcal{M}_{\text{df},3}$ and corresponding ρ terms in eq. (2.24). In the following subsections, we show that this holds as long as the contributing amplitudes, both on and off shell, satisfy unitarity. This is the case if a consistent off-shell convention is used throughout (see sec. 2.3).

All cancellations proven here have been verified using direct calculation at a selection of kinematic configurations detailed in appendix D.

C.1 Bull's head diagram

The BH diagram contributing to \mathcal{M}_3 (fig. 12 and its crossings) leads to imaginary contributions due to the presence of two two-particle cuts in the s -channel. Here, we address the issue of how these imaginary contributions are canceled in the transition to $\mathcal{K}_{\text{df},3}$. This requires both the subtraction term $\mathcal{D}^{(u,u)\text{NLO}}$ and the ρ terms in eq. (2.24), and can be broken down diagrammatically in such a way that the cancellation is straightforward.

We consider the BH diagram in fig. 9a as a contribution to the unsymmetrized amplitude, $\mathcal{M}_3^{(u,u)\text{NLO}}(\mathbf{p}, \mathbf{k})$, since the cancellation can be seen before symmetrization. We start with the NLO subtraction. The relevant part of this term is the one corresponding to the BH diagram,

$$\mathcal{D}^{(u,u)\text{NLO}}(\mathbf{p}, \mathbf{k}) \supset \mathcal{D}_{ss}^{\text{BH}}(\mathbf{p}, \mathbf{k}) \equiv \mathcal{M}_{2s}^{\text{LO}}(\mathbf{p}) \int_r \{G_{ss}^\infty(\mathbf{p}, \mathbf{r}) \mathcal{M}_{2s}^{\text{LO}}(\mathbf{r}) G_{ss}^\infty(\mathbf{r}, \mathbf{k})\} \mathcal{M}_{2s}^{\text{LO}}(\mathbf{k}). \quad (\text{C.1})$$

In the main text, all quantities were implicit matrices in ℓ, m space. Here, since $\mathcal{M}_{2s}^{\text{LO}}$ is purely s -wave, we can drop the ℓ, m indices in all quantities and leave it implicit that $\mathcal{D}_{ss}^{\text{BH}}$ is nonzero only for $\ell' = \ell = 0$ (as indicated by the subscripts). This means that G_{ss}^∞ is different here than in eq. (2.20):

$$G_{ss}^\infty(\mathbf{p}, \mathbf{r}) = \frac{H(x_p)H(x_r)}{b_{pr}^2 - M_\pi^2 + i\epsilon}, \quad b_{pr} = (P - p - r)^2. \quad (\text{C.2})$$

Note that in our calculation, $H(x_p) = 1$ because p is a momentum for which both particles in the interacting pair can be on shell. Since $\mathcal{M}_{2s}^{\text{LO}}$ is real, the imaginary part of $\mathcal{D}_{ss}^{\text{BH}}$ arises only from the $i\epsilon$ in G_{ss}^∞ , and can be pulled out using the standard Cauchy principal value,

$$\frac{1}{z + i\epsilon} = \mathcal{P} \frac{1}{z} - i\pi\delta(z). \quad (\text{C.3})$$

To proceed, we assume that \mathbf{p} and \mathbf{k} are chosen such that the poles in $G_{ss}^\infty(\mathbf{p}, \mathbf{r})$ and $G_{ss}^\infty(\mathbf{r}, \mathbf{k})$ occur for non-overlapping values of \mathbf{r} . Then we get two distinct contributions to the imaginary part, one from the left-hand cut and the other from the right-hand cut. The case where the poles overlap can be handled with a more careful application of the principal value, following ref. [78], and we have done so as a cross-check. However, it can

be circumvented with the following argument: An infinitesimal deformation of \mathbf{p} and \mathbf{k} is enough to remove the overlap, so by the smoothness of $\mathcal{K}_{\text{df},3}$, if the imaginary parts cancel in the deformed case, they must also cancel without the deformation.

Thus, assuming that the poles do not overlap, we can change to the pair CMF variables \mathbf{r}_p^* and \mathbf{r}_k^* (in the notation of sec. 2.1) *separately* for the two delta-function contributions, and it is then straightforward to evaluate them. We focus on the left-hand (LH) cut contribution, as all the following holds separately for the right-hand (RH) cut.

Although the explicit form of the imaginary part is not needed in the following, it is still instructive to compute it. We find that the LH cut contribution to the imaginary part is

$$i \text{Im} \mathcal{D}_{ss}^{\text{BH,LH}}(\mathbf{p}, \mathbf{k}) = \mathcal{M}_{2s}^{\text{LO}}(\mathbf{p}) \frac{(-i\pi)}{(2\pi)^3} \frac{q_{2,p}^*}{4E_{2,p}^*} \int d\Omega(\hat{\mathbf{r}}_p^*) \{ \mathcal{M}_{2s}^{\text{LO}}(\mathbf{r}_{\text{on}}) G_{ss}^\infty(\mathbf{r}_{\text{on}}, \mathbf{k}) \} \mathcal{M}_{2s}^{\text{LO}}(\mathbf{k}), \quad (\text{C.4})$$

where \mathbf{r}_{on} is the on-shell projection of \mathbf{r} obtained using the prescription of ref. [13]. The integral in this equation runs over the directions of \mathbf{r}_p^* , and both $\mathcal{M}_{2s}^{\text{LO}}(\mathbf{r}_{\text{on}})$ and $G_{ss}^\infty(\mathbf{r}_{\text{on}}, \mathbf{k})$ depend on this direction. The no-overlap assumption implies that the latter quantity is real, i.e., we do not have simultaneous contributions from both delta functions. We now observe that

$$\frac{q_{2,p}^*}{E_{2,p}^*} = 16i\pi\rho(\mathbf{p}), \quad (\text{C.5})$$

so the contribution from the LH cut has the form of an $\mathcal{M}_2\rho\mathcal{K}_{\text{df},3}$ term, namely

$$i \text{Im} \mathcal{D}_{ss}^{\text{BH,LH}}(\mathbf{p}, \mathbf{k}) = 2\mathcal{M}_{2s}^{\text{LO}}(\mathbf{p})\rho(\mathbf{p}) \int \frac{d\Omega(\hat{\mathbf{r}}_p^*)}{4\pi} \{ \mathcal{M}_{2s}^{\text{LO}}(\mathbf{r}_{\text{on}}) G_{ss}^\infty(\mathbf{r}_{\text{on}}, \mathbf{k}) \} \mathcal{M}_{2s}^{\text{LO}}(\mathbf{k}). \quad (\text{C.6})$$

Next, we consider the following unsymmetrized term appearing in eq. (2.24), which has the same $\mathcal{M}_2\rho\mathcal{K}_{\text{df},3}$ form,

$$\frac{1}{3}\mathcal{M}_{2s}^{\text{LO}}(\mathbf{p})\rho(\mathbf{p})\mathcal{M}_{\text{df},3}^{\text{LO}}(\mathbf{p}, \mathbf{k}). \quad (\text{C.7})$$

Again, this is purely *s*-wave (since $\mathcal{M}_2^{\text{LO}}$ and $\mathcal{M}_{\text{df},3}^{\text{LO}}$ are), so we just need to consider the $\ell = \ell' = 0$ part. Only a subset of the terms in $\mathcal{M}_{\text{df},3}^{\text{LO}}$ contribute to the cancellation of the imaginary part of the BH diagram. These are all contained in the OPE contribution

$$\mathcal{M}_{\text{df},3}^{\text{LO,OPE}}(\mathbf{p}, \mathbf{k}) = -\mathcal{S} \left\{ \mathcal{M}_{2,\text{off}}^{\text{LO}}(\mathbf{p}) \frac{1}{b_{pk}^2 - M_\pi^2 + i\epsilon} \mathcal{M}_{2,\text{off}}^{\text{LO}}(\mathbf{k}) - \mathcal{M}_{2s}^{\text{LO}}(\mathbf{p}) G_{ss}^\infty(\mathbf{p}, \mathbf{k}) \mathcal{M}_{2s}^{\text{LO}}(\mathbf{k}) \right\}. \quad (\text{C.8})$$

Here, as in the main text, $b_{pk} = P - p - k$ and the subscript “off” indicates that the b_{pk} leg is off shell. Note it is important that a consistent off-shell convention is used throughout the calculation.

We now note that the initial-state symmetrization in eq. (C.8) (i.e., that over k_1, k_2, k_3) will be repeated when the $\mathcal{M}_2\rho\mathcal{K}_{\text{df},3}$ term is symmetrized. Thus, one can drop the initial-state symmetrization in eq. (C.8) and remove the factor of 1/3 in eq. (C.7). The final-state symmetrization then yields three terms,

$$\mathcal{M}_{\text{df},3}^{\text{LO,OPE}}(\mathbf{p}, \mathbf{k}) \supset \mathcal{M}_{\text{df},3}^{(u,u)\text{LO}}(\mathbf{p}, \mathbf{k}) + \mathcal{M}_{\text{df},3}^{(u,u)\text{LO}}(\mathbf{a}_p, \mathbf{k}) + \mathcal{M}_{\text{df},3}^{(u,u)\text{LO}}(\mathbf{b}_p, \mathbf{k}), \quad (\text{C.9})$$

where $-\mathcal{M}_{\text{df},3}^{(u,u)\text{LO}}(\mathbf{p}, \mathbf{k})$ is the expression in braces in eq. (C.8) and $\mathbf{a}_p, \mathbf{b}_p$ are the momenta of the final-state interacting-pair particles. Note that while the symmetrized $\mathcal{M}_{\text{df},3}^{\text{LO,OPE}}$ is a function of the total center-of-mass energy alone, the individual terms are not. The first term, $\mathcal{M}_{\text{df},3}^{(u,u)\text{LO}}(\mathbf{p}, \mathbf{k})$, will contribute to the cancellation of the imaginary part of the NLO OPE diagram (to be discussed in the following subsection), while the other two contributions, $\mathcal{M}_{\text{df},3}^{(u,u)\text{LO}}(\mathbf{a}_p, \mathbf{k})$ and $\mathcal{M}_{\text{df},3}^{(u,u)\text{LO}}(\mathbf{b}_p, \mathbf{k})$, are needed for the cancellation of the imaginary part of the BH diagram.

In fact, since $\mathcal{M}_2^{\text{LO}}(\mathbf{p})$ is purely s -wave, there is an implicit angular integral over the first argument in both these BH contributions, arising from the projection onto $\ell' = 0$. It then follows from $\mathbf{a}_p^* = -\mathbf{b}_p^*$ that $\mathcal{M}_{\text{df},3}^{(u,u)\text{LO}}(\mathbf{a}_p, \mathbf{k}) = \mathcal{M}_{\text{df},3}^{(u,u)\text{LO}}(\mathbf{b}_p, \mathbf{k})$. We thus keep only one of these two terms and multiply by a factor of 2. This leads to the final contribution to the unsymmetrized left-hand cut part of $[\mathcal{M}_2 \rho \mathcal{K}_{\text{df},3}]_{\text{BH}}$:

$$\begin{aligned} & -2\mathcal{M}_{2s}^{\text{LO}}(\mathbf{p})\rho(\mathbf{p}) \int \frac{d\Omega(\hat{\mathbf{a}}_p^*)}{4\pi} \mathcal{M}_{2,\text{off}}^{\text{LO}}(\mathbf{a}_{p,\text{on}}) \frac{1}{b_{kr}^2 - M_\pi^2 + i\epsilon} \mathcal{M}_{2,\text{off}}^{\text{LO}}(\mathbf{k}) \\ & + 2\mathcal{M}_{2s}^{\text{LO}}(\mathbf{p})\rho(\mathbf{p}) \int \frac{d\Omega(\hat{\mathbf{a}}_p^*)}{4\pi} \mathcal{M}_{2s}^{\text{LO}}(\mathbf{a}_{p,\text{on}}) G_{ss}^\infty(\mathbf{a}_{p,\text{on}}, \mathbf{k}) \mathcal{M}_{2s}^{\text{LO}}(\mathbf{k}). \end{aligned} \quad (\text{C.10})$$

This is purely imaginary, as the pole in the b_{kr} propagator is not crossed, given our assumptions about p and k . Since \mathcal{D} enters with a minus sign, we see that the second term in eq. (C.10) exactly cancels the imaginary part of $\mathcal{D}^{\text{BH,LH}}(\mathbf{p}, \mathbf{k})$ given in eq. (C.6). This leaves the first term in eq. (C.10), which itself exactly cancels the LH cut contribution to the imaginary part of the full BH diagram in the amplitude \mathcal{M}_3 (using the cutting rules).

Exactly analogous arguments hold for the RH cut part, in which one must use the $\mathcal{K}_{\text{df},3} \rho \mathcal{M}_2$ term from the relation between \mathcal{M}_3 and $\mathcal{K}_{\text{df},3}$. Thus, altogether, we have seen how the imaginary parts must cancel in the full BH contributions to $\mathcal{K}_{\text{df},3}$.

C.2 OPE diagrams

We now consider the OPE diagrams in which the initial interaction is of NLO in ChPT and the final one of LO. The arguments are identical for the “flipped” time ordering.

Since we are here interested in the imaginary part, several simplifications occur. By construction, the OPE pole is canceled in $\mathcal{M}_{\text{df},3}$, so the only source of a imaginary part is $\mathcal{M}_2^{\text{NLO}}$, and this is present only in the s -wave, so only the ss part of G^∞ contributes. The contribution to the unsymmetrized $\mathcal{M}_{\text{df},3}$ is thus given by

$$\begin{aligned} i \text{Im} \mathcal{M}_{\text{df},3}^{(u,u)\text{NLO}}(\mathbf{p}, \mathbf{k}) & \supset -i \text{Im} [\mathcal{M}_{2,\text{off}}^{\text{NLO}}(\mathbf{p})] \frac{1}{b_{pk}^2 - M_\pi^2 + i\epsilon} \mathcal{M}_{2,\text{off}}^{\text{LO}}(\mathbf{k}) \\ & + i \text{Im} [\mathcal{M}_{2s}^{\text{NLO}}(\mathbf{p})] G_{ss}^\infty(\mathbf{p}, \mathbf{k}) \mathcal{M}_{2s}^{\text{LO}}(\mathbf{k}), \end{aligned} \quad (\text{C.11})$$

where, as usual, \mathbf{p} and \mathbf{k} are final and initial spectator momenta, respectively, and “off” indicates that the b_{pk} leg is off shell. As above, here we are using the notation without implicit ℓm indices. To this must be added the contribution from the $\mathcal{M}_2 \rho \mathcal{K}_{\text{df},3}$ term in eq. (2.24), in which the OPE part of $\mathcal{K}_{\text{df},3}^{\text{LO}} = \mathcal{M}_{\text{df},3}^{\text{LO}}$, i.e., the first term of eq. (C.9), is

included. This contribution, which is purely imaginary, is

$$\begin{aligned}
& -\mathcal{M}_{2s}^{\text{LO}}(\mathbf{p})\rho(\mathbf{p})\mathcal{M}_{2,\text{off}}^{\text{LO}}(\mathbf{p})\frac{1}{b_{pk}^2 - M_\pi^2 + i\epsilon}\mathcal{M}_{2,\text{off}}^{\text{LO}}(\mathbf{k}) \\
& + \mathcal{M}_{2s}^{\text{LO}}(\mathbf{p})\rho(\mathbf{p})\mathcal{M}_{2s}^{\text{LO}}(\mathbf{p})G_{ss}^\infty(p, k)\mathcal{M}_{2s}^{\text{LO}}(\mathbf{k}).
\end{aligned}
\tag{C.12}$$

Now, we use unitarity and cutting rules to obtain

$$i \text{Im} \mathcal{M}_{2,\text{off}}^{\text{NLO}}(\mathbf{p}) = -\mathcal{M}_{2s}^{\text{LO}}(\mathbf{p})\rho(\mathbf{p})\mathcal{M}_{2,\text{off}}^{\text{LO}}(\mathbf{p}),
\tag{C.13}$$

which applies also for the on-shell amplitude. Using this, we find that the sum of eqs. (C.11) and (C.12) vanishes.

C.3 Remaining diagrams

The remaining diagrams with an imaginary part involve a LO six-point vertex and an s -channel loop closed by a LO four-point vertex, either in the initial or final state. An example is shown in fig. 8. These diagrams are divergence-free by themselves. Thus, the imaginary parts must be canceled by $\mathcal{M}_{2\rho}\mathcal{K}_{\text{df},3}$ -like terms appearing in the six-point vertex contribution to $\mathcal{K}_{\text{df},3}$. That this is the case follows from unitarity, which introduces a factor of $-\rho$, and the double symmetrization, which cancels the $1/3$. No off-shell amplitudes appear in the imaginary parts, so the cancellation is independent of the off-shell convention.

D Threshold expansion using single-parameter kinematic configurations

In this appendix, we explain a method that we use to cross-check several of the calculations presented in the main text, and also for plotting the numerical behavior of the full NLO contribution in sec. 3.3. In particular, it provides an alternative analytic approach for obtaining the contributions of A_J , A_π , A_L , and A_I to $\mathcal{M}_{\text{df},3}^{\text{NLO,non-OPE}}$, which are discussed in sec. 4.2. It has also been used to perform a numerical check of all other contributions to $\mathcal{K}_{\text{df},3}$.

As described in the main text, $\mathcal{K}_{\text{df},3}$ is a function of eight kinematic degrees of freedom, so it is not straightforward to explore its general momentum dependence. Near threshold, however, its behavior is characterized by a few parameters, five if we work to quadratic order in Δ [see eq. (2.2)]. In order to determine these coefficients from a given contribution to $\mathcal{K}_{\text{df},3}$, one approach is to use families of momenta, each of which is a one-dimensional projection of the full momentum dependence. If one uses enough such families and controls the momentum dependence of $\mathcal{K}_{\text{df},3}$ to high-enough order for each family, then the coefficients \mathcal{K}_X of the threshold expansion can be determined.

Each family depends on a single parameter p that has dimension of momentum and, by design, vanishes at threshold. We use the five families listed in table 2. While this is more than the minimum number of families needed for our applications, using this number provides redundancy and cross-checks. Family 1 is the one used in ref. [60], while family 2 is a variant thereof, with the momenta arranged as equilateral triangles. Families 3–5 use isosceles triangles instead.

a	$p_1^{(a)}(p)$	$p_2^{(a)}(p)$	$k_1^{(a)}(p)$	$k_2^{(a)}(p)$
1	$(\omega_p, p, 0, 0)$	$(\omega_p, -\frac{1}{2}p, \frac{\sqrt{3}}{2}p, 0)$	$(\omega_p, 0, 0, -p)$	$(\omega_p, \frac{\sqrt{3}}{2}p, 0, \frac{1}{2}p)$
2	$(\omega_p, p, 0, 0)$	$(\omega_p, -\frac{1}{2}p, \frac{\sqrt{3}}{2}p, 0)$	$(\omega_p, -p, 0, 0)$	$(\omega_p, \frac{1}{2}p, \frac{\sqrt{3}}{2}p, 0)$
3	$(\omega_{2p}, 2p, 0, 0)$	$(\Omega_7, -p, \frac{\sqrt{3}}{2}p, 0)$	$(\omega_{2p}, 0, 0, -2p)$	$(\Omega_7, \frac{\sqrt{3}}{2}p, 0, p)$
4	$(\omega_{2p}, 2p, 0, 0)$	$(\Omega_3, -p, \sqrt{2}p, 0)$	$(\omega_{2p}, 0, 0, -2p)$	$(\Omega_3, \sqrt{2}p, 0, p)$
5	$(\Omega_5, p, -2p, 0)$	$(\omega_{2p}, 0, 2p, 0)$	$(\Omega_5, 0, p, 2p)$	$(\omega_{2p}, 0, 0, -2p)$

Table 2: The five families used in the calculations, labeled by a . We use $\omega_p \equiv \sqrt{p^2 + M_\pi^2}$, and, for brevity, $\Omega_3 \equiv \omega_{\sqrt{3}p}$, $\Omega_5 \equiv \omega_{\sqrt{5}p}$ and $\Omega_7 \equiv \omega_{\sqrt{7}p/2}$. All momenta are on-shell with invariant mass M_π , and in all cases, $\mathbf{P} = \mathbf{p}_1 + \mathbf{p}_2 + \mathbf{p}_3 = \mathbf{k}_1 + \mathbf{k}_2 + \mathbf{k}_3 = \mathbf{0}$. For compactness, p_3 and k_3 have been omitted but are easily inferred using $\mathbf{P} = \mathbf{0}$ and the on-shell condition.

To use the families to determine the coefficients in the threshold expansion, we note that

$$\mathcal{K}_{\text{df},3}(\mathcal{F}_a) = c_0^a + c_1^a p^2 + c_2^a p^4 + \mathcal{O}(p^6), \quad (\text{D.1})$$

where a labels the family and $\mathcal{F}_a \equiv \{p_i^{(a)}(p), k_i^{(a)}(p)\}$. The coefficients c_i^a can be determined numerically or analytically. We also need the expansions

$$\begin{aligned} \Delta(\mathcal{F}_a) &= d_1^a p^2 + d_2^a p^4 + \mathcal{O}(p^6), \\ \Delta_{\text{A}}(\mathcal{F}_a) &= d_{\text{A}}^a p^4 + \mathcal{O}(p^6), \quad \Delta_{\text{B}}(\mathcal{F}_a) = d_{\text{B}}^a p^4 + \mathcal{O}(p^6). \end{aligned} \quad (\text{D.2})$$

A closely related approach replaces the expansion in p^2 with one in E^{*2} . We have used both and checked that the results agree.

A single family is sufficient to determine

$$\mathcal{K}_0 = c_0^a, \quad \mathcal{K}_1 = c_1^a / d_1^a, \quad (\text{D.3})$$

with other families providing cross-checks. To obtain the quadratic constants, we need three families of momenta, from which we can construct the matrix

$$Q = \begin{pmatrix} (d_1^{a_1})^2 & d_{\text{A}}^{a_1} & d_{\text{B}}^{a_1} \\ (d_1^{a_2})^2 & d_{\text{A}}^{a_2} & d_{\text{B}}^{a_2} \\ (d_1^{a_3})^2 & d_{\text{A}}^{a_3} & d_{\text{B}}^{a_3} \end{pmatrix}. \quad (\text{D.4})$$

We also collect the quadratic coefficients of $\mathcal{K}_{\text{df},3}$ into a vector and subtract the p^4 term arising from \mathcal{K}_1 :

$$V = \begin{pmatrix} c_2^{a_1} - c_1^{a_1} d_2^{a_1} / d_1^{a_1} \\ c_2^{a_2} - c_1^{a_2} d_2^{a_2} / d_1^{a_2} \\ c_2^{a_3} - c_1^{a_3} d_2^{a_3} / d_1^{a_3} \end{pmatrix}. \quad (\text{D.5})$$

Then,

$$\begin{pmatrix} \mathcal{K}_2 \\ \mathcal{K}_{\text{A}} \\ \mathcal{K}_{\text{B}} \end{pmatrix} = Q^{-1} V. \quad (\text{D.6})$$

This assumes that Q is invertible, which is true for some triplets of families. In particular, for the expansion of the matrix element, it is convenient to use the triplets of families $\{1, 2, 3\}$ and $\{1, 2, 4\}$. For numerical cross-checks, on the other hand, the triplet $\{1, 4, 5\}$ turned out to be the most convenient.

E An integration method for less well-behaved \mathcal{M}_3

Sec. 4.3.4 covers the method used to calculate $\mathcal{D}^{(u,u)\text{BH}}$ without first performing a threshold expansion. The applicability of this calculation relies on the finiteness of $\mathcal{D}^{(u,u)\text{BH}}$, which in turn follows from the finiteness of the corresponding part of the amplitude, $\mathcal{M}_3^{(u,u)\text{BH}}$. If that were not the case, one would have to regularize the divergences on both sides in a consistent way before the subtraction can take place, and it is not obvious how to do that. The same situation also invalidates the threshold expansion of secs. 4.3.1 to 4.3.3 unless the divergent parts can be isolated first.

In this appendix, we present an alternative approach, which computes the difference $\mathcal{M}_3^{(u,u)\text{BH}} - \mathcal{D}^{(u,u)\text{BH}}$ without explicitly dealing with the individual terms. In the present case of NLO scattering at maximum isospin, this is nothing but an overly complicated cross-check procedure (and, in earlier stages, a contingency in case the finiteness turned out to be wrong), but it is conceivable that when the scope is generalized, one will eventually encounter a sufficiently pathological subtraction that this approach becomes worthwhile. Despite this more general outlook, we will present it as it would be applied to the present calculation, so that the technical details can be shown in full.

The goal is to write $\mathcal{M}_3^{(u,u)\text{BH}}$ as similarly as possible to $\mathcal{D}^{(u,u)\text{BH}}$, and then manipulate its expression to obtain a piece identical to $\mathcal{D}^{(u,u)\text{BH}}$ plus compensatory terms, which must then equal $\mathcal{M}_3^{(u,u)\text{BH}} - \mathcal{D}^{(u,u)\text{BH}}$. Since this quantity is always divergence-free, its evaluation should be unproblematic. To specify $\mathcal{M}_3^{(u,u)\text{BH}}$, which is parametrization-dependent, it turns out that the most convenient parametrization for our purposes is the 5th among the ones presented in ref. [60], for which the $O(N+1)/O(N)$ Lagrangian is

$$\mathcal{L} = \frac{F_\pi^2}{2} \partial_\mu \Phi^\top \partial^\mu \Phi + F_\pi^2 \chi^\top \Phi, \quad \Phi = \Phi_5 = \frac{1}{1 + \frac{1}{4} \frac{\phi^\top \phi}{F_\pi^2}} \left(1 - \frac{1}{4} \frac{\phi^\top \phi}{F_\pi^2}, \frac{\phi^\top}{F} \right)^\top, \quad (\text{E.1})$$

where ϕ is a real vector of fields transforming linearly under the unbroken part of the symmetry group. In this representation, the 4-point vertex for flavors f_i and incoming off-shell momenta p_i reads²²

$$\begin{aligned} F_\pi^2 \mathcal{M}_{(5)}^{\text{LO}}(p_1, f_1; p_2, f_2; p_3, f_3; p_4, f_4) &= \delta_{f_1 f_2} \delta_{f_3 f_4} (M_\pi^2 + p_1 \cdot p_2 + p_3 \cdot p_4) \\ &+ \delta_{f_1 f_3} \delta_{f_2 f_4} (M_\pi^2 + p_1 \cdot p_3 + p_2 \cdot p_4) \\ &+ \delta_{f_1 f_4} \delta_{f_2 f_3} (M_\pi^2 + p_1 \cdot p_4 + p_2 \cdot p_3). \end{aligned} \quad (\text{E.2})$$

²²With the momenta on-shell, this of course reduces to the parametrization-independent LO 4-particle amplitude, but the off-shell form presented here is precisely the 4-point vertex in the Φ_5 parametrization. Note that this is a different off-shell convention than anywhere else in this paper. They are compatible, however, since our main convention only separates OPE from non-OPE, whereas the one presented here separates the BH contribution from the rest of the non-OPE part (and is more convenient for that purpose).

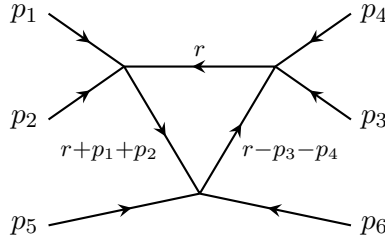


Figure 12: The bull's head diagram, showing the momentum routing used in eq. (E.4). All momenta are ingoing, following the conventions of ref. [60]; the routing of fig. 9 is straightforwardly obtained through crossing.

Now, we let $\mathcal{M}_3^{(u,u)\text{BH}}$ be precisely the contribution from the diagram fig. 12 in this parametrization. Assembling the diagram and fixing all external flavors to

$$|\pi^+\rangle = |\pi^-\rangle^* = \frac{|1\rangle + i|2\rangle}{\sqrt{2}}, \quad (\text{E.3})$$

we get considerable cancellation among the terms in the sum over internal flavors, leaving

$$\begin{aligned} \mathcal{M}_3^{(u,u)\text{BH}} &= \frac{1}{F_\pi^6} (2p_1 \cdot p_2)(2p_5 \cdot p_6) \\ &\times \frac{1}{i} \int \frac{d^4 r}{(2\pi)^4} \frac{r^2 - M_\pi^2 - 2r \cdot p_3}{[r^2 - M_\pi^2][(r + p_1 + p_2)^2 - M_\pi^2][(r - p_3 - p_4)^2 - M_\pi^2]}. \end{aligned} \quad (\text{E.4})$$

Replacing $\{p_1, \dots, p_6\}$ by $\{k_1, k_2, k_3, -p_1, -p_2, -p_3\}$ as described above eq. (2.35), this bears a striking resemblance to eq. (4.23). Indeed, comparing to eq. (4.24) reveals

$$\mathcal{M}_3^{(u,u)\text{BH}} = \frac{\Omega}{F_\pi^6} \frac{1}{i} \int \frac{d^4 r}{(2\pi)^4} \frac{G(r; p_+, k_+)}{r^2 - M_\pi^2 + i\epsilon}, \quad \mathcal{D}^{(u,u)\text{BH}} = -\frac{\Omega}{F_\pi^6} \int_r H^2(x_r) G(r; p_+, k_+), \quad (\text{E.5})$$

where $\Omega \equiv (2p_1 \cdot p_2)(2k_1 \cdot k_2)$ for brevity.

The key step is now to place the r^0 integral of $\mathcal{M}_3^{(u,u)\text{BH}}$ in the complex plane, and close the integration contour from below. This picks up three poles, one for each of the three propagators going on-shell with positive energy (closing it above would pick up the negative-energy poles). The residue at $r^2 = M_\pi^2$ contributes $-\Omega F_\pi^{-6} \int_r G(r; p_+, k_+)$; that is, it is precisely $\mathcal{D}^{(u,u)\text{BH}}$ except that there is no $H(x_r)$. However, this absence is not straightforward to compensate for, since without a cutoff the on-shell integrals become UV-divergent. Let us therefore look closer at G , whose numerator is

$$(P - r)^2 - 2M_\pi^2 = (r^2 - M_\pi^2) + (P^2 - M_\pi^2) - 2P \cdot r. \quad (\text{E.6})$$

The first term on the right-hand side vanishes on-shell, while in $\mathcal{M}_3^{(u,u)\text{BH}}$ it cancels one propagator and gives a simple, UV-divergent B integral [see eq. (B.3)]. The second term is UV-finite. The third is also UV-finite for the purposes of $\mathcal{M}_3^{(u,u)\text{BH}}$, but under an \int_r integral it diverges logarithmically. These divergences must ultimately cancel, but those cancella-

tions are very difficult to handle numerically. Therefore, we apply tensorial Passarino–Veltman reduction, replacing r with p_+ and k_+ :

$$\begin{aligned} -2P \cdot r &\longrightarrow \left([(p_+ - r)^2 - M_\pi^2] - [r^2 - M_\pi^2] - p_+^2 \right) \xi(p_+, k_+) \\ &\quad + \left([(k_+ - r)^2 - M_\pi^2] - [r^2 - M_\pi^2] - k_+^2 \right) \xi(k_+, p_+), \end{aligned} \quad (\text{E.7})$$

where we define ξ to also handle the case $p_+ = k_+$:

$$\xi(p, k) \equiv \begin{cases} \frac{p^2(P \cdot k) - (p \cdot k)(P \cdot p)}{p^2 k^2 - (p \cdot k)^2}, & \text{if } p \neq k, \\ \frac{P \cdot p}{2p^2}, & \text{if } p = k. \end{cases} \quad (\text{E.8})$$

Each term in square brackets in eq. (E.7) cancels a propagator in $\mathcal{M}_3^{(u,u)\text{BH}}$ and gives another B integral.

With this in mind, we define the fully UV-safe integrand

$$\tilde{G}(r; p, k) \equiv \frac{P^2 - M_\pi^2 - p_+^2 \xi(p_+, k_+) - k_+^2 \xi(k_+, p_+)}{[(p - r)^2 - M_\pi^2 + i\epsilon][(k - r)^2 - M_\pi^2 + i\epsilon]} \quad (\text{E.9})$$

(note that it is p, k in the denominator but p_+, k_+ in the numerator; this will be important later). Compensating for the modified numerator results in

$$\begin{aligned} \mathcal{M}_3^{(u,u)\text{BH}} = \frac{\Omega}{F_\pi^6} \left\{ \frac{1}{i} \int \frac{d^4 r}{(2\pi)^4} \frac{\tilde{G}(r; p_+, k_+)}{r^2 - M_\pi^2 + i\epsilon} + [1 - \xi(p_+, k_+) - \xi(k_+, p_+)] B((p_+ - k_+)^2) \right. \\ \left. + \xi(p_+, k_+) B(k_+^2) + \xi(k_+, p_+) B(p_+^2) \right\}, \end{aligned} \quad (\text{E.10})$$

where it is now manifest what carries the UV divergence [namely $B((p_+ - k_+)^2)$], which matches the result obtained by evaluating eq. (E.4) the standard way], while

$$\mathcal{D}^{(u,u)\text{BH}} = -\frac{\Omega}{F_\pi^6} \int_r H^2(x_r) \left\{ \tilde{G}(r; p_+, k_+) + \frac{\xi(p_+, k_+)}{(k_+ - r)^2 - M_\pi^2 + i\epsilon} + \frac{\xi(k_+, p_+)}{(p_+ - r)^2 - M_\pi^2 + i\epsilon} \right\}. \quad (\text{E.11})$$

Here, each term in the integral is individually convergent: We have moved the problematic cancellations to the extra B 's in eq. (E.10), where they are no problem at all. The extra ξ terms have at most simple poles.

Now, we apply the contour integration discussed above eq. (E.6) to the first term in eq. (E.10). The $r = M_\pi$ residue now contributes $-\Omega F_\pi^{-6} \int_r \tilde{G}(r; p_+, k_+)$, which mostly cancels against the first term in $\mathcal{D}^{(u,u)\text{BH}}$, while the remaining residues (from \tilde{G}) can either come from two simple poles or one double pole. Covering both cases, their contribution is²³

$$G_P(r) \equiv \begin{cases} \tilde{G}(r; -k_+, p_+ - k_+) + \tilde{G}(r; k_+ - p_+, -p_+), & \text{if } p_+ \neq k_+, \\ -\tilde{G}(r; -p_+, -p_+) \left[1 + \frac{2r \cdot p_+ + p_+^2 + 2\omega_r p_{+0}}{2\omega_r^2} \right], & \text{if } p_+ = k_+, \end{cases} \quad (\text{E.12})$$

²³There is no kinematic configuration that gives a triple pole; the $r = M_\pi$ pole is always separate from the others. In particular, the $p_+ = k_+$ version of G_P is appropriate at threshold.

so that

$$\frac{\Omega}{F_\pi^6} \int \frac{d^4r}{(2\pi)^4} \frac{\tilde{G}(r; p_+, k_+)}{r^2 - M_\pi^2 + i\epsilon} - \mathcal{D}^{(u,u)\text{BH}} = -\frac{\Omega}{F_\pi^6} \int_r [G_H(r) + G_P(r)], \quad (\text{E.13})$$

where we defined

$$\begin{aligned} G_H(r) &\equiv \tilde{G}(r; p_+, k_+) - H^2(x_r)G(r; p_+, k_+) \\ &= [1 - H^2(x_r)]\tilde{G}(r; p_+, k_+) - \frac{H^2(x_r)\xi(p_+, k_+)}{(k_+ - r)^2 - M_\pi^2 + i\epsilon} - \frac{H^2(x_r)\xi(k_+, p_+)}{(p_+ - r)^2 - M_\pi^2 + i\epsilon}. \end{aligned} \quad (\text{E.14})$$

Eq. (E.13), along with eq. (E.10), is the master formula for this subtraction.

The right-hand side of eq. (E.13) can be dealt with by modifying the methods of sec. 4.3.4. First, we numerically evaluate

$$\int_{r < R}^{(\diamond)} [1 - H^2(x_r)] \left\{ \tilde{G}(r; p_+, k_+) + \frac{\xi(p_+, k_+)}{(k_+ - r)^2 - M_\pi^2 + i\epsilon} + \frac{\xi(k_+, p_+)}{(p_+ - r)^2 - M_\pi^2 + i\epsilon} \right\}, \quad (\text{E.15})$$

where (\diamond) indicates that the integral is evaluated in the Breit frame, i.e., $\int^{(\diamond)} \tilde{G}(r; p, k)$ is taken in the CMF of $p + k$. By design, the integrand is entirely free from singularities. Then,

$$\begin{aligned} \int_r G_H(r) &= (\text{E.15}) + \int_{r > R}^{(\diamond)} \tilde{G}(r; p_+, k_+) \\ &\quad - \int_{r < R}^{(\diamond)} \left\{ \frac{\xi(p_+, k_+)}{(k_+ - r)^2 - M_\pi^2 + i\epsilon} + \frac{\xi(k_+, p_+)}{(p_+ - r)^2 - M_\pi^2 + i\epsilon} \right\}, \end{aligned} \quad (\text{E.16})$$

where the angles can be integrated out of the remaining integrals as in eq. (4.44). Note, however, that $a_{1,2,3}$ are now different than in eq. (4.43), while for ξ we get

$$\int_{r < R}^{(\diamond)} \frac{\xi(p, k)}{(k - r)^2 - M_\pi^2 + i\epsilon} = \int_0^R \frac{2\pi r^2 dr}{2\omega_r(2\pi)^3} \xi(p, k) g_\xi(k^2 - 2k_0^\diamond \omega_r + i\epsilon; c), \quad (\text{E.17})$$

where c is given by eq. (4.43), and

$$g_\xi(b; c) \equiv \begin{cases} \frac{2}{b}, & \text{if } c = 0, \\ \frac{1}{c} [\log(b - c) - \log(b + c)] & \text{otherwise.} \end{cases} \quad (\text{E.18})$$

Likewise, the angles can be integrated out of $\int_r G_P$. Note, however, that each individual \tilde{G} in eq. (E.12) is integrated in a different frame, as described below eq. (E.15). With that clarified, and with eq. (4.43) used in each frame separately,

$$\int_r^{(\diamond)} \tilde{G}(r; p, k) = \int \frac{2\pi r^2 dr}{2\omega_r(2\pi)^3} N g(1, 0; b_1, b_2; c), \quad (\text{E.19a})$$

$$\int_r^{(\diamond)} \tilde{G}(r; -p_+, -p_+) N' = \int \frac{2\pi r^2 dr}{2\omega_r(2\pi)^3} N g \left[1 + \frac{p_+^2 + 4p_{+0}^\diamond \omega_r}{2\omega_r^2}, -\frac{2rq}{2\omega_r^2}; b_1, b_2; c \right], \quad (\text{E.19b})$$

where [taken from eqs. (E.9) and (E.12), respectively]

$$\begin{aligned} N &\equiv P^2 - M_\pi^2 - p_+^2 \xi(p_+, k_+) - k_+^2 \xi(k_+, p_+), \\ N' &\equiv 1 + \frac{2r \cdot p_+ + p_+^2 + 2\omega_r p_{+0}}{2\omega_r^2}. \end{aligned} \tag{E.20}$$

Most of the integrands in eqs. (E.16) and (E.19) have singularities, but they are, in a sense, less severe than those encountered in sec. 4.3.4, and all give finite integrals at threshold (this is obvious for g_ξ but quite subtle for G_P). Our efforts with the numerator also ensure that the integrals to infinity can be safely done using a suitable numerical method. Assembling all these pieces completes the subtraction.

References

- [1] R. A. Briceño, J. J. Dudek and R. D. Young, *Scattering processes and resonances from lattice QCD*, *Rev. Mod. Phys.* **90** (2018) 025001 [[1706.06223](#)].
- [2] M. T. Hansen and S. R. Sharpe, *Lattice QCD and Three-particle Decays of Resonances*, *Ann. Rev. Nucl. Part. Sci.* **69** (2019) 65 [[1901.00483](#)].
- [3] A. Rusetsky, *Three particles on the lattice*, *PoS LATTICE2019* (2019) 281 [[1911.01253](#)].
- [4] B. Hörz, *Spectroscopy and Hadron Interactions*, *PoS LATTICE2021* (2022) 006.
- [5] M. Mai, M. Döring and A. Rusetsky, *Multi-particle systems on the lattice and chiral extrapolations: a brief review*, *Eur. Phys. J. ST* **230** (2021) 1623 [[2103.00577](#)].
- [6] M. Mai, U.-G. Meißner and C. Urbach, *Towards a theory of hadron resonances*, *Phys. Rept.* **1001** (2023) 1 [[2206.01477](#)].
- [7] F. Romero-López, *Three-particle scattering amplitudes from lattice QCD*, in *19th International Conference on Hadron Spectroscopy and Structure*, 12, 2021, [2112.05170](#).
- [8] F. Romero-López, *Multi-hadron interactions from lattice QCD*, in *39th International Symposium on Lattice Field Theory*, 12, 2022, [2212.13793](#).
- [9] S. R. Beane, W. Detmold and M. J. Savage, *n-Boson Energies at Finite Volume and Three-Boson Interactions*, *Phys. Rev.* **D76** (2007) 074507 [[0707.1670](#)].
- [10] W. Detmold and M. J. Savage, *The Energy of n Identical Bosons in a Finite Volume at $O(L^{-7})$* , *Phys. Rev.* **D77** (2008) 057502 [[0801.0763](#)].
- [11] R. A. Briceño and Z. Davoudi, *Three-particle scattering amplitudes from a finite volume formalism*, *Phys. Rev.* **D87** (2013) 094507 [[1212.3398](#)].
- [12] K. Polejaeva and A. Rusetsky, *Three particles in a finite volume*, *Eur. Phys. J. A* **48** (2012) 67 [[1203.1241](#)].
- [13] M. T. Hansen and S. R. Sharpe, *Relativistic, model-independent, three-particle quantization condition*, *Phys. Rev.* **D90** (2014) 116003 [[1408.5933](#)].
- [14] M. T. Hansen and S. R. Sharpe, *Expressing the three-particle finite-volume spectrum in terms of the three-to-three scattering amplitude*, *Phys. Rev.* **D92** (2015) 114509 [[1504.04248](#)].
- [15] R. A. Briceño, M. T. Hansen and S. R. Sharpe, *Relating the finite-volume spectrum and the two-and-three-particle S matrix for relativistic systems of identical scalar particles*, *Phys. Rev.* **D95** (2017) 074510 [[1701.07465](#)].

- [16] S. Koenig and D. Lee, *Volume Dependence of N-Body Bound States*, *Phys. Lett.* **B779** (2018) 9 [[1701.00279](#)].
- [17] H.-W. Hammer, J.-Y. Pang and A. Rusetsky, *Three-particle quantization condition in a finite volume: 1. The role of the three-particle force*, *JHEP* **09** (2017) 109 [[1706.07700](#)].
- [18] H. W. Hammer, J. Y. Pang and A. Rusetsky, *Three particle quantization condition in a finite volume: 2. General formalism and the analysis of data*, *JHEP* **10** (2017) 115 [[1707.02176](#)].
- [19] M. Mai and M. Döring, *Three-body Unitarity in the Finite Volume*, *Eur. Phys. J.* **A53** (2017) 240 [[1709.08222](#)].
- [20] R. A. Briceño, M. T. Hansen and S. R. Sharpe, *Numerical study of the relativistic three-body quantization condition in the isotropic approximation*, *Phys. Rev.* **D98** (2018) 014506 [[1803.04169](#)].
- [21] R. A. Briceño, M. T. Hansen and S. R. Sharpe, *Three-particle systems with resonant subprocesses in a finite volume*, *Phys. Rev.* **D99** (2019) 014516 [[1810.01429](#)].
- [22] T. D. Blanton, F. Romero-López and S. R. Sharpe, *Implementing the three-particle quantization condition including higher partial waves*, *JHEP* **03** (2019) 106 [[1901.07095](#)].
- [23] J.-Y. Pang, J.-J. Wu, H. W. Hammer, U.-G. Meißner and A. Rusetsky, *Energy shift of the three-particle system in a finite volume*, *Phys. Rev.* **D99** (2019) 074513 [[1902.01111](#)].
- [24] A. W. Jackura, S. M. Dawid, C. Fernández-Ramírez, V. Mathieu, M. Mikhasenko, A. Pilloni et al., *Equivalence of three-particle scattering formalisms*, *Phys. Rev. D* **100** (2019) 034508 [[1905.12007](#)].
- [25] R. A. Briceño, M. T. Hansen, S. R. Sharpe and A. P. Szczepaniak, *Unitarity of the infinite-volume three-particle scattering amplitude arising from a finite-volume formalism*, *Phys. Rev.* **D100** (2019) 054508 [[1905.11188](#)].
- [26] F. Romero-López, S. R. Sharpe, T. D. Blanton, R. A. Briceño and M. T. Hansen, *Numerical exploration of three relativistic particles in a finite volume including two-particle resonances and bound states*, *JHEP* **10** (2019) 007 [[1908.02411](#)].
- [27] M. T. Hansen, F. Romero-López and S. R. Sharpe, *Generalizing the relativistic quantization condition to include all three-pion isospin channels*, *JHEP* **07** (2020) 047 [[2003.10974](#)].
- [28] T. D. Blanton and S. R. Sharpe, *Alternative derivation of the relativistic three-particle quantization condition*, *Phys. Rev. D* **102** (2020) 054520 [[2007.16188](#)].
- [29] T. D. Blanton and S. R. Sharpe, *Equivalence of relativistic three-particle quantization conditions*, *Phys. Rev. D* **102** (2020) 054515 [[2007.16190](#)].
- [30] J.-Y. Pang, J.-J. Wu and L.-S. Geng, *DDK system in finite volume*, *Phys. Rev. D* **102** (2020) 114515 [[2008.13014](#)].
- [31] F. Romero-López, A. Rusetsky, N. Schlage and C. Urbach, *Relativistic N-particle energy shift in finite volume*, *JHEP* **02** (2021) 060 [[2010.11715](#)].
- [32] T. D. Blanton and S. R. Sharpe, *Relativistic three-particle quantization condition for nondegenerate scalars*, *Phys. Rev. D* **103** (2021) 054503 [[2011.05520](#)].
- [33] F. Müller, A. Rusetsky and T. Yu, *Finite-volume energy shift of the three-pion ground state*, *Phys. Rev. D* **103** (2021) 054506 [[2011.14178](#)].
- [34] T. D. Blanton and S. R. Sharpe, *Three-particle finite-volume formalism for $\pi^+\pi^+K^+$ and related systems*, *Phys. Rev. D* **104** (2021) 034509 [[2105.12094](#)].

- [35] F. Müller, J.-Y. Pang, A. Rusetsky and J.-J. Wu, *Relativistic-invariant formulation of the three-particle quantization condition*, [2110.09351](#).
- [36] T. D. Blanton, F. Romero-López and S. R. Sharpe, *Implementing the three-particle quantization condition for $\pi^+\pi^+K^+$ and related systems*, *JHEP* **02** (2022) 098 [[2111.12734](#)].
- [37] A. W. Jackura, *Three-body scattering and quantization conditions from S matrix unitarity*, [2208.10587](#).
- [38] F. Müller, J.-Y. Pang, A. Rusetsky and J.-J. Wu, *Three-particle Lellouch-Lüscher formalism in moving frames*, *JHEP* **02** (2023) 214 [[2211.10126](#)].
- [39] Z. T. Draper, M. T. Hansen, F. Romero-López and S. R. Sharpe, *Three relativistic neutrons in a finite volume*, [2303.10219](#).
- [40] S. R. Beane, W. Detmold, T. C. Luu, K. Orginos, M. J. Savage and A. Torok, *Multi-Pion Systems in Lattice QCD and the Three-Pion Interaction*, *Phys. Rev. Lett.* **100** (2008) 082004 [[0710.1827](#)].
- [41] W. Detmold and B. Smigielski, *Lattice QCD study of mixed systems of pions and kaons*, *Phys. Rev. D* **84** (2011) 014508 [[1103.4362](#)].
- [42] M. Mai and M. Döring, *Finite-Volume Spectrum of $\pi^+\pi^+$ and $\pi^+\pi^+\pi^+$ Systems*, *Phys. Rev. Lett.* **122** (2019) 062503 [[1807.04746](#)].
- [43] B. Hörz and A. Hanlon, *Two- and three-pion finite-volume spectra at maximal isospin from lattice QCD*, *Phys. Rev. Lett.* **123** (2019) 142002 [[1905.04277](#)].
- [44] T. D. Blanton, F. Romero-López and S. R. Sharpe, *$I = 3$ three-pion scattering amplitude from lattice QCD*, *Phys. Rev. Lett.* **124** (2020) 032001 [[1909.02973](#)].
- [45] M. Mai, M. Döring, C. Culver and A. Alexandru, *Three-body unitarity versus finite-volume $\pi^+\pi^+\pi^+$ spectrum from lattice QCD*, *Phys. Rev. D* **101** (2020) 054510 [[1909.05749](#)].
- [46] C. Culver, M. Mai, R. Brett, A. Alexandru and M. Döring, *Three pion spectrum in the $I = 3$ channel from lattice QCD*, *Phys. Rev. D* **101** (2020) 114507 [[1911.09047](#)].
- [47] M. Fischer, B. Kostrzewa, L. Liu, F. Romero-López, M. Ueding and C. Urbach, *Scattering of two and three physical pions at maximal isospin from lattice QCD*, *Eur. Phys. J. C* **81** (2021) 436 [[2008.03035](#)].
- [48] HADRON SPECTRUM collaboration, M. T. Hansen, R. A. Briceño, R. G. Edwards, C. E. Thomas and D. J. Wilson, *Energy-Dependent $\pi^+\pi^+\pi^+$ Scattering Amplitude from QCD*, *Phys. Rev. Lett.* **126** (2021) 012001 [[2009.04931](#)].
- [49] NPLQCD, QCDSF collaboration, S. R. Beane et al., *Charged multihadron systems in lattice QCD+QED*, *Phys. Rev. D* **103** (2021) 054504 [[2003.12130](#)].
- [50] A. Alexandru, R. Brett, C. Culver, M. Döring, D. Guo, F. X. Lee et al., *Finite-volume energy spectrum of the $K^-K^-K^-$ system*, *Phys. Rev. D* **102** (2020) 114523 [[2009.12358](#)].
- [51] R. Brett, C. Culver, M. Mai, A. Alexandru, M. Döring and F. X. Lee, *Three-body interactions from the finite-volume QCD spectrum*, *Phys. Rev. D* **104** (2021) 014501 [[2101.06144](#)].
- [52] T. D. Blanton, A. D. Hanlon, B. Hörz, C. Morningstar, F. Romero-López and S. R. Sharpe, *Interactions of two and three mesons including higher partial waves from lattice QCD*, *JHEP* **10** (2021) 023 [[2106.05590](#)].

- [53] GWQCD collaboration, M. Mai, A. Alexandru, R. Brett, C. Culver, M. Döring, F. X. Lee et al., *Three-Body Dynamics of the $a_1(1260)$ Resonance from Lattice QCD*, *Phys. Rev. Lett.* **127** (2021) 222001 [[2107.03973](#)].
- [54] S. Weinberg, *Phenomenological Lagrangians*, *Physica A* **96** (1979) 327.
- [55] J. Gasser and H. Leutwyler, *Chiral Perturbation Theory to One Loop*, *Annals Phys.* **158** (1984) 142.
- [56] FLAVOUR LATTICE AVERAGING GROUP (FLAG) collaboration, Y. Aoki et al., *FLAG Review 2021*, *Eur. Phys. J. C* **82** (2022) 869 [[2111.09849](#)].
- [57] ETM collaboration, C. Helmes, C. Jost, B. Knippschild, C. Liu, J. Liu, L. Liu et al., *Hadron-hadron interactions from $N_f = 2 + 1 + 1$ lattice QCD: isospin-2 $\pi\pi$ scattering length*, *JHEP* **09** (2015) 109 [[1506.00408](#)].
- [58] M. Mai, C. Culver, A. Alexandru, M. Döring and F. X. Lee, *Cross-channel study of pion scattering from lattice QCD*, *Phys. Rev. D* **100** (2019) 114514 [[1908.01847](#)].
- [59] Z. Fu and X. Chen, *$I = 0$ $\pi\pi$ s -wave scattering length from lattice QCD*, *Phys. Rev. D* **98** (2018) 014514 [[1712.02219](#)].
- [60] J. Bijnens and T. Husek, *Six-pion amplitude*, *Phys. Rev. D* **104** (2021) 054046 [[2107.06291](#)].
- [61] J. Bijnens, T. Husek and M. Sjö, *Six-meson amplitude in QCD-like theories*, *Phys. Rev. D* **106** (2022) 054021 [[2206.14212](#)].
- [62] A. W. Jackura, R. A. Briceño, S. M. Dawid, M. H. E. Islam and C. McCarty, *Solving relativistic three-body integral equations in the presence of bound states*, *Phys. Rev. D* **104** (2021) 014507 [[2010.09820](#)].
- [63] S. M. Dawid, M. H. E. Islam and R. A. Briceño, *Analytic continuation of the relativistic three-particle scattering amplitudes*, [2303.04394](#).
- [64] S. Scherer and M. R. Schindler, *A Primer for Chiral Perturbation Theory*, vol. 830 of *Lecture Notes in Physics*. Springer, 2012, [10.1007/978-3-642-19254-8](#).
- [65] A. Pich, *Effective Field Theory with Nambu-Goldstone Modes*, [1804.05664](#).
- [66] J. Bijnens and J. Lu, *Meson-meson Scattering in QCD-like Theories*, *JHEP* **03** (2011) 028 [[1102.0172](#)].
- [67] G. Colangelo, J. Gasser and H. Leutwyler, *$\pi\pi$ scattering*, *Nucl. Phys. B* **603** (2001) 125 [[hep-ph/0103088](#)].
- [68] MILC collaboration, A. Bazavov et al., *Results for light pseudoscalar mesons*, *PoS LATTICE2010* (2010) 074 [[1012.0868](#)].
- [69] S. Borsanyi, S. Durr, Z. Fodor, S. Krieg, A. Schafer, E. E. Scholz et al., *$SU(2)$ chiral perturbation theory low-energy constants from 2+1 flavor staggered lattice simulations*, *Phys. Rev. D* **88** (2013) 014513 [[1205.0788](#)].
- [70] BUDAPEST-MARSEILLE-WUPPERTAL collaboration, S. Dürr et al., *Lattice QCD at the physical point meets $SU(2)$ chiral perturbation theory*, *Phys. Rev. D* **90** (2014) 114504 [[1310.3626](#)].
- [71] P. A. Boyle et al., *Low energy constants of $SU(2)$ partially quenched chiral perturbation theory from $N_f=2+1$ domain wall QCD*, *Phys. Rev. D* **93** (2016) 054502 [[1511.01950](#)].
- [72] S. R. Beane, W. Detmold, P. M. Junnarkar, T. C. Luu, K. Orginos, A. Parreno et al.,

- SU(2) Low-Energy Constants from Mixed-Action Lattice QCD*, *Phys. Rev. D* **86** (2012) 094509 [[1108.1380](#)].
- [73] Wolfram Research, Inc., *Mathematica, Version 12.2*, Champaign, IL, 2020.
- [74] J. A. M. Vermaseren, *New features of FORM*, [math-ph/0010025](#).
- [75] J. Bijnens, *CHIRON: a package for ChPT numerical results at two loops*, *Eur. Phys. J. C* **75** (2015) 27 [[1412.0887](#)].
- [76] T. Hahn and M. Perez-Victoria, *Automatized one loop calculations in four-dimensions and D-dimensions*, *Comput. Phys. Commun.* **118** (1999) 153 [[hep-ph/9807565](#)].
- [77] M. Galassi et al., *GNU scientific library*. Network Theory Limited Godalming, 2002.
- [78] K. T. R. Davies, M. L. Glasser, V. Protopopescu and F. Tabakin, *The mathematics of principal value integrals and applications to nuclear physics, transport theory, and condensed matter physics*, *Math. Models Methods Appl. Sci.* **06** (1996) 833.
- [79] O. Costin and H. M. Friedman, *Foundational aspects of singular integrals*, *Journal of Functional Analysis* **267** (2014) 4732 [[1401.7045](#)].
- [80] Z. T. Draper, A. D. Hanlon, B. Hörz, C. Morningstar, F. Romero-López and S. R. Sharpe, *Interactions of πK , $\pi\pi K$ and $KK\pi$ systems at maximal isospin from lattice QCD*, [2302.13587](#).